



ISAAC ALVES DE OLIVEIRA

**PRODUCTION AND CHARACTERIZATION OF FLY ASH-
BASED GEOPOLYMER CONCRETE**

LAVRAS-MG

2024

ISAAC ALVES DE OLIVEIRA

**PRODUCTION AND CHARACTERIZATION OF FLY ASH-BASED
GEOPOLYMER CONCRETE**

Monografia apresentada à Universidade Federal de Lavras, como parte das exigências do Curso de Engenharia Civil, para a obtenção do título de Bacharel.

Prof. Dr. Rodrigo Allan Pereira

Orientador

Prof. Dra. Débora Macanjo Ferreira

Coorientadora

Prof. Dr. Helder Teixeira Gomes

Coorientador

LAVRAS-MG

2024

ISAAC ALVES DE OLIVEIRA

**PRODUCTION AND CHARACTERIZATION OF FLY ASH-BASED
GEOPOLYMER CONCRETE**

**PRODUÇÃO E CARACTERIZAÇÃO DE BETÃO GEOPOLIMÉRICO À BASE
DE CINZAS VOLANTES**

Monografia apresentada à Universidade Federal de Lavras, como parte das exigências do Curso de Engenharia Civil, para a obtenção do título de Bacharel.

APROVADA em 13 de junho de 2024.

Dra. Sílvia Maria Afonso Fernandes IPB

Dr. Rodrigo Allan Pereira UFLA

Dra. Eduarda Cristina Pires Luso IPB

Prof. Dr. Rodrigo Allan Pereira

Orientador

Prof. Dra. Débora Macanjo Ferreira

Coorientadora

Prof. Dr. Helder Teixeira Gomes

Coorientador

LAVRAS-MG

2024

ACKNOWLEDGEMENTS

First, I would like to thank God for the uncountable blessings and opportunities to do my best every day. To my parents, Rosana and Pedro, and my sister, Yasmin, for their trust, incentive, support, and always believing in me. I always had the best for my life, and I am really grateful for all the opportunities. I want to extend my gratitude to all my family, especially my grandparents Otaviano, Lulu, Dico and Marieta for providing me the best advice.

I sincerely thank my supervisors, Prof. Dr. Débora Macanjo Ferreira and Prof. Dr. Helder Teixeira Gomes from the Polytechnic Institute of Bragança (IPB), and Prof. Dr. Rodrigo Allan Pereira from University Federal of Lavras (UFLA), for guiding me, for all support, meetings, their teachings, and assistance in this research. I am also grateful to MSc. Ana Paula Ferreira da Silva for helping me since the beginning, providing me great knowledge, laboratory techniques, assistance in computer tools, support, advice, and everything that I needed to successfully complete my work.

To UFLA, for providing me the opportunity to study this double degree in Portugal, and to IPB, for offering the structure, laboratories, and materials necessary to the development of this work. I am also grateful to MSc. Hermínia Maria Mesquita Morais, and the technicians João Pires and Octávio Pereira, for providing me assistance and guidance during the tests conducted at the laboratories of geotechnics and building materials.

I want to thank my friends João Lucas Rezende and Natan Franco Martins for all their support and incentive during my journey despite the distance. To my friend Maria Luiza Monteiro for encouraging me front international opportunities. To my friend João Victor Rosa for the friendship and experiences in Portugal.

ABSTRACT

Increasing urbanization presents environmental, economic, and social concerns, mainly derived from the impact of carbon dioxide emissions and rapid waste generation. Geopolymer concrete (GPC) is an innovative construction material with the potential to minimize the environmental threat due to fly ash (FA) waste disposal and reduce cement consumption. In this study, cement-free GPC mixes are prepared using FA as a source of aluminosilicate material. Sodium silicate (SS) and sodium hydroxide (SH) solutions were used as alkaline activators with varying SH concentrations of 4 M, 10 M, and 16 M; sodium silicate to sodium hydroxide (SS/SH) ratios of 1.5, 2.0, and 2.5; and alkaline liquids to fly ash (AL/FA) ratios of 0.35, 0.525, and 0.70. The influence of the alkaline liquids on the mechanical properties of fly ash-based geopolymer concrete (FA-BGPC) were investigated through flexural strength and compressive strength tests in preliminary tests using prismatic molds. Additionally, water absorption tests through capillarity and immersion, and another trial of compressive strength tests were done in final tests using cubic molds. A reference composition using ordinary Portland cement (OPC) was produced to compare the results. All samples were cured at controlled temperature of 25°C. The optimum flexural strength in the initial tests (6 MPa), and optimum compressive strength in the final tests (29.4 MPa) was attained with a GPC mix using 10 M, 1.5 SS/SH ratio, and 0.70 AL/FA ratio. It was found that the mechanical behavior of GPC is similar to that of OPC concrete.

Keywords: Geopolymer; Fly ash; Concrete; Carbon dioxide; Portland cement; Mechanical proprieties.

RESUMO

A crescente urbanização envolve preocupações ambientais, econômicas e sociais, principalmente devido o impacto das emissões de gás carbônico e rápida geração de resíduos. Betão geopolimérico (GPC) é um inovador material de construção com o potencial de minimizar os impactos ambientais do descarte de cinzas volantes (FA) e reduzir o consumo de cimento. Neste trabalho, misturas de betões geopoliméricos, sem cimento, foram produzidas a partir da utilização de cinzas volantes como fonte de material aluminossilicato. Soluções de silicato de sódio (SS) e hidróxido de sódio (SH) foram utilizadas como ativadores alcalinos com concentrações variáveis de SH de 4 M, 10 M, e 16 M; razões de silicato de sódio para hidróxido de sódio (SS/SH) de 1.5, 2.0 e 2.5; e razão de líquidos alcalinos para cinzas volantes (AL/FA) de 0.35, 0.525 e 0.70. Foi investigado a influência dos líquidos alcalinos nas propriedades mecânicas do betão geopolimérico à base de cinzas volantes (FA-BGPC) através de testes de resistência à flexão e compressão em testes preliminares em moldes prismáticos. Adicionalmente, testes de absorção de água por capilaridade e imersão, e uma nova série de testes de resistência à compressão foram realizadas em testes finais em moldes cúbicos. Foi produzida uma mistura de referência com cimento Portland (OPC) para comparar os resultados. Todas as amostras foram curadas em uma temperatura controlada de 25 °C. A maior resistência à flexão nos testes iniciais (6 MPa), e a maior resistência à compressão nos testes finais (29.4 MPa) foi obtida por uma mistura de betão geopolimérico com concentração de SH de 10 M, razão SS/SH de 1.5 e razão AL/FA de 0.70. Foi constatado que o comportamento mecânico das amostras de GPC foram similares ao betão de OPC.

Palavras-chave: Geopolímero; Cinzas volantes; Betão; Gás carbônico; Cimento Portland; Propriedades mecânicas.

LIST OF CONTENTS

LIST OF FIGURES	v
LIST OF TABLES	vi
LIST OF ABBREVIATIONS	vii
1 INTRODUCTION	1
2 STATE OF THE ART	3
2.1 Climate change and CO ₂	3
2.2 Cement Production.....	4
2.3 Mitigation strategies in the cement industry	5
2.4 Alternative solutions to Ordinary Portland Cement.....	7
2.5 Geopolymer technology	8
2.5.1 Precursor	10
2.5.2 Alkaline solution	12
2.5.3 Water Absorption	16
3 OBJECTIVES	21
3.1 General Objective.....	21
3.2 Specific Objectives.....	21
4 MATERIALS AND METHODS	22
4.1 Materials.....	22
4.2 Design of Experiments	23
4.3 Mixture proportions	26
4.4 Mixing, sample preparation, and curing	32
4.5 Experimental tests	35
4.5.1 Preliminary tests - Flexural and compressive strength testing in prismatic molds	35
4.5.2 Final tests	38
5 RESULTS AND DISCUSSION	44
5.1 Preliminary tests.....	44
5.2 Final tests	49
5.2.1 Capillarity Water absorption Tests	49

5.2.2 Immersion water absorption Tests.....	57
5.2.3 Compressive strength cubic molds	62
6 CONCLUSIONS AND FUTURE RESEARCH	67
6.1 Conclusions	67
6.2 Future research	67
REFERENCES	69
APPENDIX	81

LIST OF FIGURES

Figure 1 - Simplified diagram of the cement production process.	5
Figure 2 - Geopolymerization process.....	9
Figure 3 - Fly ash, sand, gravel, and distilled water weighed.	33
Figure 4 - (a) Acrylic molds (b) Prismatic molds filled with geopolymer concrete.....	33
Figure 5 - (a) Compaction of the first layer (b) Fresh concrete at the vibrating table....	34
Figure 6 - (a) Cubic molds filled with GPC (b) GPC storage inside the chamber.	34
Figure 7 - Simplified FA-BGPC mixing procedure.....	35
Figure 8 - (a) Flexural Strength machine (b) Prismatic mold placed in the machine.....	37
Figure 9 - Compressive strength prismatic molds.	38
Figure 10 - Capillarity test.....	39
Figure 11 - (a) GP4, GP5, and GP6 (b) cement reference composition underwater.	40
Figure 12 - (a) First, (b) second and (c) third layer of water, respectively.	41
Figure 13 - (a) Sample inside the metallic container (b) thermometer.....	41
Figure 14 - (a) Hydrostatic balance (b) drying process in the oven.	42
Figure 15 - (a) Weight of the specimen (b) Compression test cubic molds.	43
Figure 16 - Average flexural and compressive strength in the preliminary tests.	45
Figure 17 - Prisms a-b) GP7 c-d) REF after flexural strength test.	49
Figure 18 - Water absorption by capillarity of GP1, GP2, GP4, GP5, GP6, GP8, GP9, GP10, and GP13.	51
Figure 19 - (a) GP2 and (b) GP5, the highest water absorptions through capillarity.	53
Figure 20 - (a) Comparison between geopolymers GP1, GP2 (b) GP4, GP5, and GP6, respectively.	54
Figure 21 - The water absorption by capillarity of REF, GP3, GP7, GP11, GP12, GP14, and GP15.	55
Figure 22 - Reference composition at a-d) 24h, b-e) 48h, and c-f) 72h, respectively.	56
Figure 23 - Results of absorption of water by immersion.	59
Figure 24 - Average compressive strength at 28 days in cubs.	62
Figure 25 - (a-f) Geopolymers GP3, GP7, GP11, GP12, GP14, and GP15, respectively (g) REF composition.	66
Figure 26 - Selection of samples to future research.	66

LIST OF TABLES

Table 1 - Chemical characterization of the FA.	23
Table 2 - Summary of previous studies of GPC.	25
Table 3 - Experimental variables and their levels used in the DOE.	26
Table 4 - Design of Experiments.	26
Table 5 - Reference mixture proportion in the preliminary tests.	28
Table 6 - Mixture proportions in the preliminary tests.	29
Table 7 - Reference mixture proportion in the final tests.	30
Table 8 - Mixture proportions in the final tests.	30
Table 9 - Final unit weight of concrete.	32
Table 10 - Average, standard deviation, and coefficient of variation.	44
Table 11 - Water absorption at 72 h from the highest to the lowest value.	50
Table 12 - Immersion test.	57
Table 13 - Immersion test GP10.	57
Table 14 - Dry mass immersion test.	58

LIST OF ABBREVIATIONS

FA	Fly Ash
OPC	Ordinary Portland Cement
GPC	Geopolymer Concrete
GHG	Greenhouse Gas
CCS	Carbon Capture and Storage
CCU	Carbon Capture and Use
SCM	Supplementary Cementitious Material
AAM	Alkali Activated Material
GGBFS	Ground granulated blast-furnace slag
SS	Sodium Silicate
SH	Sodium Hydroxide
AL/FA	Alkaline liquids to fly ash ratio
SEM	Scanning Electron Microscope
XRD	X-ray Diffraction
FTIR	Fourier Transform Infrared Spectroscopy

1 INTRODUCTION

Concrete is one of the most used building materials in the construction sector. Regarding concrete production, one of its main ingredients is cement, a massive contributor to carbon dioxide emissions due to the combustion process involved in its production. Over 4 billion tons of cement are produced yearly, representing 8% of global carbon dioxide emissions (Lehne; Preston, 2018; Poloju; Srinivasu, 2021; Yang *et al.*, 2024).

It is predicted that production of OPC will increase by 200% from 2015 to 2025 due to global construction sector demand (Ghafoor *et al.*, 2021; Xie; Ozbakkaloglu, 2015). Cement production requires a high amount of energy, which results in environmental issues such as increasing emissions of greenhouse gases (GHGs), particularly carbon dioxide (CO₂), nitrogen oxides (NO_x) and sulfur oxides (SO_x), although in smaller quantities compared to CO₂ (Ghafoor *et al.*, 2021; Xie *et al.*, 2019). Considering all the GHGs, CO₂ emissions are responsible for 65% of global warming, and according to specialists, the global average temperature could probably increase about 1.4 - 5.8 °C over the next 100 years (Rehan; Nehdi, 2005; Zhou *et al.*, 2016).

The manufacture of cement affects the environment in a series of ways; the procurement of limestone leads to the pollution of land and water and affects the local ecosystem, flora, and fauna (Ganesh; Muthukannan, 2021). Production of OPC liberates almost equal amounts of CO₂, which leads to air pollution (Ganesh; Muthukannan, 2021), an increase in global temperature (Benhelal; Shamsaei; Rashid, 2021), and climate changes (Töbelmann; Wendler, 2020).

Because of environmental concerns, much research is carried out worldwide to replace conventional concrete with eco-friendly solutions. One of them, Geopolymer technology, was introduced to the world by Professor Davidovits in France in 1970 (Ahmed *et al.*, 2021; Bellum; Muniraj; Madduru, 2020). Geopolymer is a novel binder, the chemistry of which is based on aluminosilicate sources, which means it is synthesized with minerals that have Al and Si in it (Bajpai *et al.*, 2020; Ganesh; Muthukannan, 2021). These aluminosilicate sources can be of natural origin like metakaolin or be an industrial by-product like Fly Ash (FA), Ground Granulated Blast Furnace Slag (GGBFS), rice husk ash, high calcium wood ash, and waste glass powder, mostly industrial materials worthless after their production (Bajpai *et al.*, 2020; Ganesh; Muthukannan, 2021).

As a potential substitute for OPC, geopolymer is a low-carbon binder and clinker-free material made by activating aluminosilicate resources with alkaline sols like silicate, carbonate, alkali hydroxide, and sulfate (Qaidi *et al.*, 2022). It was reported that resorting to GPC would lessen about 80 percent of the impact caused by cement production over global warming, and it could reduce the problems caused by limestone mining and FA, GGBFS disposal as well (Ganesh; Muthukannan, 2021).

The use of industrial wastes in alkali-activated geopolymer concrete has become a matter of recent research on concrete sustainability, not just because of environmental concerns but also because it was discovered that the material possesses high compressive strength due its three-dimensional structure (Bajpai *et al.*, 2020). Furthermore, GPC could replace traditional cement-based concrete once presented with similar mechanical properties, durability, and less environmental impact (Bellum; Muniraj; Madduru, 2020).

2 STATE OF THE ART

2.1 Climate change and CO₂

It is well known that over the last few years, climate change has been one of the most significant concerns due to its direct impact on the environment and global economy (Hanifa *et al.*, 2023). GHGs emissions mainly cause climate change; the Kyoto Protocol defines these gases as CO₂, methane (CH₄), nitrous oxide (N₂O), and fluorinated gases such as hydrofluorocarbons (HFCs), perfluorocarbons (PFCs) and sulfur hexafluoride (SF₆) (Fawzy *et al.*, 2020). The major influencing gas and the primary cause of global warming is considered CO₂ (Fawzy *et al.*, 2020; Hanifa *et al.*, 2023; World Meteorological Organization, 2022).

The increasing levels of CO₂ emissions in the atmosphere affect life on earth once it changes in climate indicators, precipitation, rise in temperatures, sea level, and acidification of oceans (Fawzy *et al.*, 2020; Hanifa *et al.*, 2023). In 2018, the world faced 315 cases of natural disasters, most of them were storms, floods, wildfires, and droughts, mainly attributed to climate change, where 68.5 million people were affected and economic losses of about 131.7 billion dólares (Fawzy *et al.*, 2020).

In 2015, the Paris Agreement was an important international treaty where 195 nations agreed to combat climate change. The main goal was to limit the global average temperature increase to 2 °C above pre-industrial levels and pursue efforts to limit the temperature increase to 1.5 °C by the end of the century in 2100 (Fawzy *et al.*, 2020; Hanifa *et al.*, 2023). However, the temperature has increased by 1 °C above pre-industrial levels and will reach 1.5 °C between 2030 and 2052 and 2.7 °C until 2100 if nothing changes in current emission rates (Fawzy *et al.*, 2020; World Meteorological Organization, 2022).

According to the 2022 World Meteorological Organization report (World Meteorological Organization, 2022), real-time data indicate that global GHGs emissions continued to increase in 2022. In 2021, the latest data available, record values were reached in the atmosphere: CO₂ at 149% of pre-industrial levels, CH₄ at 262% of pre-industrial levels, and N₂O at 124% of pre-industrial levels. On top of that, in 2022, the temperature achieved approximately 1.15 °C above the pre-industrial average, being the last 8 years the warmest registered (World Meteorological Organization, 2022).

As can be seen, since the Paris Agreement in 2015, global GHGs emissions have grown, leading to the necessity of strategies for emissions reduction and mitigation in all sectors immediately. Otherwise, it will not be possible to keep warming below 1.5 °C by the end of the century in 2100.

Concerning CO₂ emissions to the atmosphere caused by human activities, the primary sources are the oxidation of fossil fuels, deforestation, and carbonate decomposition (Andrew, 2019). Cement, the second-most consumed material after water on earth (Busch *et al.*, 2022), is the highest contributor to CO₂ emissions from carbonate decomposition (Andrew, 2019).

2.2 Cement Production

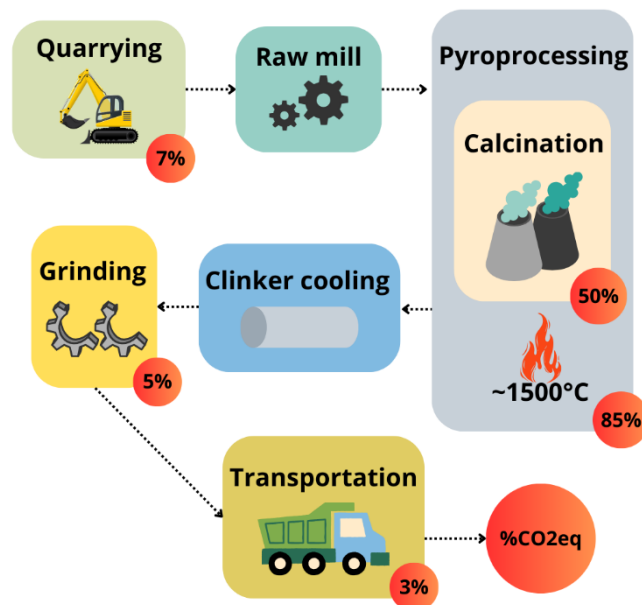
Cement is a binder material primarily used in the construction and geotechnical industries, although its applications are expanding into various emerging fields. These include nuclear waste containment, biological and dental ceramics, and water filtration (Maddalena; Roberts; Hamilton, 2018). Concerning its use in the construction sector, it can be used as a source material associated with other ingredients, such as water, sand, and gravel, for concrete and mortar manufacturing, for instance. After that, cement-based materials are employed worldwide to produce structures, buildings, roads, bridges, dams, railways, and many other construction applications (Maddalena; Roberts; Hamilton, 2018).

Due to the increasing urbanization and rapid infrastructural development, especially in developing countries, cement consumption is expected to increase. Consequently, the impact of cement production on CO₂ emissions is expected to increase as well (Almutairi *et al.*, 2021; Busch *et al.*, 2022). According to many authors, reducing CO₂ emissions from the construction industry is essential to reaching climate change targets (Hanifa *et al.*, 2023).

Cement manufacturing comprises the following steps: quarrying, raw mill, pyro processing/calcination, clinker cooling, grinding, and transportation (Maddalena; Roberts; Hamilton, 2018). CO₂ emissions associated with each production stage can be measured and are usually expressed as CO₂ equivalent (CO_{2eq}), as can be seen in Figure 1. The majority of CO_{2eq} emissions in cement manufacture is from calcination during clinker production, the main component of cement. The chemical reaction to produce

clinker, in which carbonates (largely CaCO_3 , found in limestone) are decomposed into oxides (largely lime, CaO) and CO_2 by adding heat (Andrew, 2019), is responsible for 50% of all emissions from cement production (Maddalena; Roberts; Hamilton, 2018). In the second place is the combustion of fossil fuels for calcination because of the high temperature needed to heat the materials in a furnace to well over $1400\text{ }^\circ\text{C}$ (Andrew, 2019). The 85% of pyroprocessing $\text{CO}_{2\text{eq}}$ emissions include the 50% of calcination $\text{CO}_{2\text{eq}}$ emissions. Finally, the remaining emissions come from excavation, transportation, milling, and grinding processes (Maddalena; Roberts; Hamilton, 2018).

Figure 1 - Simplified diagram of the cement production process.



Source: Adapted from Maddalena, Roberts, and Hamilton (2018).

2.3 Mitigation strategies in the cement industry

In 2009, the International Energy Agency (IEA) proposed Carbon Capture and Storage (CCS) as the primary strategy to mitigate CO_2 emissions from the cement industry. Since then, researchers have kept efforts on track to improve the existing solutions on the market and explore new strategies, such as Carbon Capture and Utilization (CCU) (Scrivener; John; Gartner, 2018).

A recent study review by Busch et al. (2022) shows a consensus between common strategies currently deployed on cement and concrete decarbonization. The technical measures include improved energy efficiency, fuel switching, carbon capture utilization

and storage, and reduced clinker-to-cement ratio (low-carbon cement) for cement production. Similarly, alternative binders, material efficiency, construction efficiency, and CO₂ uptake by concrete are used for concrete production. Moreover, other strategies were also mentioned, such as electricity decarbonization and reduction of transport emissions (Busch *et al.*, 2022).

Regarding the decarbonization techniques, fuel switching, and energy efficiency are widespread in any industry, whereas carbon capture, use, and storage are less commercialized. All three solutions can mitigate CO₂ emissions and are linked to the clinker production level (Busch *et al.*, 2022). On the other hand, at the cement level, it is possible to reduce emissions by reducing the clinker percentage, using different clinker compositions, or using alkali-activated materials (Busch *et al.*, 2022). Finally, at the concrete level, it is possible to fix CO₂ during curing using carbon utilization technologies and increasing the natural carbonation process by concrete. This means some CO₂ uptake will occur naturally in concrete, but additional methods can improve it. Also, at the concrete level still, other possibilities are related to material efficiency strategies, efficient design (reduced use of concrete and cement), reuse of materials, recycling, and others (Busch *et al.*, 2022).

Meanwhile, there are barriers to the complete adoption of the mitigation measures mentioned by the authors, such as higher cost, lack of demand or incentives for low-carbon products, new standards, market acceptance, technologies in early stages of development, lack of adequate training, little support for testing and upscaling new technologies, and so many others (Busch *et al.*, 2022).

Reducing CO₂ emissions from the cement industry will require policy interventions such as reducing transaction costs, reducing fossil fuel use, increasing the demand for low-carbon cement and concrete, promoting research of new technologies, and promoting circularity in new materials, for instance (Busch *et al.*, 2022).

Among all these mitigation strategies mentioned for reducing CO₂ emissions in the cement industry, this work mainly discusses reducing the clinker-to-cement ratio and alternative binders for concrete once clinker production is where the most emissions occur.

2.4 Alternative solutions to Ordinary Portland Cement

It is well known that cement based on Portland cement clinker is very dominant in the global market nowadays; consequently, replacing cement with new materials in the construction industry is not a simple task. There are reasons for that: economy of scale production and optimized processing, affecting both cost and energy requirements; widespread availability of raw materials; excellent workability before setting; and deep knowledge in long-term properties and durability (Scrivener; John; Gartner, 2018).

One of the possibilities for decarbonizing the construction industry is to replace clinker used in Portland cement systems with lower carbon materials, such as reused waste, industrial by-products, or biomass wastes like rice husk ash (Maddalena; Roberts; Hamilton, 2018). These are mineral additions or supplementary cementitious materials (SCMs) and include almost inert materials called fillers (Scrivener; John; Gartner, 2018). Fillers are fine particulate materials, inert or weakly reactive, produced by grinding, that can partially replace clinker or other reactive SCMs. Many materials, such as limestone fillers, can be used as fillers, and they do not require calcining, their production needs only energy for grinding (Scrivener; John; Gartner, 2018).

Among all the materials that can be used as partial clinker replacement, there are two by-products from other industries that are commonly utilized: GGBFS, from pig-iron production in blast furnaces, and FA, generated by burning coal to produce electricity. However, the most common SCM is the almost inert limestone filler (Scrivener; John; Gartner, 2018). In addition, there are other possible sources of SCMs and fillers, such as natural pozzolans, calcined clays, vegetable ashes, waste glass, and silica fume. In summary, any amorphous or imperfectly crystalline material containing silica, alumina, or lime can be potentially a reactive SCM (Scrivener; John; Gartner, 2018).

The Getting the Numbers Right (GNR) database from the Cement Sustainability Initiative (CSI) showed the evolution of clinker substitutes from CSI World Business Council for Sustainable Development (WBCSD) companies. It is possible to notice that the rate level of clinker substitution was almost stabilized in the last years of the database. This corresponds to the fact that the supply of slags and FA, the most desirable substitutes, was not proportional to the increasing cement production. In other words, the FA and slag supplies are limited compared to the cement demand. As new SCMs are discovered and

available, they are expected to reduce cement use further (Scrivener; John; Gartner, 2018).

In most scenarios, clinker is just partially replaced by these novel materials, which is advantageous from a regulatory perspective once the existing Portland cement standards can be adapted. On the other hand, especially for novel cement-free binders, their adoption in construction can be difficult due the lack of regulatory standards backed by long term testing and development (Maddalena; Roberts; Hamilton, 2018).

2.5 Geopolymer technology

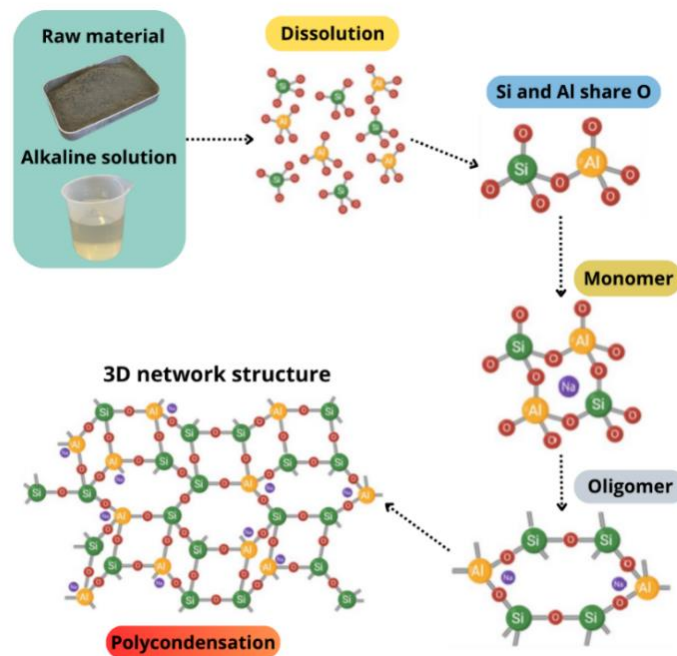
Geopolymer, first introduced by Professor Davidovits (Davidovits, 2020), is an inorganic polymer usually produced at temperatures below 100 °C, by a reaction between an alkali-activated solution (alkali activators) and a raw material rich in aluminum and silicon (aluminosilicate precursors) (Davidovits, 2020; Ferdous; Kayali; Khennane, 2013; Reddy; Dinakar; Rao, 2018). In other words, the process occurs through dissolution at high pH under alkaline conditions, atmospheric pressure, and at considerably low temperatures, from room temperature to slightly elevated temperatures (Luhar; Luhar, 2022).

The French scientist Joseph Davidovits discovered that alternative binders for concrete could be produced through the process of geopolymerization by using different wastes, such as FA (B. Siva Konda Reddy; J. Varaprasad; K. Naveen Kumar Reddy, 2010; Baharom *et al.*, 2019; Fang *et al.*, 2018; Mustafa *et al.*, 2012; Sumajouw *et al.*, 2007), GGBFS (Hadi; Farhan; Sheikh, 2017; Nath; Sarker, 2014), metakaolin (Aswathy; Ritzky, 2020; Eisa; Fahmy; Basiouny, 2022; Nuaklong; Sata; Chindaprasirt, 2018), fibres (Verma *et al.*, 2022), volcanic ash (Luhar *et al.*, 2019), glass wastes (Manikandan; Vasugi, 2021; Siddika *et al.*, 2021), and farming wastes (Luhar; Luhar, 2022; Sulthan, 2019). These precursors' reaction depends on their chemical and physical properties, such as fineness, glassy phase composition, and mineralogy (Almutairi *et al.*, 2021).

The geopolymerization reaction, which leads to geopolymer product, is divided into dissolution, transportation, orientation, condensation, and poly-condensation (Davidovits, 2020; Reddy; Dinakar; Rao, 2018). The first step is the dissolution of silicates and aluminates in an alkali solution to form precursor ions, which are reoriented and condensed to form monomers. Dissolved AlO_4 and SiO_4 tetrahedrons combine to

form monomers by sharing one oxide (O) atom (Zhang *et al.*, 2020a). Monomers interact to form oligomers. Ultimately, the poly-condensed process leads to a three-dimensional structure of silicates and aluminates (Fernández-Jiménez; Palomo; Criado, 2005; Reddy; Dinakar; Rao, 2018). This dissolution and polycondensation process is called geopolymerization. The geopolymerization process leading the raw material to a synthesized 3D network of aluminosilicate structures is summarized in Figure 2. Also, during geopolymerization, an important information is that it occurs with nine times fewer emissions of CO₂, requires 60% less energy, and is approximately 10-30% cheaper compared with OPC (Luhar; Luhar, 2022).

Figure 2 - Geopolymerization process.



Source: Adapted from Zhang *et al.* (2020a).

The geopolymer binder possesses amorphous and semi-crystalline framework structures created by the accompanying $(\text{SiO}_4)^{-4}$ and $(\text{AlO}_4)^{-5}$ tetrahedral (Almutairi *et al.*, 2021). Also, the material possesses higher compressive strength due to the creation of a three-dimensional structure of aluminosilicate hydrate associated with primary bonding compared to calcium silicate hydrate of one-dimensional structure with secondary van der Waals bonding (Bajpai *et al.*, 2020).

The GPC consists of three components: a source of aluminosilicate (precursor), coarse and fine aggregates, and an activating (alkali) solution. Additionally, as GPC may

utilize waste materials, they are considered a sustainable alternative to OPC concrete (Assi *et al.*, 2020).

GPC has been shown to have excellent properties, including high compressive strength, reaching more than 85% of its final compressive strength within 48 h. Also, compared to OPC, the geopolymer has superior durability, higher resistance under elevated heat, higher resistance to acid attack when exposed to varied acid concentrations for a year or more, and generally higher resistance against freeze-thaw cycles and salt scaling (Assi *et al.*, 2020).

Studies have shown a broad set of novel binder materials (Ahmed *et al.*, 2021; Shi; Qu; Provis, 2019; Zhang *et al.*, 2020a). However, there are challenges in standardization and specification, as it is challenging to combine all these materials' information in the same content. So, this highlights the need for performance-based specification of alkali-activated binders rather than relying on a prescriptive approach (Shi; Qu; Provis, 2019).

2.5.1 Precursor

In GPC, the precursor can be the inorganic binder agent in the chemical reaction to bind other materials together. Different kinds of materials are already demanded for use in Portland cement blends. Consequently, alternative precursors with less competition in demand have been targeted for their use in alkali activation. For example, calcined non-kaolinitic clays, palm oil fuel ash, or other minerals. Also, various industrial by-products or wastes, such as red mud, slags, and FA (Shi; Qu; Provis, 2019).

Geopolymer precursors are typically composed of a high amount of silicate and aluminate. These aluminosilicate precursors are critical components of geopolymers, and their chemical composition plays a vital role in the geopolymerization. It happens because when these materials are placed in an alkaline medium, they will hydrolyze and condense, forming new inorganic polymers that can develop load-bearing capacity. In other words, aluminosilicate precursors used in geopolymers will dissolve in an alkaline/acidic medium to form a gel that hardens (Almutairi *et al.*, 2021).

FA, GGBFS, and metakaolin are examples of aluminosilicate precursors used to produce GPC. FA and GGBFS are by-products, and metakaolin is a manufactured material. However, this study mainly discusses the utilization of FA to produce GPC.

FA comprises powdery, fine particles mainly of spherical shape, which may be hollow or solid, that constitutes a by-product obtained when coal, biomass, municipal solid waste, or a mixture of these are combusted. It should be emphasized that all types of FA are rich sources of SiO_2 and Al_2O_3 , and their recovery is a waste management issue (Grabias-Blicharz; Franus, 2023).

FA is a waste material produced primarily from coal-fired power production. It is produced by burning finely ground coal in a boiler to produce electricity and is captured in a power plant's chimney through a particulate control device (Assi *et al.*, 2020). The mineralogical and chemical composition of FA is diverse, and depends on the combusted coal, combustion conditions, and the type of emission control devices (Grabias-Blicharz; Franus, 2023). In Portugal, most of the concrete used is made with coal FA as a SCM. However, Portuguese coal-fired power plants are being closed as the energy sector and the local government are committed to producing energy using low carbon sources. So, coal FA supply is expected to decrease, and it is important to find alternatives to substitute the utilization of coal FA in the concrete industry (Teixeira; Camões; Branco, 2022).

FA can also be produced from the combustion of municipal solid waste, such as wood, textiles, food waste, paper, and plastics (Grabias-Blicharz; Franus, 2023). Similarly to coal FA, the chemical and physical properties of FA are highly dependent on the type of waste being incinerated, combustion technology, and devices to control air pollution. The current global municipal solid waste generation is 2.01 billion tons per year and is expected to keep increasing due to urbanization and people's living standards (Grabias-Blicharz; Franus, 2023). The incineration of solid waste is a very effective procedure due to its capacity to reduce the waste volumes. This method varies from country to country and the municipal solid waste incineration rate can reach as high as 50-58% in some northern Europe countries (Cristelo *et al.*, 2020). Significant volumes of FA are still produced by incineration and their recycling by integration in any industrial process constitutes an attractive possibility (Cristelo *et al.*, 2020).

In general, FA is considered a waste of public concern because it contains a tremendous amount of soluble constituents and toxic heavy metals such as arsenic, mercury, copper, cobalt, chromium, and lead, with potential negative impacts on the environment as well as large land area occupation, which includes fertile farmland (Grabias-Blicharz; Franus, 2023; Nguyen *et al.*, 2023).

At present, FA is deposited in huge quantities in landfills, dumps, or settling ponds. Due to its relatively low reactivity and heterogeneity, FA is commonly landfilled (Grabias-Blicharz; Franus, 2023). However, the disposal methods are far from being environmentally friendly because heavy elements can easily migrate from FA and through interaction with water, leading to soil and groundwater contamination. Also, exposure to wind contributes to environmental pollution by spreading FA particles in the air (Grabias-Blicharz; Franus, 2023).

Global FA utilization is lower than its annual production, with the reuse rate of FA recycled being only up to 30% (Assi *et al.*, 2020; Grabias-Blicharz; Franus, 2023). The disposal of an excessive quantity of FA is not preferred, and hence, the modification of waste FA to beneficial and useful materials is crucial (Nguyen *et al.*, 2023).

As an emerging, useful, and low-cost material, several review articles regarding the utilization of FA have been reported in the literature (Nguyen *et al.*, 2023). For example, manufacturing membranes for oil-in-water emulsion and wastewater treatment (Goswami; Pakshirajan; Pugazhenthii, 2022); the production of porous materials including thermal insulation, adsorbents, and ceramic membranes (Wang *et al.*, 2021); FA (Fu *et al.*, 2021) and FA/GGBFS (Zhang *et al.*, 2020b) derived GPC (Nguyen *et al.*, 2023).

FA-BGPC is one possibility that could turn waste material (primarily from the combustion of coal and municipal solid waste) into a useable product, avoiding the environmental concerns of disposal of FA; FA-BGPC has superior performance and results in a 40% reduction of CO₂ relative to OPC concrete (Assi *et al.*, 2020).

2.5.2 Alkaline solution

The alkaline solution used in geopolymerization is generally a combination of alkali hydroxides and alkali silicates; the most common are sodium hydroxide (SH) with sodium silicate (SS) and potassium hydroxide (KOH) with potassium silicate (K₂SiO₃) (Ferdous; Kayali; Khennane, 2013), individually or in combination (Reddy; Dinakar; Rao, 2018).

The KOH exhibited a higher degree of alkalinity, whereas it has been reported that SH acquires higher efficiency in dissolved silicate and aluminate monomers in the aluminosilicate precursors (Almutairi *et al.*, 2021). Specifically, many studies suggest the

combination of SH with SS for GPC production (Deb; Nath; Sarker, 2014; Ghafoor *et al.*, 2021; Nath; Sarker, 2014, 2017; Ramujee; PothaRaju, 2017).

The activator solution is usually the most expensive component of an alkali-activated binder; it happens because the commercial solutions are produced at high purity for other industry sectors' applications, which in most cases for commercial alkali silicate solutions, like sodium silicate solutions, but purity could not be required at a high level for alkali-activation. Thus, alternative activators, such as silicate activators from olivine or waste glass, biomass ashes, and near-neutral salts, have been studied in the literature (Shi; Qu; Provis, 2019).

Some alkali-activated solution parameters could influence the properties of the geopolymer produced, such as SH molarity, silicates to hydroxide ratio, and alkaline solution to binder ratio.

2.5.2.1 NaOH Molarity

The SH molarity is an important parameter that has a direct influence on the properties of the material. Some studies were selected to review the impact of this parameter in FA-BGPC.

A study was carried out by Ghafoor *et al.* (2021) to evaluate the mechanical properties of FA-BGPC cured at ambient temperature. It was observed that with increasing molarity of SH, the average compressive strengths of GPC were also increased from 8 M to 10 M, 10 M to 12 M, and 12 M to 14 M, by 55,8%, 10,5%, and 33,0%, respectively. However, the average compressive strength decreased as the molarity of SH varied by 9% from 14 M to 16 M (Ghafoor *et al.*, 2021). Similar results can be seen in other studies, some using different molarity (Ahmed *et al.*, 2021; Chithambaram *et al.*, 2018a; Sumajouw *et al.*, 2007).

In contrast, B. Siva Konda Reddy, J. Varaprasad, and K. Naveen Kumar Reddy (2010), explain that the compressive strength of FA-BGPC was improved at 28 days and curing temperature of 60°C with increased molarity of SH by 8.5%, 14,7%, and 19,2% at 12 M, 14 M, and 16 M, respectively, compared to the molarity of 10 M (Ahmed *et al.*, 2021; B. Siva Konda Reddy; J. Varaprasad; K. Naveen Kumar Reddy, 2010). Similarly, it was also observed by some other authors (Baharom *et al.*, 2019; Das; Shrivastava, 2021; Jaydeep; Chakravarthy, 2013; Vora; Dave, 2013).

In general, increasing the molarity of SH improves the compression strength of GPC, which could be attributed to the higher dissolution of silicon and aluminum particles in the geopolymerization process (Ahmed *et al.*, 2021; Ghafoor *et al.*, 2021; Görhan; Kürklü, 2014; Nath; Sarker, 2017); through the leaching out of silica and alumina with the high concentration of SH (Aliabdo; Abd Elmoaty; Salem, 2016; Chindaprasirt *et al.*, 2009a). The improvement in GPC properties when increasing molarity up to 16 M were reported in these studies (Al Bakri, A M M *et al.*, 2012; Aliabdo; Abd Elmoaty; Salem, 2016; Hardjito *et al.*, 2004).

Some authors reported decreased compression strength while increasing the molarity of SH (Ahmed *et al.*, 2021; Aliabdo; Abd Elmoaty; Salem, 2016; Ghafoor *et al.*, 2021; Nath; Sarker, 2017). Usually, it happens in high molarity solutions, such as 16 M or higher. Beyond 16 M, the GPC properties decreases due to a lower rate of polymerization taking place, resulting in a decreased strength (Aliabdo; Abd Elmoaty; Salem, 2016). Also, other studies attributed decreased strength while increasing molarity due to congestion of hydroxide ions in high molarity mix (OH^-) (Ghafoor *et al.*, 2021; Nath; Sarker, 2017); to the fact that overflowing alkali concentration prevents the condensation of silicate elements (Ahmed *et al.*, 2021).

In addition, in the study by Joseph, and Mathew (2012), the compressive strength behavior was changed while varying SH molarities around 10 M. It was observed that the compressive strength of GPC increased with increase in SH molarity up to a value of 10 M and on further increase, the compressive strength decreases. So, according to the authors, this behavior is mainly due to the fact that SH molarity used for geopolymer synthesis has a positive influence on dissolution, hydrolysis, and condensation reactions, but excess alkali concentration hinders the condensation of the silicate species (Joseph; Mathew, 2012).

2.5.2.2 Silicates to hydroxide ratio

Regarding FA-BGPC production, the parameter silicates to hydroxide ratio represents the ratio between SS and SH by weight. This ratio directly affects the geopolymerization reaction between the alkali solution and the precursor FA.

A study was carried out by Joseph, and Mathew (2012) to investigate parameters on the performance of FA-BGPC. After casting, the specimens were cured at 100° C for

24 hours and kept at room temperature until testing. The experiment showed that the compression strength increased while the SS/SH ratio increased from 1.5 to 2 and 2 to 2.5. On the other hand, the compressive strength decreased when the ratio moved from 2.5 to 3 and from 3 to 3.5. In other words, the authors showed that the compressive strength increased while the SS/SH ratio increased to a value of 2.5 and then decreased (Joseph; Mathew, 2012). Regarding the same authors, increase in compressive strength is mainly due to the change in microstructure of GPC, which was influenced by the quantity of SS. On the other hand, the decrease in compressive strength is because at high SS/SH ratios, the quantity of SH is not sufficient for the completion of dissolution process during the formation of GPC (Joseph; Mathew, 2012). Similarly, other studies reached similar conclusions (Ahmed *et al.*, 2021; Mustafa *et al.*, 2012). The improvement in GPC strength also may be due to SS solution improving the polymerization process leading to reaction products with more Si and, hence, higher mechanical strength (Aliabdo; Abd Elmoaty; Salem, 2016; Pacheco-Torgal; Castro-Gomes; Jalali, 2008). The increase in strength with increase in SS/SH ratio were also reported in these studies (Aliabdo; Abd Elmoaty; Salem, 2016; Sathonsaowaphak; Chindaprasirt; Pimraksa, 2009a).

The same research conducted by Ghafoor *et al.* (2021), mentioned in previous topics, also analyzed the effect of the SS/SH ratio on the compressive strength of FA-BGPC cured at ambient temperature. Their findings demonstrate that increasing the SS/SH ratio from 1.5 to 2 decreased the compressive strengths of GPC by 5.2%, 7.6%, 7.6%, 10.8%, and 12.8% at 8 M, 10 M, 12 M, 14 M, and 16 M, respectively. In addition, a second increase from 2 to 2.5 showed a new reduction of about 4.3%, 2.9%, 12.2%, 15.4%, and 7% at 8 M, 10 M, 12 M, 14 M, and 16 M, respectively. The author mentioned that the reductions in compressive strength while increasing the SS/SH ratio were due to the consequent reduction in SH solution and hydroxide ions (OH⁻), which reduces the formation of the three-dimensional network of sodium aluminosilicates hydrate [N-A-S-H] gel (Ghafoor *et al.*, 2021).

2.5.2.3 Alkaline solution to binder ratio

The alkaline hydroxide and alkaline silicate solutions are referred to as alkaline liquids, and the ratio of their sum by mass to the total mass of FA is defined as AL/FA ratio or alkaline liquid to binder ratio (l/b) (Talha Junaid *et al.*, 2015).

Based on the findings of Joseph, and Mathew (2012), it was discovered that as the AL/FA ratio increased up to 0.55, the compressive strength increased, and beyond that, the compressive strength was negatively affected. They reported that the compressive strength results of 39, 47, 58, and 44 MPa were obtained with AL/FA ratios of 0.35, 0.45, 0.55, and 0.65, respectively (Joseph; Mathew, 2012). The improvement in GPC properties as a result of increasing AL/FA ratio were reported in these studies (Ahmed *et al.*, 2021; Aliabdo; Abd Elmoaty; Salem, 2016; Hardjito *et al.*, 2004; Scholar; Ganesh Babu-Professor; Santhanam-Assistant Professor, 2008). The increasing in the alkaline activator content increases the GPC strength because increases the Si species content and the $\text{SiO}_2/\text{Al}_2\text{O}_3$ ratio, resulting in more Si-O-Si bonds which are stronger in comparison with Si-O-Al (Al Bakri, A.M.M. *et al.*, 2012; Aliabdo; Abd Elmoaty; Salem, 2016).

In contrast to the earlier findings, an experimental study by Xie, and Ozbakkaloglu (2015) observed that increasing the AL/FA ratio decreased the compression strength of FA-BGPC. So, at 28 days, the compressive strength of GPC was 18.8, 27.2, and 34.3 MPa, respectively, with AL/FA ratios of 0.5, 0.35, and 0.3. This was attributed to the fact that any increase in the AL/FA ratio leads to decreased friction between the particles due to increased water content in the reaction medium of the GPC mixtures and a reduction in the compressive strength (Ahmed *et al.*, 2021; Xie; Ozbakkaloglu, 2015).

2.5.3 Water Absorption

In this section it will be discussed the effects of the alkaline solution (SH and SS) on microstructural properties of GPC, such as the influence of SH molarity, SS/SH, and AL/FA on water absorption by immersion and capillarity.

In geopolymers, excessive alkali ions in the system leak through the pores and interact with the CO_2 in the atmosphere; this mostly results in the formation of white salt deposits on the surface of samples. This phenomenon is called efflorescence. In general, when it is not excessive, efflorescence does not affect the mechanical performance of the material, but it implies deficiencies in the matrix properties and porosity (Ozcelikci *et al.*, 2023). Zhou *et al.* (2020) reported that efflorescence increased the water absorption of geopolymers due to the deterioration of pore structures caused by the crystallization pressure. Apart from efflorescence, pore structure is likely to be affected by the formation of drying shrinkage and related microcracks increasing the water absorption results (Ozcelikci *et al.*, 2023).

A study carried out by Zaidi et al. (2021) reported the influence of alkali activators ratio on GPC for underwater concreting. The geopolymers were synthesized from FA and kaolin and activated at 1.5, 2.0, 2.5, and 3.0 SS/SH ratios. The results showed that the water absorption percentage decreases as the alkaline activator ratio increases up to 2.5. The lowest water absorption of 0.12% was reported using a 2.5 ratio, while the highest water absorption of 0.41% was achieved using a 1.5 alkaline activator ratio. Lower water absorption is preferred due to its lower porosity. The sample using 2.5 ratios resulted in the highest density (Zaidi *et al.*, 2021). At lower alkaline activator ratios, the workability of the mixture is low, which results in poor bonding between the raw materials and alkaline activators, which increases the possibility of segregation and cement washout during concrete placement, resulting in low strength, density, and water absorption (Ibrahim *et al.*, 2020; Zaidi *et al.*, 2021).

Based on previous study (Aliabdo; Abd Elmoaty; Salem, 2016; Sathonsaowaphak; Chindaprasirt; Pimraksa, 2009b), it may be concluded that the reduction in mechanical properties and the increase in absorption and porosity because of increasing additional water content could be due to the increase of voids resulting from the increase of water content, which has no role in chemical reaction.

The effect of SH solution molarity on 28-day absorption of FA-BGPC was reported by Aliabdo, Abd Elmoaty, and Salem (2016). The SH molarity in this study showed an insignificant role in water absorption, but generally, the increase in molarity from 12 M to 18 M decreases water absorption. From test results, the increase in molarity from 12 M, 16 M, and 18 M decreases water absorption by 5.4% and 1.4%, respectively, compared with the mix with 12 M (Aliabdo; Abd Elmoaty; Salem, 2016). The same study reported the effect of 0.30, 0.35, 0.40, and 0.45 AL/FA ratios on water absorption. The increase in the AL/FA ratio reduced water absorption. The reduction in absorption was 8.6%, 12.2%, and 11.2% for GPC mixes with 0.35, 0.40, and 0.45 AL/FA ratios, respectively, compared with the mix with 0.30 AL/FA ratio (Aliabdo; Abd Elmoaty; Salem, 2016). The same study also reported the effect of the NaOH to Na₂SiO₃ (SH/SS) ratio on GPC absorption. The results showed that an increase in the SH/SS ratio significantly increases water absorption. The increase in absorption was 9.3% and 11.3% for mixes with 0.40 and 0.50 SH/SS ratios, respectively, compared to the mix with 0.30 SH/SS ratio (Aliabdo; Abd Elmoaty; Salem, 2016).

A study synthesized GPC by using FA, SH and SS (Wongkeo; Seekaew; Kaewrahan, 2019). The effects of SH concentration at 7.5, 10 and 12.5 M, SS/SH ratio at 1, 1.5 and 2, and AL/FA ratio at 0.50 on pore morphology and water absorption were investigated. The pore morphology was studied by using photograph and the pore diameters were in the range of 1 – 5 mm approximately. It was found that the increase of SH concentration enlarges the pore size of the samples. GPC using SH at 7.5 M showed the finer pore than the other mixtures. When increasing SH concentration, the hydrogen gas is violent and macropores are formed inside the sample. In addition, the water absorption of GPC was in the range of 22 to 30%. The water absorption increased as the SH concentration increased. The less pore structure of GPC was observed at SS/SH ratio of 2, resulting in sample dense. It was indicated that the increase of SS/SH ratio obstructs the pore formation. Similarly, water absorption decreased with increasing SS/SH ratio. Also, when increasing SS/SH, small pore size and less pore connection were formed. It was concluded that the pore structure had a significant role on the water absorption of GPC. Regarding the authors, the water absorption is the measurement of the ability of sample to absorb water by pore structure, which can be related to the pore volume of sample. In practice, pore structure including pore connection and pore size of each sample cannot be controlled to equivalent achieve, even though it is the same condition (Wongkeo; Seekaew; Kaewrahan, 2019).

In the study by Abdullah et al. (2012) was produced lightweight GPC mixing FA with a mixture of SS and SH as alkaline activator solution. The water absorption, porosity, chemical composition, microstructure, X-ray Diffraction, Fourier Transform Infrared Spectroscopy, and Scanning Electron Microscope analyses were studied. The samples were cured at room temperature (LW1) and heat cured at 60 °C (LW2). The compressive strength of the LW2 samples was greater than the compressive strength of the LW1 samples. This was attributed to the fact that the porosity and water absorption of the LW2 samples, at 6.78% and 1.22% respectively, were lower than the porosity and water absorption of the LW1 samples, at 15.29% and 2.35%, respectively. The SEM showed that LW2 had a denser matrix than LW1, because heat cured increased the rate of geopolymerization and hence, increased the strength. However, for LW1, microcrack were present on the surface, which increased water absorption and porosity, thus strength was reduced (Abdullah *et al.*, 2012).

The study by Shahedan et al. (2021) obtained water absorption percentage of GPC using FA around 3.5 – 4%. The water absorption was increased with increasing placement of glass bubble in GPC but remained within a comparable percentage of 3 – 6.5% of standard concrete (Shahedan *et al.*, 2021).

This investigation by Ojha, and Aggarwal (2023) manufactured FA-BGPC using SH of 14 M, SS/SH ratio of 2.5, and AL/FA ratio of 0.55. The concrete samples were subjected to water absorption, water permeability, sorptivity, acid resistance, sulphate resistance, and rapid chloride penetration tests. Water absorption findings revealed less water absorption by GPC than OPC. The water absorption study was conducted as per ASTM C 642 (2006), and the tests were performed on three different cubic samples of 150 mm dimensions for FA-BGPC and OPC concrete. The average weight gain for FA-BGPC was 1.409% and for OPC was 1.428%. Higher water absorption rates of OPC concrete may be attributed to the existence of larger voids in the concrete, whereas lower values of water absorption of FA-BGPC may be ascribed to the formation of a more compact microstructure (polymerization process develops a three-dimensional network that fills the voids) leading to the fewer vacancies. In addition, the water permeability test was performed in accordance with DIN 1048 part 5 (1996). For FA-BGPC samples, the maximum water penetration under pressure was found to be 39 mm, compared to 45 mm for OPC concrete. Compared to OPC, low pore interconnectivity in the GPC matrix may be attributed to the formation of dense microstructure leading to low water permeability (Ojha; Aggarwal, 2023). These water absorption studies reported similar findings (Hannanee Ahmad Zaidi *et al.*, 2019; Lavanya; Jegan, 2015; Luhar; Khandelwal, 2015).

A study by Hannanee Ahmad Zaidi et al. (2019) analyzed the performance of GPC when exposed to marine environment. Based on the results, it is identified that the water absorption of GPC is lower than of OPC concrete, which obtained 4.58% and 11.33%, respectively. The author mentioned that water absorption with value ranged 3 – 5% is classified as “average” concrete, and above 6% is classified as “bad” concrete. Low water absorption is a good indicator that there is limited open porosity that can inhibit high flow of water into the concrete. Since OPC concrete is a water-based concrete, it is expected that it will absorb more water than GPC (Hannanee Ahmad Zaidi *et al.*, 2019). However, there is studies where OPC concrete had a lower water absorption rate than fly ash geopolymer concretes (Albitar *et al.*, 2017).

The study by Lavanya, and Jegan (2015) presents an investigation of FA-BGPC measuring water absorption and sorptivity. It was used a combination of SH and SS as alkaline activator with the ratio of 2.5. The SH molarity was fixed as 12 M. The water absorption results were in the range of approximately 1 – 3%. From test results, the increase in water absorption indicated the presence of higher void content due to incomplete process of geopolymerization. The lower water absorption was observed in GPC compared to OPC concrete. The presence of higher silica content formed higher quantity of aluminosilicate gel and provides very good interparticle bonding. Hence, the silicate occupies the void spaces between the fly ash particles resulting in lower water absorption (Lavanya; Jegan, 2015).

3 OBJECTIVES

3.1 General Objective

This study aims to develop FA-BGPC in the laboratory to achieve maximum compressive strength under a controlled temperature of 25 °C and $90 \pm 10\%$ relative humidity curing conditions. Additionally, the study includes testing for flexural strength, water absorption through capillarity and immersion, and a comparison of the results with a reference composition employing OPC.

3.2 Specific Objectives

The specific objectives of this research are to:

- I. Characterize the FA and aggregates;
- II. Developing a Design of Experiment for the optimized production of GPC;
- III. Determine a production methodology for GPC based on the literature;
- IV. Produce FA-BGPC and a reference composition using OPC;
- V. Preliminary tests: compressive and flexural strength in prismatic molds;
- VI. Final tests: compressive strength and water absorption tests by immersion and capillarity in cubic molds;
- VII. Compare results according to the literature.

4 MATERIALS AND METHODS

4.1 Materials

The reactants used in this work are described below.

- FA provided by Central Termoelétrica Pego – Abrantes;
- SH pearls (98%) provided by Labkem;
- SS ($\text{Na}_2\text{O} = 10.6\%$ and $\text{SiO}_2 = 26.5\%$), provided by Fisher Chemical;
- Sand provided by David & Nuno SA.;
- Gravel provided by Nordeste Betão Lda.;
- Portland Cement CEM II/B-L 32.5N provided by Secil;
- Distilled water.

The chemical composition of FA is presented in Table 1. A mixture of SH and SS solutions was used as the activator solution. SH solution of concentrations 4 M, 10 M, and 16 M were prepared by mixing 98% pure NaOH pearls with distilled water (86.17%, 71.37%, and 60.91% water by mass, respectively). The mass ratio of SiO_2 to Na_2O of the SS was 2.50 with chemical compositions of 26.5% SiO_2 , 10.6% Na_2O and 62.9% water. The fine and coarse aggregates used have nominal maximum sizes as indicated in APPENDIX A and APPENDIX B, respectively, adapted from a particle analysis of gravel and sand carried out in previous work at IPB (Vinício Tiozzi Schincaglia, 2022) meeting the European Standard specifications (European Standard; European Committee for Standardization, 2003b, 2014). Several authors have used the aggregates in saturated surface dry (SSD) conditions (Deb; Nath; Sarker, 2014; Nath; Sarker, 2014). However, fine, and coarse aggregates were used in dry condition after 24 hours in an oven at 105 °C.

Table 1 - Chemical characterization of the FA.

Sample	Fly Ash (%)
Ca	27.47
Si	12.17
Al	9.60
K	2.92
Fe	2.10
Mg	1.87
Zn	0.43
Cu	0.15
Mn	0.08
Total	56.79
g/g	100 g

Source: Author (2024).

4.2 Design of Experiments

A Design of Experiment (DOE) has been employed in the present study to optimize the synthesis of FA-BGPC. The design matrix was composed by a combination of three levels (-1, 0, +1) for three selected variables. It means that each factor is tested at low, medium, and high component levels, respectively. Maximum and minimum limits found in the literature were used in the DOE to expand the realm of possibilities involving the production of GPC.

It was carried out a preliminary research based on FA-BGPC papers to select three experimental variables and their levels to use in the DOE. This study adopted Web of Science as its main source of data. The keyword used for the initial search was “geopolymer”. To extract relevant documents and data, it was used the quick filter “highly cited papers”. This search resulted in 133 results. However, 73 documents were opened one by one to be carefully analyzed. The abstracts for each document were read to ensure that the papers fall within the research of geopolymer. Several studies using different precursors appeared in the search, such as papers about geopolymer concrete, mortars, pastes, mix design procedures, and study reviews.

All 73 documents were downloaded and read to get an overview of the geopolymer topic. Then, the documents were filtered to get closer to the main objective of the work. Firstly, the documents were filtered to “geopolymer concrete”. After removing 35 files about mortars, pastes, and binders, 38 documents were left. Secondly, the documents were filtered to “production of fly ash-based geopolymer concrete” and

“production of blended fly ash-based geopolymer concrete”. This second filter removed 5 files about mix design procedures and study reviews. From the 33 papers left, the three variables and their ratio were chosen to be used in the DOE. Regarding the selection of the variables, the objective was to select the three main variables that could affect the compressive strength of FA-BGPC. It was noticed that some of the variables selected could be:

- Si/Al ratio of FA;
- AL/FA;
- Superplasticizer dosage and extra water;
- FA content;
- Aggregate content;
- SS/SH;
- SH molar concentration (M);
- Curing conditions and curing ages;

Among all parameters found in the literature, three were selected as the core of the work: SH molarity, SS/SH ratio, and AL/FA ratio. Following, Table 2 presents a summary of noteworthy studies of FA-BGPC found in the literature that were used to select the range of the three variables chosen to be used in the DOE.

Table 2 - Summary of previous studies of GPC.

Research Study	Precursor	Variables Investigated			Curing	Compression Strength (MPa)
		SH Molarity	SS/SH	AL/FA		
(Nath; Sarker, 2014)	FA, GGBFS	14M	1.5, 2.0, 2.5	0.35, 0.40, 0.45	Controlled temperature of 20–23 °C and 65 ± 5% relative humidity	25
(Deb; Nath; Sarker, 2014)	FA, GGBFS	14M	1.5, 2.5	0.35, 0.40	Ambient condition at 20 ± 2 °C and 70 ± 10% relative humidity	27
(Ramujee; PothaRaju, 2017)	FA	8M, 16M	2.0, 2.5	0.35, 0.40, 0.50	Heat cured at 60 °C for 24 h	31
(Ghafoor <i>et al.</i> , 2021)	FA	8M, 10M, 12M, 14M, 16M	1.5, 2.0, 2.5	0.40, 0.50, 0.60	Room temperature of 23 ± 2 °C	21.5
(Nath; Sarker, 2017)	FA, GGBFS, OPC	14M	2.5	0.35, 0.40	Room temperature of 18-23 °C and 70 ± 10% relative humidity	25.6
(Karthik; Sudalaimani; Vijaya Kumar, 2017)	FA, GGBFS	4M, 8M	2.5	0.45	Ambient condition at 30 ± 2 °C and relative humidity of 65 ± 5%	28.4
(Pavithra <i>et al.</i> , 2016)	FA	16M	1.5	0.40, 0.50, 0.60, 0.70, 0.80	Oven at 60 °C for 24 h	38.7

Source: Author (2024).

Regarding the papers mentioned in Table 2, while some researchers have produced combinations of FA with other materials like GGBFS (Deb; Nath; Sarker, 2014; Nath; Sarker, 2014, 2017) and OPC (Nath; Sarker, 2017) as precursors in GPC, this work exclusively produces fly ash-based precursors. Also, some researchers used heat-cured conditions above 60 °C (Pavithra *et al.*, 2016; Ramujee; PothaRaju, 2017), but this work only used curing under a controlled temperature of 25 °C. Nevertheless, all these studies were analyzed in this preliminary research.

In advance of creating the DOE, the three parameters chosen were selected in a range to use and define each mixture composition. Regarding Table 2, these 7 studies were selected from the 33 papers filtered previously because they represent the maximum and minimum limits of the three variables chosen. So, the NaOH molarity was defined in the range from 4 M to 16 M, the SS/SH from 1.5 to 2.5, and AL/FA from 0.35 to 0.70. The AL/FA ratio of 0.80 from the study of Pavithra *et al.* (Pavithra *et al.*, 2016) wasn't used in this analysis because the authors reported collapse in the slump test due high content of water in the mixture. Each factor was tested at three levels of component content, high (1), medium (0), and low (-1). Table 3 shows the ranges and experimental

values of the independent variables that were considered for the design (Ana Paula Silva Natal, 2023).

Table 3 - Experimental variables and their levels used in the DOE.

Factor	Original Factor (x)	Levels		
		-1	0	1
SH (M)	x ₁	4	10	16
SS/SH	x ₂	1.5	2.0	2.5
AL/FA	x ₃	0.35	0.525	0.70

Source: Author (2024).

The design was created using Minitab 16 Statistical software, which was only used for design conception. Then, fifteen geopolymer experiments were synthesized using the DOE approach to start the laboratory activities of FA-BGPC production. The parameters not analyzed in this study were kept constant. Table 4 displays the experimental design matrix used in the work.

Table 4 - Design of Experiments.

Experiment			Coded Factors			SH (M)	SS/SH	AL/FA
Logical	Random	Mix ID	x1	x2	x3			
1	6	GP1	1	0	-1	16	2	0.35
2	5	GP2	-1	0	-1	4	2	0.35
3	14	GP3	0	0	0	10	2	0.525
4	3	GP4	-1	1	0	4	2.5	0.525
5	9	GP5	0	-1	-1	10	1.5	0.35
6	1	GP6	-1	-1	0	4	1.5	0.525
7	12	GP7	0	1	1	10	2.5	0.70
8	8	GP8	1	0	1	16	2	0.70
9	7	GP9	-1	0	1	4	2	0.70
10	2	GP10	1	-1	0	16	1.5	0.525
11	11	GP11	0	-1	1	10	1.5	0.70
12	13	GP12	0	0	0	10	2	0.525
13	10	GP13	0	1	-1	10	2.5	0.35
14	15	GP14	0	0	0	10	2	0.525
15	4	GP15	1	1	0	16	2.5	0.525

Source: Author (2024).

4.3 Mixture proportions

The fifteen experiments presented in the DOE (Table 4) were used to produce fifteen compositions of geopolymer concrete. However, the experiments 3, 12 and 14 are the three center nodes, which means these experiments present the same factors. The DOE

provides the parameters of the activator solution, which is the ratio and molarity of SH and SS, but it doesn't provide the quantity of FA/cement, coarse and fine aggregates to produce geopolymer concrete. These mixture parameters, such as quantity of FA and aggregates were included in the literature research on geopolymer concrete before starting laboratory activities, but they weren't considered as factors in the DOE.

The mixture quantities are usually in SSD condition of the aggregates. Although when aggregates are either dry, partially dry, or moist, the water and aggregate adjustments need to be done similar to the practice in OPC. Once the values of all constituents are determined, a final volume check is performed, and fine adjustments can be made (Talha Junaid *et al.*, 2015). The workability of the samples wasn't measured. From laboratory tests, mixes produced using higher volume of alkaline solution presented higher workability, compared to those mixes produced using lower volume of alkaline solution. In general, it was observed that the workability of GPC was similar to the workability of OPC concrete.

In this study, the aggregates were used in dry conditions, and trial mixtures were tested to adjust the water content in the mix using GP9 (Table 4) as a reference. It wasn't performed final volume check and fine adjustments in the proportions and volume of the total aggregates. FA, coarse, and fine aggregates were fixed in all geopolymers according to reference compositions found in the literature. The final unit weight of the GPC was varied according to the amount of alkaline solution and the addition of water. However, these studies suggest the development of a mixed design procedure for FA-BGPC where adjustments using specific gravity of the materials, proportion and volume of aggregates, and density variability were done (Pavithra *et al.*, 2016; Talha Junaid *et al.*, 2015).

GP9 is the geopolymer mix with the highest water content, because this composition has 0.70 AL/FA and 4 M. This composition was expected to present the lowest addition of water, compared to other geopolymers. From laboratory tests, GP9 mix achieved good workability without any extra water. For this reason, this composition was used as a reference to keep a similar amount of water in all geopolymer mixes. Similarly to OPC concrete, it is possible to calculate the water content, or the addition of water required to achieve a specific water ratio in geopolymer concrete. From geopolymer literature, several studies (Nath; Sarker, 2014; Pavithra *et al.*, 2016; Ramujee; PothaRaju, 2017; Talha Junaid *et al.*, 2015) suggest the utilization of the equation (1) to calculate the water to geopolymer solids ratio by weight (W/GPS). So, this equation was employed in

this study to calculate the addition of water in geopolymers. Where, W_{OH} is the water content in the hydroxide solution, W_{Si} is the water content in the silicate solution, W_{free} is any extra water added, $Solids_{OH}$ is the solid content in the hydroxide solution, and $Solids_{Si}$ is the solid content in the silicate solution. Using the equation (1), considering trial mixtures using 350 kg/m^3 and 400 kg/m^3 of FA and no extra water added, GP9 mix achieved 0.41 W/GPS ratio. Then, this ratio was fixed to all geopolymers produced. It was reported in this study (Pavithra *et al.*, 2016) the utilization of 0.37 W/GPS ratio, which also was used high ratio of alkaline solutions, such as 0.60 and 0.70 for FA-BGPC production. The required amount of water for each geopolymer mix was calculated according to the equation (1).

$$\frac{W_{free} + W_{OH} + W_{Si}}{FA + Solids_{OH} + Solids_{Si}} = \frac{W}{GPS} \quad (1)$$

This study was divided into two parts. First, preliminary tests were conducted to evaluate the mechanical properties of FA-BGPC. Then, final tests were carried out with a focus on the best geopolymers from the preliminary tests. The mixture proportion, the molds, and the tests weren't the same in the preliminary and final tests. The reference mixture proportion used in the preliminary and final tests will be presented next, whereas the molds and tests will be furthered in the following topics.

In the preliminary tests, a reference mixture proportion of concrete was used from previous studies carried out at IPB regarding concrete blocks incorporating diatomaceous earth (Vinicio Tiozzi Schincaglia, 2022). This reference mixture proportion of concrete is outlined below in Table 5.

Table 5 - Reference mixture proportion in the preliminary tests.

Designation	Preliminary tests - Reference mixture proportion (kg/m ³)			
	Cement	Coarse Agg.	Fine Agg.	H ₂ O
Reference Composition	350.00	1010.06	804.35	218.50

Source: Adapted from Vinicio Tiozzi Schincaglia (2022).

Then, using the reference mixture proportion (Table 5) and the DOE presented previously combined (Table 4), the mixture proportions of FA-BGPC produced in the preliminary tests are presented in Table 6. The designation of GP means the mix number, SH molarity, SS/SH ratio, and the AL/FA ratio, respectively. Only REF-OPC was

produced using Portland cement at 0.62 water to cement ratio (a/c). All geopolymers were produced using only FA as a precursor at a 0.41 W/GPS ratio. It was used the same quantity of cement and FA by mass following the reference mixture in Table 5.

Table 6 - Mixture proportions in the preliminary tests.

Designation	Preliminary tests - Concrete mixture quantity (kg/m ³)						
	FA	Coarse Agg.	Fine Agg.	SS	SH	H ₂ O	W/GPS
GP1-16-2.0-0.35				81.67	40.83	86.36	
GP2-4-2.0-0.35				81.67	40.83	71.81	
GP3-10-2.0-0.525				122.50	61.25	48.69	
GP4-4-2.5-0.525				131.25	52.50	38.78	
GP5-10-1.5-0.35				73.50	49.00	79.36	
GP6-4-1.5-0.525				110.25	73.50	31.88	
GP7-10-2.5-0.70				175.00	70.00	18.44	
GP8-16-2.0-0.70	350	1010.06	804.35	163.33	81.67	29.10	0.41
GP9-4-2.0-0.70				163.33	81.67	0.00	
GP10-16-1.5-0.525				110.25	73.50	58.07	
GP11-10-1.5-0.70				147.00	98.00	15.10	
GP12-10-2.0-0.525				122.50	61.25	48.69	
GP13-10-2.5-0.35				87.50	35.00	81.03	
GP14-10-2.0-0.525				122.50	61.25	48.69	
GP15-16-2.5-0.525				131.25	52.50	57.48	

Source: Author (2024).

In the final tests, the reference mixture proportion was changed based on previous work exclusively on GPC (Nath; Sarker, 2014). The quantity of FA, sand, and gravel was changed from 350.00 kg/m³ to 400.00 kg/m³, from 804.35 kg/m³ to 651.00 kg/m³, and from 1010.06 kg/m³ to 1209.00 kg/m³, respectively. Also, according to this reference mixture proportion, the alkali solution is the only water source; no extra water or superplasticizer was added. However, trial mixes carried out at the laboratory required the addition of water to achieve minimum workability. Then, similarly to the preliminary tests, extra water was added in the final tests. These studies reported using extra water (Nath; Sarker, 2017) and superplasticizers (Nath; Sarker, 2017; Pavithra *et al.*, 2016) to improve workability of GPC. Several authors reported that similar mixture proportions achieved higher compressive strength in GPC (Deb; Nath; Sarker, 2014; Ghafoor *et al.*, 2021; Nath; Sarker, 2014, 2017; Ramujee; PothaRaju, 2017). The reference mixture proportion used in the final tests is presented in the Table 7:

Table 7 - Reference mixture proportion in the final tests.

Designation	Final tests - Reference mixture proportion (kg/m ³)		
	FA	Coarse Agg.	Fine Agg.
Reference Composition	400.00	1209.00	651.00

Source: Author (2024).

The quantity of alkali solution depends on the quantity of FA in the binder. Once the quantity of FA is changed, the quantity of alkali solution is also changed. The higher the amount of FA, the higher the alkali solution amount. So, the mixture proportions of GPC produced in the final tests are presented in the Table 8. In the same way, the designation of GP means the mix number, SH molarity, SS/SH ratio, and the AL/FA ratio, respectively. Also, REF and GPC were produced at the same water ratios of preliminary tests, which is 0.62 and 0.41, respectively.

Table 8 - Mixture proportions in the final tests.

Designation	Final tests - Concrete mixture quantity (kg/m ³)						
	FA	Coarse Agg.	Fine Agg.	SS	SH	H ₂ O	W/GPS
GP1-16-2.0-0.35				93.33	46.67	98.69	
GP2-4-2.0-0.35				93.33	46.67	82.06	
GP3-10-2.0-0.525				140.00	70.00	55.65	
GP4-4-2.5-0.525				150.00	60.00	44.31	
GP5-10-1.5-0.35				84.00	56.00	90.69	
GP6-4-1.5-0.525				126.00	84.00	36.44	
GP7-10-2.5-0.70				200.00	80.00	21.08	
GP8-16-2.0-0.70	400	1209	651	186.67	93.33	33.26	0.41
GP9-4-2.0-0.70				186.67	93.33	0.00	
GP10-16-1.5-0.525				126.00	84.00	66.37	
GP11-10-1.5-0.70				168.00	112.00	17.26	
GP12-10-2.0-0.525				140.00	70.00	55.65	
GP13-10-2.5-0.35				100.00	40.00	92.60	
GP14-10-2.0-0.525				140.00	70.00	55.65	
GP15-16-2.5-0.525				150.00	60.00	65.69	

Source: Author (2024).

Studies suggest that GPC has final unit weight of 2420 kg/m³ (Deb; Nath; Sarker, 2014; Nath; Sarker, 2014, 2017); 2400 kg/m³ (Ghafoor *et al.*, 2021; Pavithra *et al.*, 2016). As is the case with OPC concrete, total aggregates make up 70% (Joseph; Mathew, 2012); 75% (Talha Junaid *et al.*, 2015); 80% (Pavithra *et al.*, 2016); from 74% to 82% (Chithambaram *et al.*, 2018b); of the mass of GPC while the percentage of fines may be taken as about 30% (Karthik; Sudalaimani; Vijaya Kumar, 2017; Talha Junaid *et al.*, 2015)

or 35% (Ahmed *et al.*, 2021; Deb; Nath; Sarker, 2014; Joseph; Mathew, 2012; Nath; Sarker, 2014) of the total aggregates. The final unit weight of the GPC was varied according to the amount of alkaline solution and the addition of water. Geopolymers that were produced with higher quantity of alkaline solution will have higher final unit weight, even having the same W/GPS ratio compared to other geopolymers. It happens because any addition in a mass of extra water only increases the water content in the mixture, whereas as part of the alkaline solution is composed of solids, any addition in a mass of the alkaline solution increases the water content and the solids content. Increasing the mixture's water and solids content reduces the variation of W/GPS ratio. In other words, the same addition in mass of alkaline solution results in higher final unit weight and lower increase in W/GPS, compared to only water addition. As can be seen in Table 9, the final unit weight of GPC was slightly lower in the preliminary tests, and slightly higher in the final tests, compared to the literature 2420 kg/m³ (Deb; Nath; Sarker, 2014; Nath; Sarker, 2014, 2017); 2400 kg/m³ (Ghafoor *et al.*, 2021; Pavithra *et al.*, 2016). The variation of the final unit weight could be resolved through fine adjustments in the proportions and volume of the total aggregates in the mixtures. Altering the values of FA, AL/FA ratio or water may have significant effect on the strength (Talha Junaid *et al.*, 2015). The total aggregates were between 72% and 77% of the mass of GPC, while the final combined aggregate volume was a combination of 44% of fine aggregate and 56% of coarse aggregates (Vinicio Tiozzi Schincaglia, 2022), and 35% fine aggregate and 65% of coarse aggregates (Deb; Nath; Sarker, 2014) in the preliminary and final tests, respectively. In this study review of FA-BGPC (Ahmed *et al.*, 2021), the optimum fine aggregate to the total aggregate was 35% (Joseph; Mathew, 2012). Also, the optimum total aggregate content was 78%, higher content declined compressive strength of FA-BGPC due to insufficient binding material for holding the aggregates together (Chithambaram *et al.*, 2018b). As a result, a limit proportion of fine aggregate and total aggregate content for a given type of coarse and fine aggregate produces the best compressive strength for the FA-BGPC (Ahmed *et al.*, 2021).

Table 9 - Final unit weight of concrete.

Designation	Preliminary tests		Final tests	
	Unit weight (kg/m ³)	Agg. Cont./Total mass (%)	Unit weight (kg/m ³)	Agg. Cont./Total mass (%)
REF-OPC	2382.91	0.76	2509.71	0.74
GP1-16-2.0-0.35	2373.27	0.76	2498.70	0.74
GP2-4-2.0-0.35	2358.64	0.77	2481.98	0.75
GP3-10-2.0-0.525	2396.86	0.76	2525.66	0.74
GP4-4-2.5-0.525	2386.87	0.76	2514.23	0.74
GP5-10-1.5-0.35	2366.26	0.77	2490.68	0.75
GP6-4-1.5-0.525	2380.00	0.76	2506.39	0.74
GP7-10-2.5-0.70	2427.88	0.75	2561.11	0.73
GP8-16-2.0-0.70	2438.64	0.74	2573.40	0.72
GP9-4-2.0-0.70	2409.41	0.75	2540.00	0.73
GP10-16-1.5-0.525	2406.34	0.75	2536.49	0.73
GP11-10-1.5-0.70	2424.60	0.75	2557.37	0.73
GP12-10-2.0-0.525	2396.86	0.76	2525.66	0.74
GP13-10-2.5-0.35	2367.90	0.77	2492.55	0.75
GP14-10-2.0-0.525	2396.86	0.76	2525.66	0.74
GP15-16-2.5-0.525	2405.68	0.75	2535.74	0.73

Source: Author (2024).

4.4 Mixing, sample preparation, and curing

The sodium hydroxide solution of the desired concentration (4 M, 10 M, 16 M) was prepared 24 hours earlier to ensure the complete dissolution in distilled water. The NaOH pearls were weighed using an analytical balance, and then the solution was prepared by mixing the pearls in distilled water for 15 min in a magnetic stirrer. After 24 hours, the SS and SH solutions were mixed for 10 min in the magnetic stirrer for 30 min before mixing with other ingredients to enhance the reactivity of the solution. The coarse and fine aggregates and FA were weighed (Figure 3) and dry-mixed in a laboratory pan for 1 min. Then, the alkali solution was added to the mixer for 2 more minutes. Finally, the extra water was gradually added for 2 – 5 minutes until uniform consistency was achieved. The amount of extra water was registered for each composition.

Figure 3 - Fly ash, sand, gravel, and distilled water weighed.



Source: Author (2024).

In the initial tests, 160 x 40 x 40 mm dimensions acrylic molds were filled with geopolymer concrete in one layer and compacted on a vibrating table for 2 min. An elastic around the prismatic molds was used to avoid material loss between the faces of the molds, as presented in Figure 4.

Figure 4 - (a) Acrylic molds (b) Prismatic molds filled with geopolymer concrete.



a)

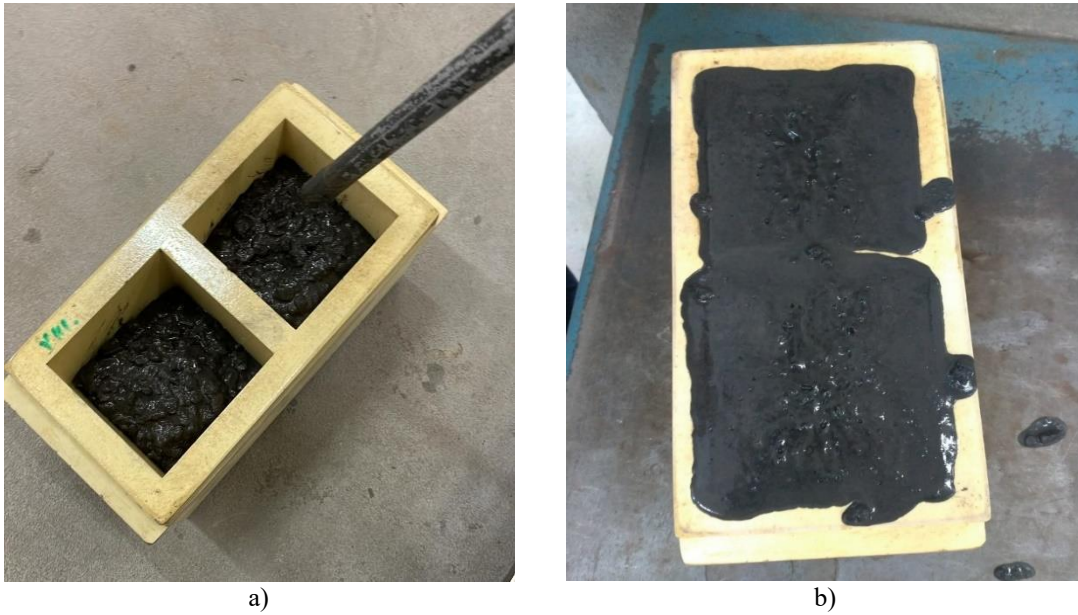


b)

Source: Author (2024).

Meanwhile, in the final tests, cubic molds of 100 mm dimensions were compacted into 2 layers; in this case, the first layer was compacted with 25 strokes using a metal rod, and the second layer on a vibrating table for 2 min (Figure 5).

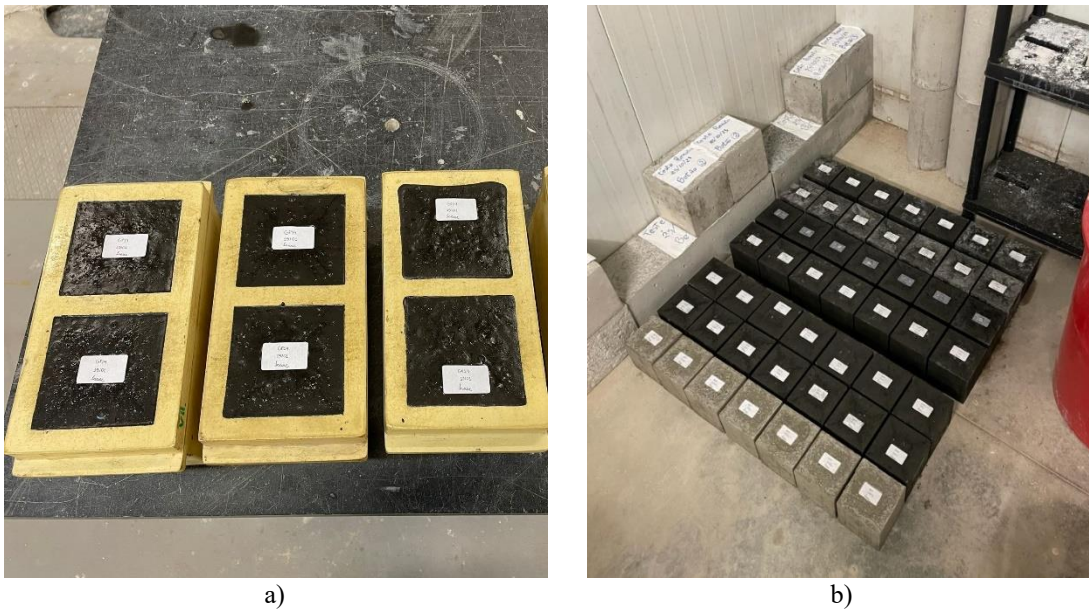
Figure 5 - (a) Compaction of the first layer (b) Fresh concrete at the vibrating table.



Source: Author (2024).

The molds were then cured in a chamber with a controlled temperature of 25 °C and 90 ± 10 % relative humidity for 28 days. The samples were de-molded 48 hours after casting using a compressed-air pistol and remained inside the chamber in the same temperature and humidity conditions until being tested at 28 days (Figure 6).

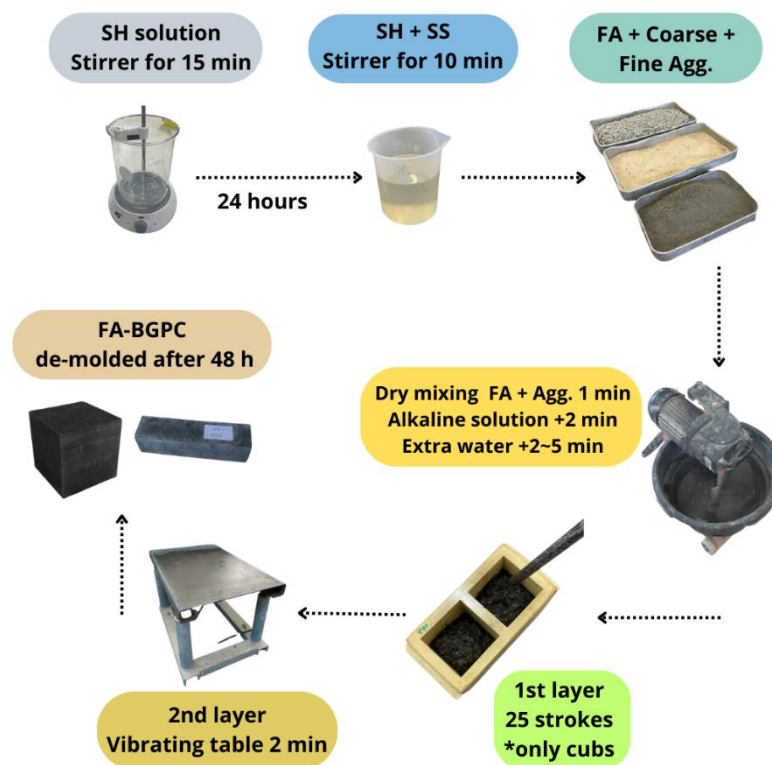
Figure 6 - (a) Cubic molds filled with GPC (b) GPC storage inside the chamber.



Source: Author (2024).

The mixing procedure adopted in this study is summarized in Figure 7. Similar mixing procedures were reported in these studies (Ghafoor *et al.*, 2021; Ramujee; PothaRaju, 2017).

Figure 7 - Simplified FA-BGPC mixing procedure.



Source: Author (2024).

4.5 Experimental tests

4.5.1 Preliminary tests - Flexural and compressive strength testing in prismatic molds

In the preliminary tests, three samples were made and cast in prismatic molds for each of the fifteen geopolymers concrete compositions and the cement reference composition. The concrete standard EN 12390-1 (2003) requires a minimum dimension of the prismatic mold of 100 mm. However, in order to reduce the quantity of materials spent in this preliminary test, the samples were cast into prismatic molds of 40 x 40 x 160 mm dimensions and tested for flexural and compressive strength, respectively, following the standard of cement NP EN 196-1 (2006). The samples were tested at the age of 28 days and removed from the humidity chamber 24 hours before being tested to avoid

excess moisture. Accordingly, the standard for the same sample is tested for flexural strength, and then the two remaining parts are tested for compressive strength. So, it means each specimen provides one result from flexural strength and two results from compressive strength. All the prismatic samples were weighed and measured at the beginning of the initial tests. Due to the weakness of the acrylic molds, even using elastic bands around the mold, some samples lost material during compaction through the mold connections. Also, some molds could not support the weight of the GPC and became deformed after compaction in the vibration table. So, taking this into account, some samples presented less weight and irregular dimensions.

Regarding the test procedure, the prism is first placed in the testing machine between the three supporting rollers, one at the top of the mold and the other at the bottom (Figure 8). The distance between the two supports is 100 ± 0.5 mm. The load is applied vertically in the middle of the specimen at the rate of 50 ± 10 N/s until fracture. The flexural strength is calculated from the equation (2), which was taken from the European Standard (2006):

$$R_f = \frac{1.5 \times F_f \times l}{b^3} \quad (2)$$

Where:

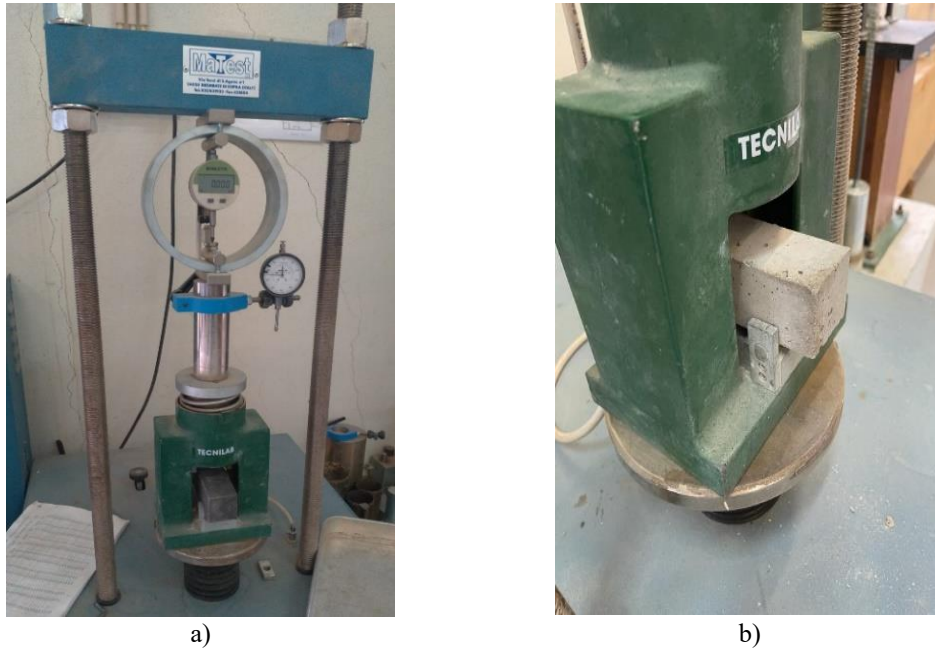
R_f = Flexural Strength [MPa]

F = Maximum load [N]

l = Distance between the bottom supports [mm]

b = side of square section [mm]

Figure 8 - (a) Flexural Strength machine (b) Prismatic mold placed in the machine.



Source: Author (2024).

After the flexural strength test, the prism halves are tested for compression strength. The center of the prism halves is placed between 40 x 40 mm platens of hard steel, and the load is increased at 2400 ± 200 N/s until fracture of the specimen (Figure 9). The compressive strength is calculated from the equation (3), which was taken from the European Standard (2006):

$$R_c = \frac{F_c}{1600} \quad (3)$$

Where:

R_c = Compressive strength [MPa]

F_c = Maximum load at fracture [N]

1600 = section area = area of the platens (40 mm x 40 mm = 1600 mm²) [mm²]

Figure 9 - Compressive strength prismatic molds.



Source: Author (2024).

The final test results are defined as the arithmetic mean of the three flexural strength determinations and the six compressive strength determinations conducted on a set of three prisms for each of the fifteen geopolymer concrete compositions and for the reference composition of cement.

4.5.2 Final tests

In the final tests were made 2 samples in cubic molds of 100 mm dimensions for each geopolymer and cement composition to be tested for water absorption through capillarity and immersion tests. The determination of water absorption through capillarity and immersion was carried out following the standards from the National Laboratory of Civil Engineering, LNEC E 393 (1993), and LNEC E 394 (1993), respectively. These standards recommend that specimens age of at least 28 days. In addition, for the seven highest average compressive strength compositions from the initial tests were made three more samples in cubic molds to being tested at the age of 28 days for compressive strength following the standard NP EN 12390-3 (2009).

4.5.2.1 Capillarity Water Absorption Tests

The water absorption tests through capillarity were carried out following the standard LNEC E 393 (1993). The standard recommends that specimens be placed in an oven for fourteen days at 40 ± 5 °C to ensure complete moisture removal. Conversely, it is allowed to adopt other strategies since the information is recorded in the report and applied similarly to all samples. Then, the strategy adopted in this study was to remove the specimen from the humidity chamber 24 hours before the test, which is the same procedure for the flexural and compressive strength tests.

The initial step was to record the initial mass of the specimens and place them in a straight tray. The bottom of the tray must have support, which are not specified in the standard LNEC E 393 (1993), but they are essential not to allow contact between the specimen and the tray to keep the flow of the water. For this reason, two plastic pipes were used for each sample. After that, the tray was filled with water until the height of 5 ± 1 mm using a metal ruler (Figure 10). The standard recommends the utilization of a desiccator dryer vacuum to cover the specimens to avoid water loss; nevertheless, there was not enough equipment for all samples, so it was not utilized, and the samples were left to the air at room temperature of 17.5 °C and 54% relative humidity during all measurements of the test.

Figure 10 - Capillarity test.



Source: Author (2024).

After the beginning of the test, the weight of the specimens was registered at 3, 6, 24, 48, and 72 hours. Before measuring the weight, the specimen was placed on a non-absorbent balcony for 60 ± 5 s to remove the excess water, and then the specimen returned

to the tray until the next measurement of the test. The water absorption through capillarity is defined by the equation (4), as indicated in the standard LNEC E 393 (1993):

$$A_i = \frac{M_i - M_0}{10.000} \quad (4)$$

Where:

A_i = Water absorption in a specific time [g/mm²]

M_i = Mass in a specific time[g]

M_0 = Initial mass of the specimen [g]

10.000 = Section area (100 x 100 mm = 10.000 mm²) [mm²]

4.5.2.2 Immersion Water Absorption Tests

The water absorption tests by immersion were carried out following the standard LNEC E 394 (1993). The specimens must be placed in a container and filled with water at 20 ± 3 °C until saturated mass. The procedure is divided into three parts with breaks of 1 hour. So, at the beginning of the test, the container is filled up to 1/3 of the specimen's height, then 1 hour later up to 2/3, and more 1 hour up to a maximum of 20 mm above the surface of the specimen. The container was marked outside using a green pen at the height of the three levels of water, as represented in the figures Figure 11 and Figure 12:

Figure 11 - (a) GP4, GP5, and GP6 (b) cement reference composition underwater.



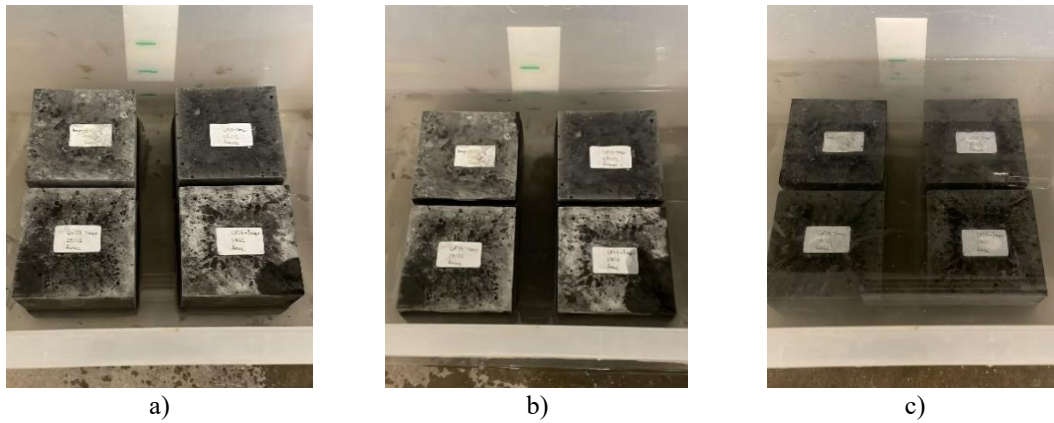
a)



b)

Source: Author (2024).

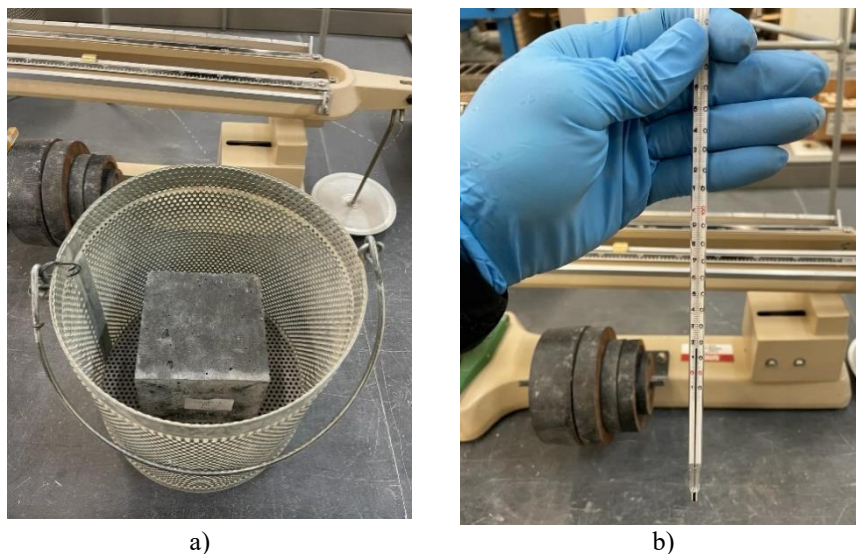
Figure 12 - (a) First, (b) second and (c) third layer of water, respectively.



Source: Author (2024).

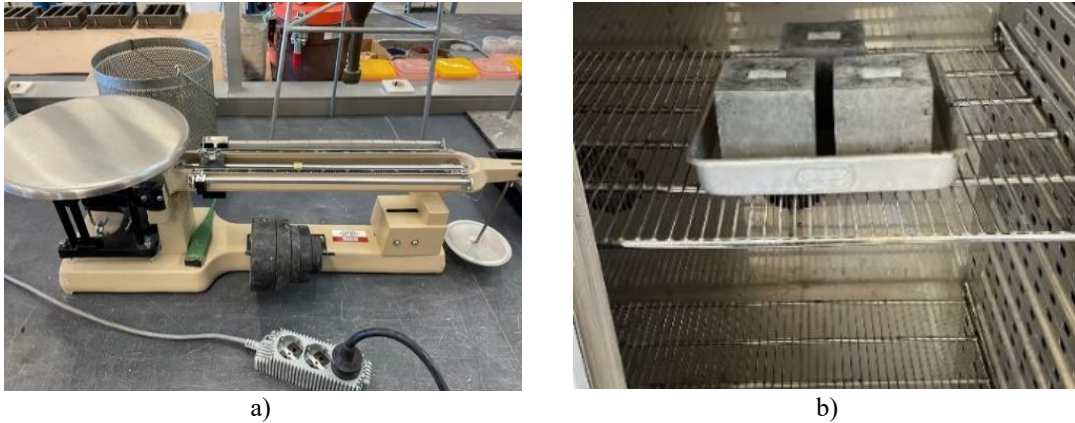
After 24 hours of immersion, the first measurement is done, so the specimen is removed from the plastic container and dried. Then, the sample is weighed, and the saturated mass of 24 hours is measured. The saturated mass is obtained when the difference between two measurements in intervals of 24 hours is less than 0.1 % of the average of the exact measurements. Therefore, 48 hours after the beginning of the immersion test, the same process must be followed, and the weight variation must be analyzed to stop the test or keep it going until the mass is almost stable. Once the saturated mass of the specimen is obtained, the next step is to weigh it underwater using a hydrostatic balance to find its hydrostatic mass. The water must be at 20 ± 3 °C; the temperature must be verified before weighing the specimen using a thermometer (Figure 13).

Figure 13 - (a) Sample inside the metallic container (b) thermometer.



Source: Author (2024).

Figure 14 - (a) Hydrostatic balance (b) drying process in the oven.



Source: Author (2024).

The final step is to dry the specimen in the oven at 105 ± 5 °C temperature to take the dry mass (Figure 14). The dry mass is achieved in the same situation as the saturated mass, so when the difference of two measurements in intervals of 24 hours is less than 0.1 % of the average. The water absorption by immersion is obtained from the equation (5), which was taken from the standard LNEC E 394 (1993):

$$A_i = \frac{m_1 - m_3}{m_1 - m_2} \times 100 \quad (5)$$

Where:

m_1 = Saturated mass [g]

m_2 = Hydrostatic mass [g]

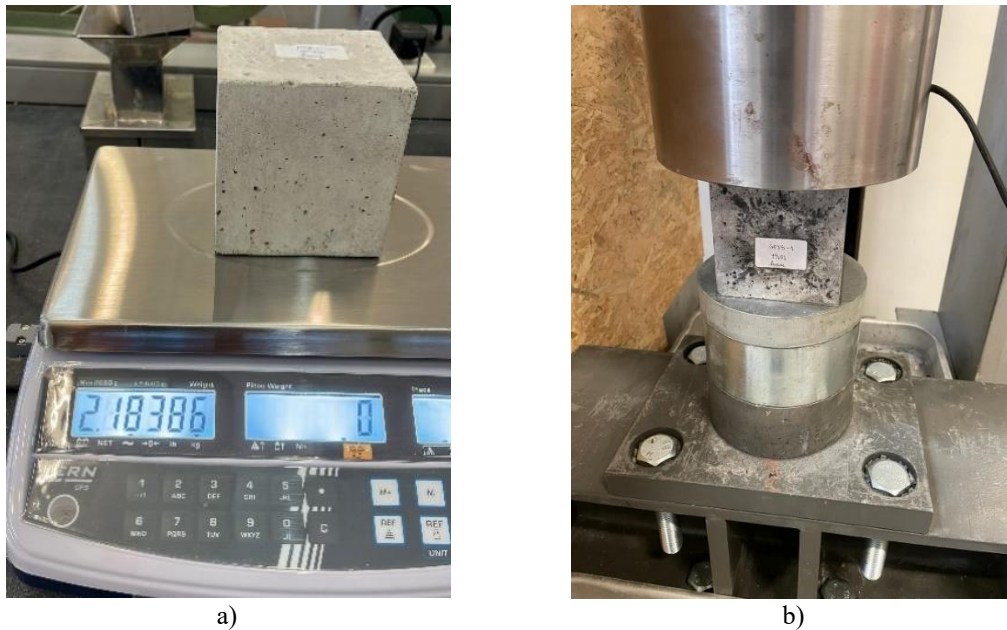
m_3 = Dry mass [g]

4.5.2.3 Compressive strength testing in cubic molds

The specimens were tested following the standard NP EN 12390-3 (2009) at the age of 28 days, and they were removed from the humidity chamber 24 hours before being tested to avoid excess moisture.

Regarding the test procedure, the specimen was weighed and positioned centrally within the load cell, which had a maximum capacity of 1000 kN, and was subjected to axial compression testing under displacement control. The tests were conducted at a constant speed of 0.1 mm/s until failure. The testing procedure is illustrated in Figure 15:

Figure 15 - (a) Weight of the specimen (b) Compression test cubic molds.



Source: Author (2024).

The rate of the load must be in the range of 0.6 ± 0.2 MPa/s ($\text{N}/\text{mm}^2.\text{s}$), and the initial load should be applied as close as possible to the specimen and without shock; after that, the load continuously increases until failure.

The final compressive strength is expressed as the arithmetic mean of the three specimens to the nearest 0.1 MPa (N/mm^2). After the type of failure is identified, the test can be classified as satisfactory or unsatisfactory, and this shall be recorded once many factors cause the type of failure.

5 RESULTS AND DISCUSSION

5.1 Preliminary tests

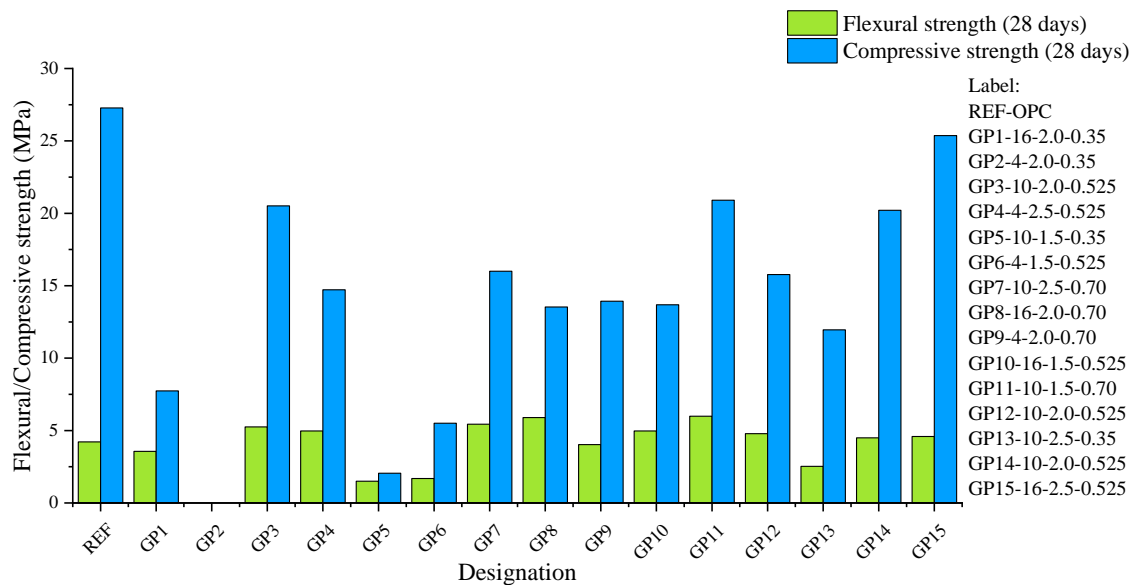
The preliminary tests assessed the samples' flexural and compressive strength using prismatic molds. The weight and measurements of each specimen are presented in APPENDIX C. Following these measurements, the specimens were subjected to flexural strength and compressive strength tests. The results for all geopolymers and reference compositions are presented in APPENDIX D. In summary, Table 10 and Figure 16 present the average results, standard deviation, and coefficient of variation of GPC and OPC mixes.

Table 10 - Average, standard deviation, and coefficient of variation.

Designation	Flexural Strength			Compressive Strength		
	Average (MPa)	Standard deviation (MPa)	Coefficient of variation (%)	Average (Mpa)	Standard deviation (MPa)	Coefficient of variation (%)
REF-OPC	4.2	0.49	11.55	27.3	2.32	8.51
GP1-16-2.0-0.35	3.6	0.32	9.12	7.7	2.12	27.37
GP2-4-2.0-0.35	0.0	0.00	0.00	0.0	0.00	0.00
GP3-10-2.0-0.525	5.3	0.16	3.09	20.5	6.80	33.15
GP4-4-2.5-0.525	5.0	0.32	6.54	14.7	5.89	39.99
GP5-10-1.5-0.35	1.5	0.86	57.28	2.1	2.91	141.65
GP6-4-1.5-0.525	1.7	0.28	16.67	5.5	1.14	20.75
GP7-10-2.5-0.70	5.4	0.16	2.99	16.0	5.57	34.83
GP8-16-2.0-0.70	5.9	0.27	4.57	13.5	3.74	27.68
GP9-4-2.0-0.70	4.0	0.16	4.03	13.9	3.88	27.84
GP10-16-1.5-0.525	5.0	0.16	3.3	13.7	1.58	11.5
GP11-10-1.5-0.70	6.0	0.42	6.96	20.9	1.41	6.73
GP12-10-2.0-0.525	4.8	0.28	5.88	15.8	3.45	21.89
GP13-10-2.5-0.35	2.5	0.28	11.11	12.0	1.32	11.01
GP14-10-2.0-0.525	4.5	0.28	6.25	20.2	1.61	7.98
GP15-16-2.5-0.525	4.6	0.16	3.53	25.4	3.71	14.62

Source: Author (2024).

Figure 16 - Average flexural and compressive strength in the preliminary tests.



Source: Author (2024).

The GP1, GP5, GP6, GP13, and REF mixes presented higher coefficients of variation in the flexural strength results, while the GP3, GP4, GP5, and GP7 mixes showed higher coefficients of variation in the compressive strength results. One reason for this variation is the irregular shape of some samples, which became deformed after the compaction process, as mentioned previously in section 4.6.1 of the experimental procedure chapter.

The GP3, GP4, GP7, GP8, GP10, GP11, GP12, GP14, and GP15 mixes exhibited higher flexural strength than REF. Among all compositions, including the reference cement composition (REF), the geopolymer GP11 presented the highest average flexural strength result, approximately 6 MPa, whereas REF achieved 4.2 MPa. Conversely, the average compressive strength of GP11 was 20.9 MPa, while REF recorded 27.3 MPa. Therefore, compared to REF, the GP11 composition presented higher flexural strength but lower compressive strength. Usually, the flexural strength of GPC is significantly higher than the flexural strength of OPC for similar compressive strengths (Ghafoor *et al.*, 2021). Previous studies have also reported that the flexural strengths of ambient cured GPC were higher than those of OPC concrete for similar compressive strengths (Ghafoor *et al.*, 2021; Nath; Sarker, 2017).

The GP11 mix, which achieved the highest flexural strength, was synthesized using medium SH molarity, 10 M. Joseph, and Mathew (2012) analyzed varying SH

molarities, determining that an SH concentration of 10 M was optimal. In the study Ghafoor et al. (2021), it has been reported that increasing SH molarity from 8 M up to 14 M increases GPC strength, but with higher molarities, the strength decreases. Similar results were achieved in other studies (Ahmed *et al.*, 2021; Chithambaram *et al.*, 2018a; Sumajouw *et al.*, 2007). According to Joseph, and Mathew (2012) the SH molarity used for geopolymer synthesis has a positive influence on dissolution, hydrolysis, and condensation reactions, but excess alkali concentration hinders the condensation of the silicate species (Joseph; Mathew, 2012). In contrast with the previous findings, these studies (Ahmed *et al.*, 2021; Aliabdo; Abd Elmoaty; Salem, 2016; Ghafoor *et al.*, 2021; Nath; Sarker, 2017) reported decreased strength while increasing SH molarity. These decreased in strength was attributed to the congestion of hydroxide ions in high molarity mixes (OH⁻) (Ghafoor *et al.*, 2021; Nath; Sarker, 2017) and the overflowing alkali concentration, which prevents the condensation of silicate elements (Ahmed *et al.*, 2021). In the present work, the medium molarity used in the GP11 synthesis may have positively affected the flexural strength result.

In addition, GP11 was synthesized using a high AL/FA ratio of 0.70. Joseph, and Mathew (2012) reported increased FA-BGPC strength while increasing the AL/FA ratio. The higher GPC strength at high AL/FA ratios may be attributed to the fact that increasing the Si species content and the SiO₂/Al₂O₃ ratio results in more Si-O-Si bonds, which are stronger in comparison with Si-O-Al (Al Bakri, A.M.M. *et al.*, 2012; Aliabdo; Abd Elmoaty; Salem, 2016).

Compared to all mixes in Figure 16, REF-OPC achieved the highest compression strength, 27.3 MPa. Among the geopolymers alone, GP15 presented the highest compression strength, 25.4 MPa. The higher compressive strength result of the GP15 may be attributed to some facts. Firstly, GP15 composition has a molarity of 16 M, an SS/SH ratio of 2.5, and an AL/FA ratio of 0.525. Compared to GP4, which has the same SS/SH ratio and AL/FA ratio but a molarity of 4 M, the compressive strength observed in the GP15 composition can be attributed to the higher dissolution of silicon and aluminum particles in the geopolymerization process, while increasing the molarity of SH. These studies reported that increasing the molarity of SH improved the compressive strength of GPC (Ahmed *et al.*, 2021; B. Siva Konda Reddy; J. Varaprasad; K. Naveen Kumar Reddy, 2010; Baharom *et al.*, 2019; Das; Shrivastava, 2021; Ghafoor *et al.*, 2021; Görhan; Kürklü, 2014; Jaydeep; Chakravarthy, 2013; Nath; Sarker, 2017; Vora; Dave, 2013).

Second, the GP15 mix was synthesized at high SS/SH ratio. In this study, Aliabdo, Abd Elmoaty, and Salem (2016) reported an increase in strength with an increase in the SS/SH ratio. The test results showed that the optimum SS/SH ratio was 2.5, the same SS/SH ratio used in the GP15 synthesis. The improvement in GPC strength while increasing the SS/SH ratio may be due to the SS solution improving the polymerization process, leading to reaction products with more Si and, hence, higher mechanical strength (Aliabdo; Abd Elmoaty; Salem, 2016; Pacheco-Torgal; Castro-Gomes; Jalali, 2008). The studies reported increased strength of FA-BGPC with increasing the SS/SH ratio (Aliabdo; Abd Elmoaty; Salem, 2016; Sathonsaowaphak; Chindaprasirt; Pimraksa, 2009a).

The GP2 composition did not register flexural or compressive strength in the tests. One of the reasons can be due to that GP2 was synthesized at low SH molarity, which was 4 M. Therefore, the result may be explained by the fact that lower SH molarities, in general, negatively affect the compressive strength of GPC. In other words, it is established that an alkaline activator solution with a higher SH concentration is usually advantageous for achieving elevated compressive strength (De Vargas *et al.*, 2011). Also, according to Luhar (2022), it could happen because the concentration of SH affects the release of Si^{4+} and Al^{3+} ions from fly ash during geopolymerization reaction kinetics (Luhar; Luhar, 2022); silica and alumina are filtered more in a highly concentrated SH solution (Chindaprasirt *et al.*, 2009; Görhan; Kürklü, 2014); higher SH concentration is more effective in dissolving FA particles and can result in a better geopolymerization (Álvarez-Ayuso *et al.*, 2008; Görhan; Kürklü, 2014). These studies recommend the utilization of concentrations of SH in the range of 8 to 16 M to achieve higher compressive strength results in FA-BGPC (Mustafa *et al.*, 2012).

In addition, the GP2 mix was synthesized using an AL/FA ratio of 0.35. Based on the findings of the study by Joseph, and Mathew (2012), while the AL/FA ratio increased from 0.35 up to 0.55, the compressive strength increased, and beyond that, the compressive strength was negatively affected. From the test results, the compressive strength of 39, 47, 58, and 44 MPa was obtained with AL/FA ratios of 0.35, 0.45, 0.55, and 0.65, respectively (Joseph; Mathew, 2012). So, in the study by Joseph, and Mathew (2012), the mix synthesized using the same AL/FA ratio of GP2, which is 0.35, achieved the lowest compressive strength. Similarly to GP11, which may be positively influenced by the high AL/FA ratio, the opposite effect may be expected at low AL/FA ratios, resulting in less stronger bonds Si-O-Si and reduced compressive strength (Al Bakri,

A.M.M. *et al.*, 2012; Aliabdo; Abd Elmoaty; Salem, 2016; Joseph; Mathew, 2012). The improvement in GPC properties because of the increasing AL/FA ratio were reported in these studies (Ahmed *et al.*, 2021; Aliabdo; Abd Elmoaty; Salem, 2016; Hardjito *et al.*, 2004; Scholar; Ganesh Babu-Professor; Santhanam-Assistant Professor, 2008).

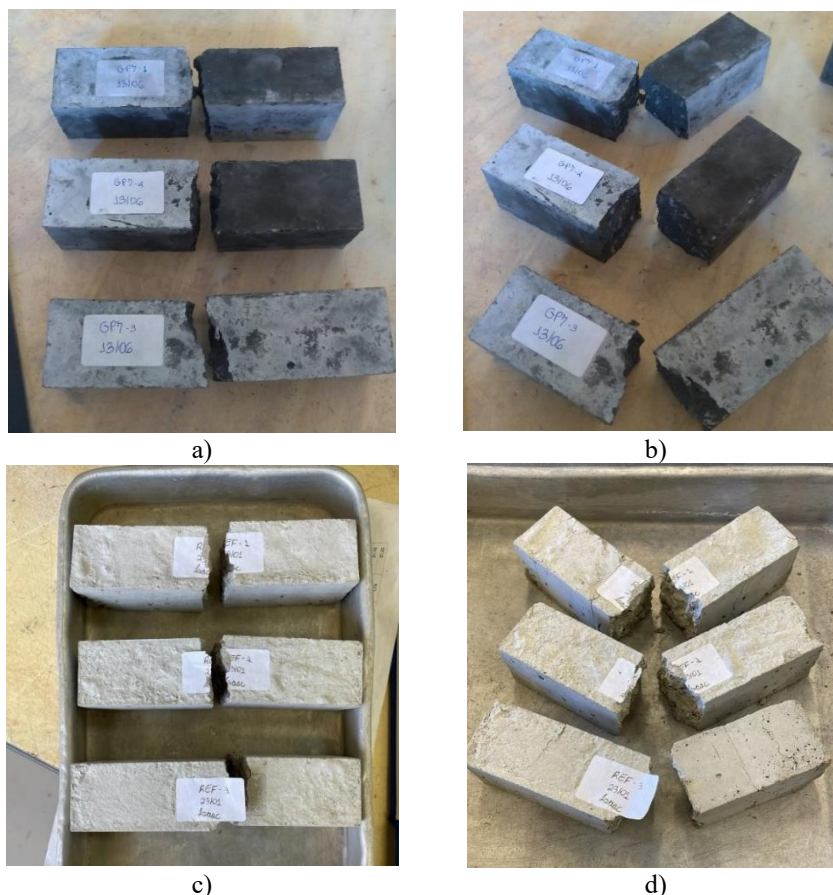
The GP5 mix presented the lowest average flexural strength and compressive strength results, which was 1.5 MPa, and 2.1 MPa, respectively. Compared to GP11, which achieved higher flexural and compressive strength results, the geopolymer GP5 had the same molarity (10 M) and SS/SH (1.5). However, the geopolymer GP5 has AL/FA ratio of 0.35, whereas GP11 has an AL/FA ratio of 0.70. So, even having the same W/GPS ratio, GP5 has less water content in the mixture, compared to GP11. It happens because most of the alkaline solutions are composed by water. These results may be attributed to the fact that the water contents played an important role during the dissolution stage in the geopolymerization phenomena (Ghafoor *et al.*, 2021). Also, according to Hu *et al.* (2018), water is important in the geopolymer formation and properties of the final products since it provides the reaction medium for the dissolution of aluminosilicates and the transfer of various ions, implying that the existence of sufficient water is vital for geopolymerization (Hu *et al.*, 2018).

In addition, considering that the GP5 mix was synthesized using an SS/SH ratio of 1.5, the lowest flexural and compressive strength of GP5 may be attributed to another fact. In the study by Joseph, and Mathew (2012), FA-BGPC strength increased while increasing SS/SH ratio from 1.5 to 2.0 and from 2.0 to 2.5. The higher GPC strength was at an SS/SH ratio of 2.5, and the lower strength was at the SS/SH ratio of 1.5, the same SS/SH ratio of the GP5 mix. Regarding the same author, the increase in mechanical properties while increasing the SS/SH ratio is mainly due to the change in the microstructure of GPC, which is influenced by the quantity of SS (Joseph; Mathew, 2012). Then, reduced FA-BGPC strength in mixes synthesized at an SS/SH ratio of 1.5 may be due to possessing lower SS quantity than mixes synthesized at SS/SH ratios of 2.0 and 2.5.

Similarly to the GP2 mix, which did not present flexural and compressive strength, the GP5 was also synthesized using AL/FA of 0.35. As is the case with using a lower AL/FA ratio in the GP2 synthesis, the same reasons also may be attributed to the lower strength in the GP5 mix. To illustrate the flexural and compressive strength test procedure,

the figures displaying concrete rupture of geopolymer GP7 and REF are presented in Figure 17.

Figure 17 - Prisms a-b) GP7 c-d) REF after flexural strength test.



Source: Author (2024).

5.2 Final tests

In the final tests, water absorption was assessed through capillarity and immersion using cubic molds with dimensions of 100 mm. Additionally, the mixes that achieved the highest compressive strength in the preliminary tests, REF, GP3, GP7, GP11, GP12, GP14, and GP15, were also tested for compression strength at 28 days.

5.2.1 Capillarity Water absorption Tests

The weight measurements and the water absorption results at each time (0 h, 3 h, 6 h, 24 h, 48 h, and 72 h) are presented in APPENDIX E and APPENDIX F, respectively. In summary, the water absorption results through capillarity at 72 hours, which are listed in descending order in Table 11, will be discussed next.

Table 11 - Water absorption at 72 h from the highest to the lowest value.

Designation	Water absorption (g/mm ²)
GP5-10-1.5-0.35	0.00960
GP2-4-2.0-0.35	0.00833
GP13-10-2.5-0.35	0.00490
GP6-4-1.5-0.525	0.00389
GP14-10-2.0-0.525	0.00318
GP15-16-2.5-0.525	0.00308
GP10-16-1.5-0.525	0.00258
GP1-16-2.0-0.35	0.00245
GP4-4-2.5-0.525	0.00225
GP3-10-2.0-0.525	0.00217
GP9-4-2.0-0.70	0.00180
GP11-10-1.5-0.70	0.00150
REF-OPC	0.00143
GP12-10-2.0-0.525	0.00113
GP8-16-2.0-0.70	0.00103
GP7-10-2.5-0.70	0.00055

Source: Author (2024).

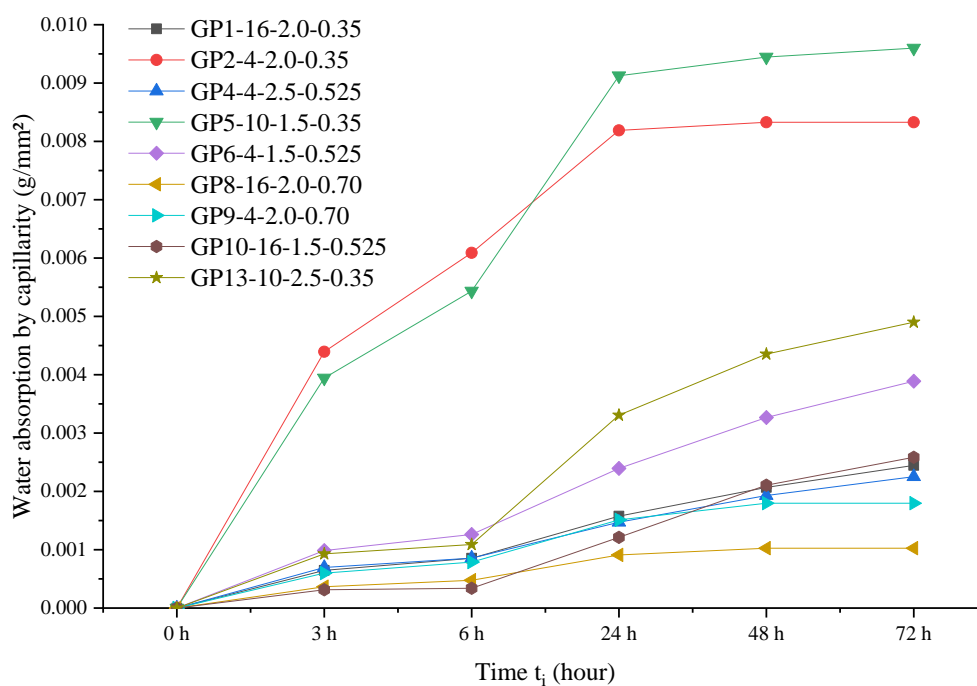
As shown in Table 11, the mixes GP7, GP8, and GP12 presented the lowest water absorption results at 72 hours. These lower values can be attributed to forming a more compact and denser microstructure, with low pore interconnectivity in the GPC matrix, compared to the OPC mix. This occurs because the geopolymerization process develops a three-dimensional network that fills the voids, leading to fewer vacancies and low water permeability (Ojha; Aggarwal, 2023). As reported in similar studies (Hannanee Ahmad Zaidi *et al.*, 2019; Lavanya; Jegan, 2015; Luhar; Khandelwal, 2015; Ojha; Aggarwal, 2023), lower water absorption by GPC compared to OPC mixes was expected. In the study by Zaidi *et al.* (2021), a connection between water absorption and porosity was established, indicating that the lower water absorption of GPC is preferred due to its lower porosity. Low water absorption is a good indicator of limited open porosity, which inhibits the high flow of water into the concrete (Hannanee Ahmad Zaidi *et al.*, 2019). This other study found that FA-BGPC samples with lower water absorption and porosity achieved higher mechanical properties under compressive strength tests compared to GPC samples with higher water absorption and porosity (Abdullah *et al.*, 2012).

However, in general, the GPC mixes presented higher water absorption through capillarity than the OPC mix (Table 11). The mixes GP5, GP2, and GP13 presented the highest water absorption results. This trend aligns with previous studies that reported a

lower water absorption rate for OPC concrete than FA-BGPC (Albitar *et al.*, 2017). The higher absorption rates of GPC mixes may be attributed to the presence of larger voids in the concrete (Ojha; Aggarwal, 2023) and the presence of microcracks, which increase water absorption and porosity (Abdullah *et al.*, 2012). In the study by Wongkeo, Seekaew, and Kaewrahan (2019), the pore morphology and water absorption of FA-BGPC were investigated, concluding that the pore structure, including pore connection and pore size, significantly influenced the water absorption of GPC.

The mixes were divided into groups for analysis, and the results of water absorption by capillarity are presented in Figure 18 and Figure 21. These figures illustrate measurements from the beginning of the test at 0 hours to the final of the test at 72 hours.

Figure 18 - Water absorption by capillarity of GP1, GP2, GP4, GP5, GP6, GP8, GP9, GP10, and GP13.



Source: Author (2024).

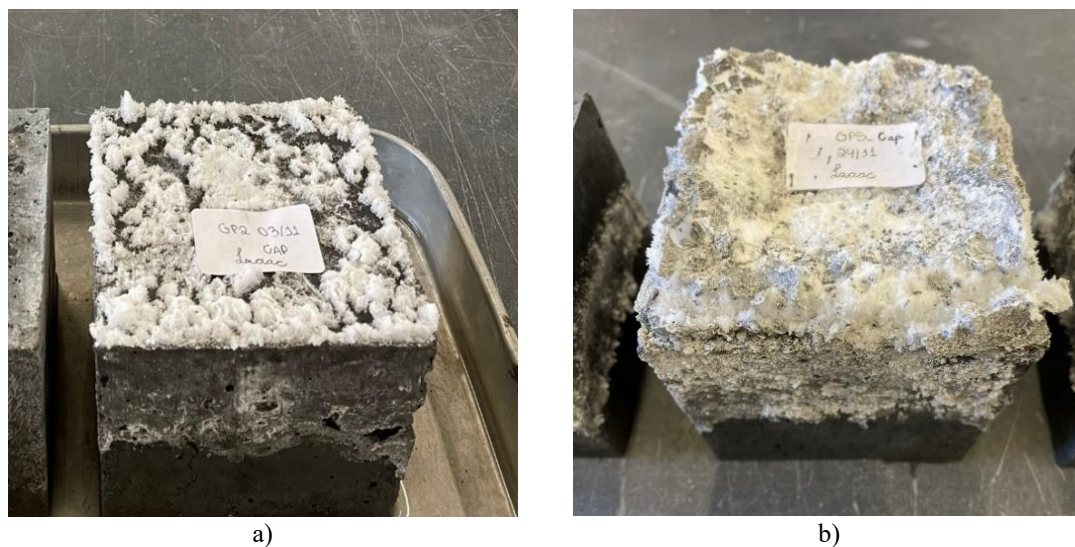
The GP2 and GP5 registered the highest water absorption, mainly in the first 24 hours of the test, after which they maintained almost the same mass until the end of the test at 72 hours. Compared to other geopolymers, the higher water absorption results of the mixes GP2 and GP5 can be attributed to several factors. Firstly, these mixes were synthesized using the lowest factor AL/FA ratio level of 0.35. According to previous

studies (Aliabdo; Abd Elmoaty; Salem, 2016), a decrease in the AL/FA ratio increased water absorption. Also, the highest water absorption was observed when using AL/FA ratio of 0.30, which is a very similar to the 0.35 ratio used in the GP2 and GP5. Secondly, GP2 and GP5 were produced with medium and low levels of SS/SH ratios of 2.0 and 1.5, respectively. Studies (Aliabdo; Abd Elmoaty; Salem, 2016; Wongkeo; Seekaew; Kaewrahan, 2019; Zaidi *et al.*, 2021) have reported that the decrease in the SS/SH ratio significantly increases water absorption. Also, in the study by Zaidi *et al.* (2021), the highest water absorption was reported using SS/SH ratio of 1.5, which is the same SS/SH ratio used in GP5, while the lowest water absorption was achieved using SS/SH ratio of 2.5, which is a higher than the 2.0 and 1.5 ratios used in GP2 and GP5, respectively. The study by Wongkeo, Seekaew, and Kaewrahan (2019) suggests that the increase of SS/SH ratio obstructs the pore formation, resulting in small pore size, fewer pore connections, and lower water absorption. Then, it was expected the opposite effect at low (1.5) and medium (2.0) SS/SH ratios. From the test results, GP2 and GP5 agreed with this trend.

Among all fifteen mixes in Table 11, the GP5 mix presented the highest water absorption. Also, compared to all GPC mixes, GP5 mix was synthesized using the third highest water addition, 90.69 kg/m³ (Table 8). Previous studies by Aliabdo, Abd Elmoaty, and Salem (2016); Sathonsaowaphak, Chindaprasirt, and Pimraksa (2009) have concluded that an increase in water absorption because of increasing additional water content could be due to the increase of voids resulting from increased water content, which had no role in chemical reaction. Therefore, the higher water addition in the GP5 mix likely contributed to this high-water absorption.

The phenomenon of efflorescence was primarily identified in the mixes with higher water absorption, specifically GP2 and GP5. Efflorescence occurs when excessive alkali ions in the system leak through the pores and interact with the CO₂ in the atmosphere, forming white salt deposits on the surface of the samples. This phenomenon implies deficiencies in the matrix properties and porosity of GPC (Ozcelikci *et al.*, 2023). In the present work, efflorescence was studied by using photographs. The test results for the mixes with higher water absorption, which are GP2 and GP5, are shown in Figure 19. These results align with those of Zhou *et al.* (2020), who reported that efflorescence increased the water absorption of GPC due to the deterioration of pore structures caused by the crystallization pressure.

Figure 19 - (a) GP2 and (b) GP5, the highest water absorptions through capillarity.



Source: Author (2024).

The mixes GP4, GP8, and GP9 presented the lowest water absorption rates. GP8 and GP9 registered water absorption until 48 hours, after their mass remained constant. On the other hand, the mixes GP1, GP4, GP6, GP10, and GP13 presented high water absorption rate until the end of the test at 72 hours. Even though, all these GPC mixes presented significantly lower water absorption at 72 hours, compared to GP2 and GP5.

These mixes' lower water absorption results may be attributed to some facts. Firstly, GP4, GP6, and GP9 were synthesized using a low SH molarity of 4 M, a low-level concentration, compared to other mixes that used SH molarity of 10 M and 16 M. In the study by Wongkeo, Seekaew, and Kaewrahan (2019), the authors reported that the increase of SH molarity enlarges the pore size of the samples because higher SH molarity causes more violent hydrogen gas release, forming macropores inside the sample. It was reported that the water absorption increased as the SH molarity increased (Wongkeo; Seekaew; Kaewrahan, 2019). The same study found that synthesized with 7.5 M SH showed finer pores and lower water absorption than mixed with 12.5 M SH. So, in the present work, the lower water absorption of the mixes GP4, GP6, and GP9 can be attributed to their synthesis using a low SH molarity of 4 M.

Also, in the study by Zaidi et al. (2021), reported the lowest water absorption with an SS/SH ratio of 2.5. The high-level SS/SH ratio of 2.5 was used to produce the mixes GP4 and GP13, which showed less water absorption compared to GP2 and GP5 synthesized with SS/SH ratios of 2.0 and 1.5, respectively.

Finally, the mixes GP1, GP8, and GP10 also presented lower water absorption. Among all geopolymers in Figure 18, GP8 presented the lowest water absorption. These mixes were produced using medium and high SS/SH and AL/FA ratios. High levels of these factors contribute to higher silica in the mixture. The study by Lavanya, and Jegan (2015) attributed lower water absorption to higher silica content which forms a greater quantity of aluminosilicate gel, providing strong interparticle bonding. Hence, the silicate occupies the void spaces between the FA particles, resulting in lower water absorption (Lavanya; Jegan, 2015). So, in the present work, the low water absorption of the mixes GP1, GP8, and GP10 may be attributed to this fact.

As shown in Figure 20, there is a comparison of efflorescence between the mixes with higher water absorption (GP2 and GP5) and those with lower water absorption (GP1, GP4, and GP6). Similarly, the mixes GP1, GP4, and GP6 exhibit less efflorescence compared to GP2 and GP5, which correlates with their lower water absorption, as reported by the trend of Zhou et al. (2020).

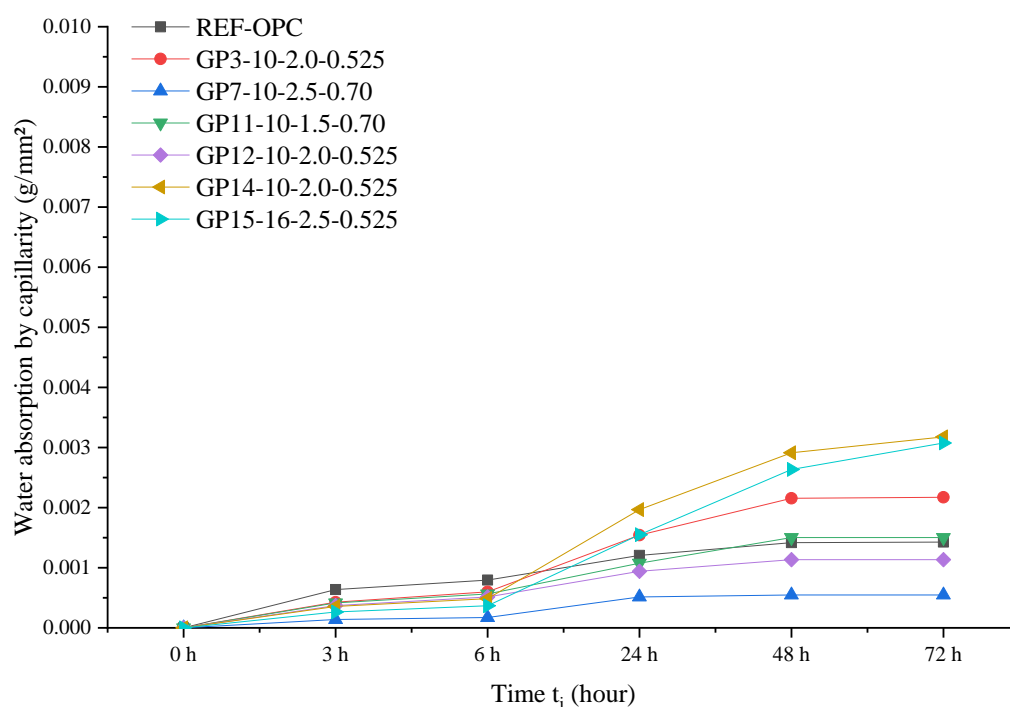
Figure 20 - (a) Comparison between geopolymers GP1, GP2 (b) GP4, GP5, and GP6, respectively.



Source: Author (2024).

The water absorption results of the mixes REF, GP3, GP7, GP11, GP12, GP14, and GP15 is presented in the Figure 21. Except for GP14 and GP15, the other mixes maintained almost the same measurement between 48 and 72 hours.

Figure 21 - The water absorption by capillarity of REF, GP3, GP7, GP11, GP12, GP14, and GP15.



Source: Author (2024).

In general, lower water absorption was observed in the mixes presented in Figure 21, compared to those in Figure 18. Also, the differences in water absorption between the mixes in Figure 21 were not significantly pronounced compared to those in Figure 18. Similar factors may explain these lower water absorption results.

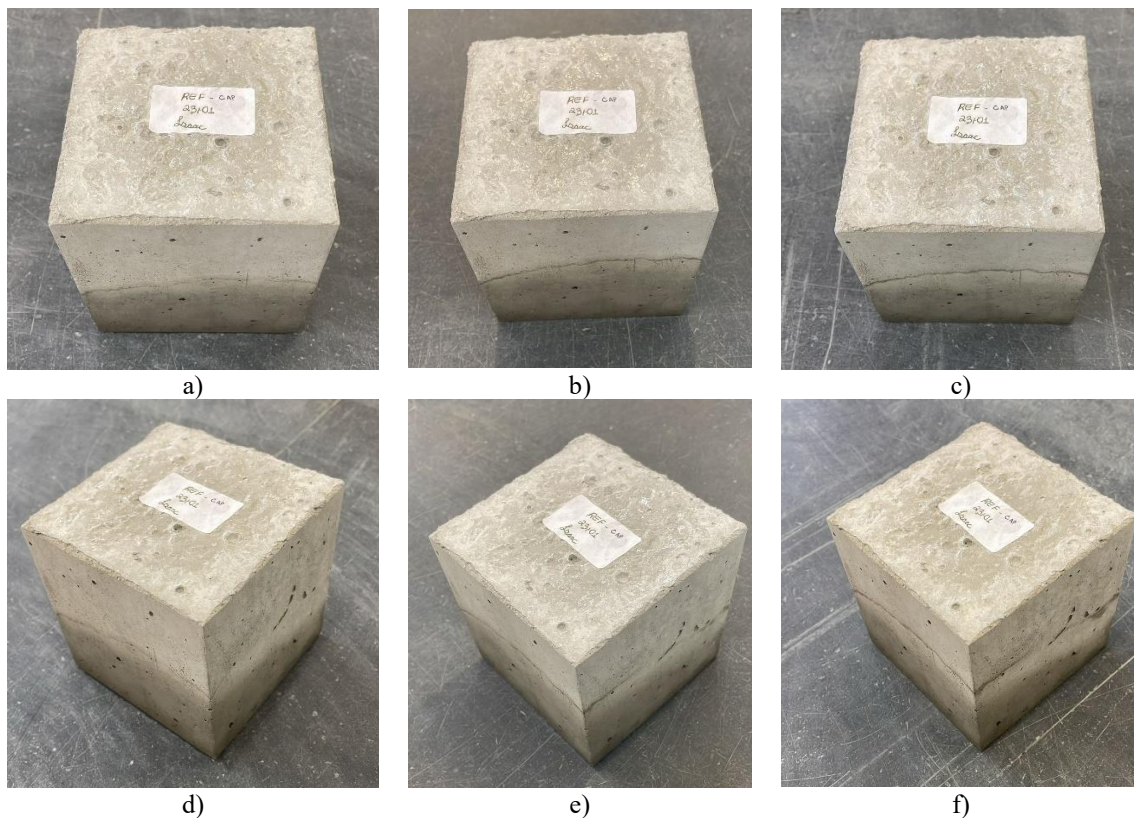
Of the six GPC mixes presented in the Figure 21, five were synthesized at an SH molarity of 10 M, considered in the DOE. The study by Wongkeo, Seekaew, and Kaewrahan (2019) showed that decreasing SH molarity from 12.5 M to 7.5 M decreased water absorption, with the samples using lower SH molarity presenting finer pores and lower water absorption, compared to 12.5 M. Therefore, one reason for the lower water absorption results of mixes GP3, GP7, GP11, GP12, and GP14 may be their synthesis at medium SH molarity (10 M).

Compared to REF, only the mixes GP7, GP8, and GP12 registered lower water absorption. Similar to the discussion regarding mixes GP1, GP8, and GP10 from Figure 18, GP7 and GP12 were produced using medium and high levels of the factors SS/SH and AL/FA. So, the GP7 and GP12 results can be attributed to the presence of higher silica

content, resulting in higher formation of aluminosilicate gel and higher interparticle bonding. Also, the silicate occupies the void spaces between the FA particles, resulting in lower water absorption (Lavanya; Jegan, 2015). Also, the GP7 mix presented the lowest water absorption among all sixteen mixes. GP7 mix barely presented water absorption after 24 hours. The lowest water absorption result of the GP7 mix may be attributed to the fact that only the GP7 mix was synthesized using a high SS/SH ratio (2.5) and high AL/FA ratio (0.70), which means this mixture presents the highest silica content, which increases the formation of aluminosilicate gel, resulting in lower water absorption (Lavanya; Jegan, 2015).

Figure 22 shows a photograph report of the REF-OPC mix taken at 24, 48, and 72 hours during the capillarity test. As can be seen, most water absorption happens in the first 48 hours, with lower water absorption rates thereafter and a nearly constant weight measurement. GPC mixes with lower water absorption presented similar behavior to the OPC mix.

Figure 22 - Reference composition at a-d) 24h, b-e) 48h, and c-f) 72h, respectively.



Source: Author (2024).

5.2.2 Immersion water absorption Tests

Regarding the immersion test of the specimens, the results were divided into Table 12, Table 13, and Table 14. This division was necessary because the test procedure required weight verification at each 24-hour test interval, including the saturation and drying procedures. Table 12 shows the results of saturated mass at 24 and 48 hours. Besides GP10, all the mixes presented low water absorption between 24 and 48 hours. Then, they underwent hydrostatic mass measurement, also presented in Table 12.

Table 12 - Immersion test.

Designation	Saturated mass 24 h (g)	Saturated mass 48 h (g)	Verification <1	Water temperature (°C)	Container mass under water (g)	Hydrostatic mass with container (g)	Hydrostatic mass without container (g)
REF-OPC	2351.03	2352.81	0.76	20	1025	2367	1342
GP1-16-2.0-0.35	2311.60	2311.60	0.15	20	1023	2349	1326
GP2-4-2.0-0.35	2341.05	2341.05	0.32	20	1023	2355	1332
GP3-10-2.0-0.525	2275.02	2275.68	0.29	19.5	1025	2317	1292
GP4-4-2.5-0.525	2340.24	2340.90	0.28	19	1023	2363	1340
GP5-10-1.5-0.35	2348.86	2348.97	0.05	19	1023	2355	1332
GP6-4-1.5-0.525	2346.25	2346.61	0.15	19	1023	2360	1337
GP7-10-2.5-0.70	2339.30	2339.30	0.03	19.5	1025	2354	1329
GP8-16-2.0-0.70	2327.43	2329.21	0.76	19.5	1025	2358	1333
GP9-4-2.0-0.70	2305.84	2308.11	0.98	19.5	1025	2345	1320
GP10-16-1.5-0.525	2324.41	2327.57	1.36	-	-	-	-
GP11-10-1.5-0.70	2345.36	2346.42	0.45	19	1027	2358	1331
GP12-10-2.0-0.525	2288.02	2288.87	0.37	19	1027	2315	1288
GP13-10-2.5-0.35	2319.61	2319.89	0.12	19	1024	2349	1325
GP14-10-2.0-0.525	2301.99	2302.73	0.32	19	1024	2333	1309
GP15-16-2.5-0.525	2281.79	2282.24	0.20	19	1024	2315	1291

Source: Author (2024).

The GP10 mix presented water absorption between 24 hours and 48 hours above the maximum allowed by the standard LNEC E 393-1993 (1993). Therefore, keeping underwater for 96 hours was necessary until the saturated mass stabilized. Table 13 shows the saturated and hydrostatic mass at 72 hours of the GP10 mix.

Table 13 - Immersion test GP10.

Designation	Saturated mass 72 h (g)	Verification <1	Saturated mass 96 h (g)	Verification <1	Water temperature (°C)	Container mass underwater (g)	Hydrostatic mass with container (g)	Hydrostatic mass without container (g)
GP10-16-1.5-0.525	2330.33	1.19	2331.3	0.43	19.5	1025	2357	1332

Source: Author (2024).

Finally, after getting the results of saturated and hydrostatic mass for all mixes, the results of dry mass and water absorption are shown in Table 14.

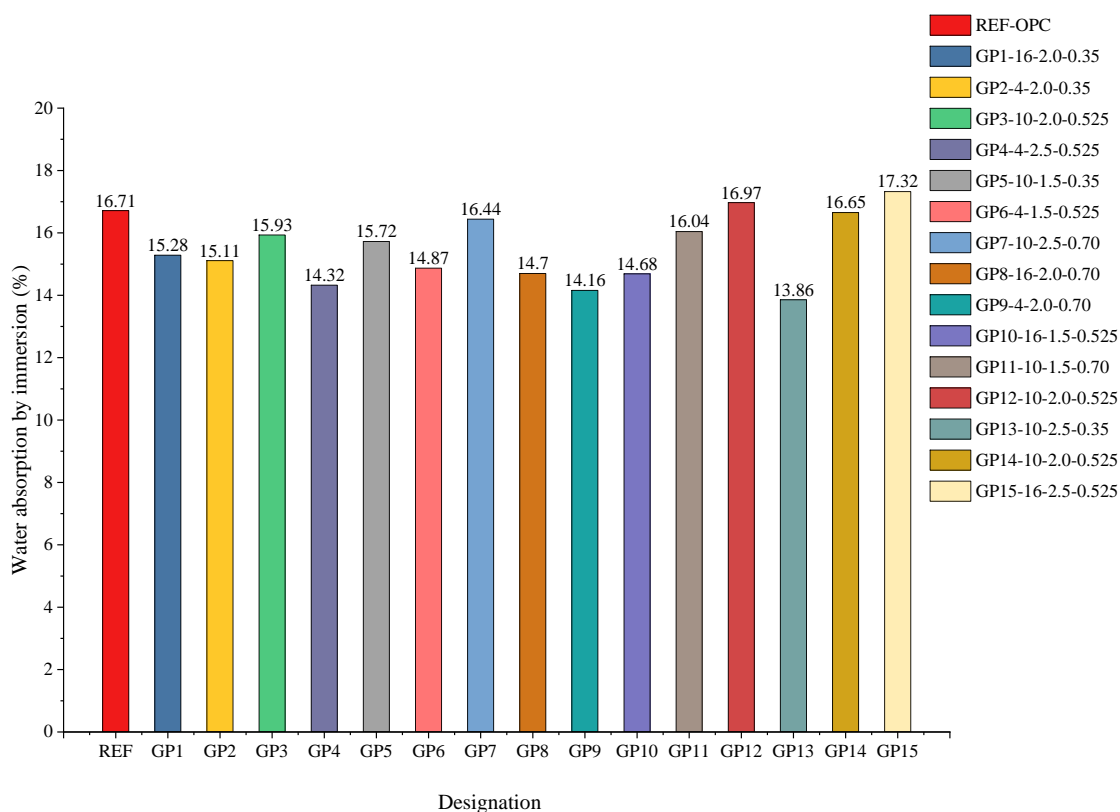
Table 14 - Dry mass immersion test.

Designation	Dry mass 24 h (g)	Dry mass 48 h (g)	Verification <1	Dry mass 72 h (g)	Verification <1	Dry mass 96 h (g)	Verification <1	Dry mass 120 h (g)	Verification <1	Water absorption (%)
REF-OPC	2205.37	2187.61	8.09	2184.72	1.32	2183.86	0.39	-	-	16.71
GP1-16-2.0-0.35	2189.08	2172.39	7.65	2161.55	5.00	2160.35	0.56	-	-	15.28
GP2-4-2.0-0.35	2189.92	2187.80	0.97	-	-	-	-	-	-	15.11
GP3-10-2.0-0.525	2130.61	2118.96	5.48	2116.66	1.09	2115.41	0.59	-	-	15.93
GP4-4-2.5-0.525	2215.65	2202.13	6.12	2198.02	1.87	2197.54	0.22	-	-	14.32
GP5-10-1.5-0.35	2193.10	2190.20	1.32	2189.08	0.51	2188.8	-	-	-	15.72
GP6-4-1.5-0.525	2214.88	2200.96	6.30	2196.97	1.81	2196.48	0.22	-	-	14.87
GP7-10-2.5-0.70	2190.66	2178.12	5.74	2175.14	1.37	2173.47	0.77	-	-	16.44
GP8-16-2.0-0.70	2214.13	2196.73	7.89	2190.41	2.88	2184.67	2.62	2182.79	0.86	14.70
GP9-4-2.0-0.70	2186.47	2173.28	6.05	2170.11	1.46	2168.24	0.86	-	-	14.16
GP10-16-1.5-0.525	2211.74	2193.54	8.26	2185.83	3.52	2182.65	1.46	2181.08	0.72	14.68
GP11-10-1.5-0.70	2207.74	2191.03	7.60	2185.6	2.48	2183.54	0.94	-	-	16.04
GP12-10-2.0-0.525	2140.31	2123.98	7.66	2120.22	1.77	2119.02	0.57	-	-	16.97
GP13-10-2.5-0.35	2194.91	2183.55	5.19	2182.04	0.69	-	-	-	-	13.86
GP14-10-2.0-0.525	2155.90	2140.54	7.15	2138.26	1.07	2137.26	0.47	-	-	16.65
GP15-16-2.5-0.525	2129.33	2113.84	7.30	2111.45	1.13	2110.52	0.44	-	-	17.32

Source: Author (2024).

In summary, only the water absorption results through immersion were presented in the Figure 23. Then, the test results of GPC and OPC mixes will be discussed.

Figure 23 - Results of absorption of water by immersion.



Source: Author (2024).

The GP13 presented the lowest water absorption value by immersion, around 13.86 %, while GP15 showed the highest value of 17.32 %. The geopolymer compositions recorded similar values to the reference cement composition, with water absorption averaging around 16.71% at the end of the test. Also, considering the sixteen mixes submitted to the immersion test, the OPC mix was the third in higher water absorption. Only GP15 and GP11 presented higher water absorption compared to REF-OPC. This trend agreed with these studies (Hannanee Ahmad Zaidi *et al.*, 2019; Lavanya; Jegan, 2015) where OPC mixes achieved higher water absorption, compared to GPC mixes.

In general, the water absorption results through immersion in the present work showed higher values compared to most studies found in the literature. For example, in the study by Lavanya, and Jegan (2015), FA-BGPC produced using SS/SH ratio of 2.5 and SH molarity fixed at 12 M exhibited water absorption results in the range of approximately 1 – 3%. Another study, Shahedan et al. (2021), reported FA-BGPC water absorption percentage was around 3.5 – 4%. The authors mentioned that water absorption around 3 – 6.5% remained within a comparable percentage of standard concrete

(Shahedan *et al.*, 2021). Lastly, in the study by Hannanee Ahmad Zaidi *et al.* (2019), GPC was exposed to a marine environment. Based on the results, the water absorption of GPC was lower than that of OPC concrete, which obtained 4.58% and 11.33%, respectively. Regarding the same study, low water absorption is a good indicator of limited open porosity, which can inhibit the high water flow into the concrete. The authors of Hannanee Ahmad Zaidi *et al.* (2019) considered water absorption value ranging from 3% to 5% as an average concrete, and they regarded water absorption of up to 6% as desirable. As shown in Figure 23, the water absorption results of the GPC and OPC mixes in the present work ranged from 13.86% to 17.32%. Compared to the literature, the nearest results were found in the study by Wongkeo, Seekaew, and Kaewrahan (2019). Lightweight FA-BGPC was produced using aluminum powder as a foaming agent. Also, GPC was synthesized using SH molarity at 7.5, 10, and 12.5 M, SS/SH ratio at 1.0, 1.5, and 2.0, and AL/FA ratio of 0.5. The water absorption results of this study, which used similar factors compared to the present study, range from 22 to 30% (Wongkeo; Seekaew; Kaewrahan, 2019).

The GP13, GP9, and GP4 mixes presented the lowest water absorption by immersion of 13.86%, 14.16%, and 14.32%, respectively. This lower water absorption results may be attributed to some reasons. Firstly, GP4 and GP13 were synthesized using a high SS/SH ratio (2.5). Also, GP9 was synthesized using a medium SS/SH ratio (2.0). So, neither of them was synthesized using a low SS/SH ratio (1.5). In the study by Zaidi *et al.* (2021), the lowest water absorption was achieved using SS/SH ratio of 2.5. Also, these studies (Aliabdo; Abd Elmoaty; Salem, 2016; Wongkeo; Seekaew; Kaewrahan, 2019; Zaidi *et al.*, 2021) reported that the increase in the SS/SH ratio significantly reduces water absorption. This study by Wongkeo, Seekaew, and Kaewrahan (2019) suggests that an increased SS/SH ratio obstructs the pore formation, resulting in small pore size, less pore connections, and lower water absorption. In addition, GP4 and GP9 were synthesized using low SH molarity (4 M), and GP13 was synthesized using medium SH molarity (10 M). This study by Wongkeo, Seekaew, and Kaewrahan (2019) showed that samples produced using lower SH molarities, around 7.5 M, presented finer pore and lower water absorption, compared to higher molarities around 12.5 M. It happened because the samples produced using higher SH molarities increased the formation of macropores, increasing the water absorption. So, from the test results of the study by Wongkeo, Seekaew, and Kaewrahan (2019), the water absorption decreased as the SH

molarity decreased. Similarly, in the present work, the lower water absorption results of the GP4, GP9, and GP13 mixes may also be attributed to the fact that they were synthesized at low (4 M) and medium (10 M) SH molarity.

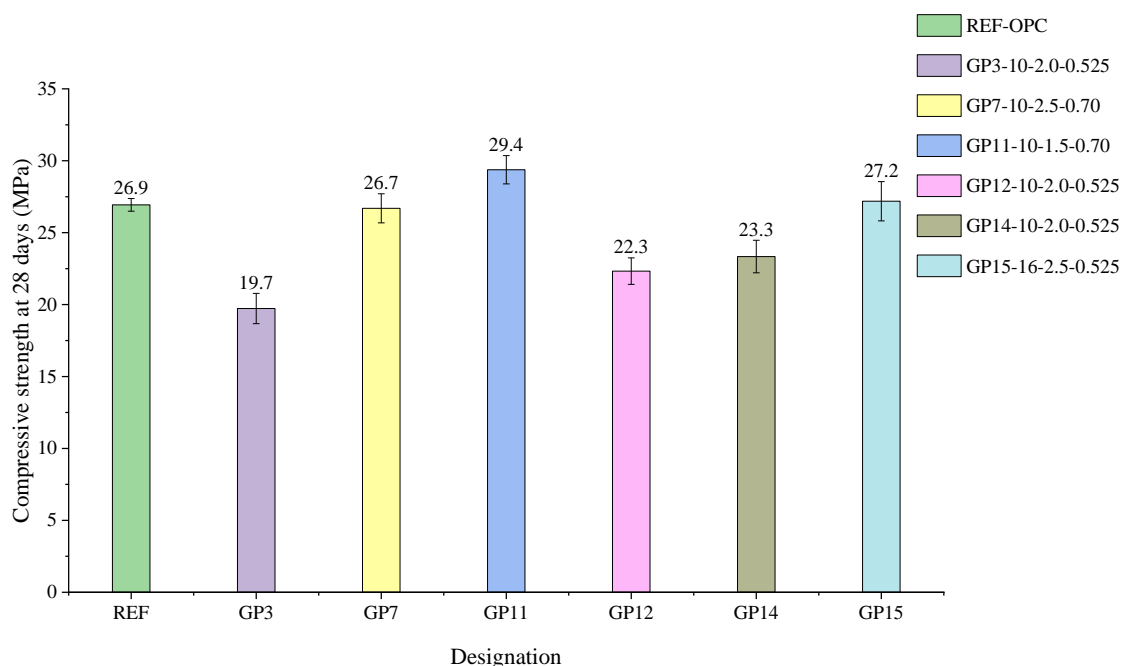
The GP15, GP12, REF, and GP14 mixes presented the highest water absorption by immersion of 17.32%, 16.97%, 16.71%, and 16.65%, respectively. This higher water absorption results may be attributed to some reasons. Firstly, GP15 was synthesized using high SH molarity (16 M), and GP12 and GP14 were synthesized using medium SH molarity (10 M). By contrast to GP4, GP9, and GP13, which were synthesized at low/medium SH molarities and presented lower absorption, the GP12, GP14, and GP15 mixes were synthesized at medium/high molarities and presented higher water absorption. Similarly, the water absorption increased as the SH molarity increased. So, the higher water absorption results of the GP12, GP14, and GP15 mixes may be attributed to the fact that the higher molarities result in higher formation of hydrogen gas and macropores inside the sample, resulting in higher water absorption (Wongkeo; Seekaew; Kaewrahan, 2019).

In addition, GP12, GP14, and GP15 were synthesized at the same AL/FA ratio, which was 0.525. Also, other than GP15, which was synthesized at SS/SH ratio of 2.5, GP12 and GP14 were both synthesized at SS/SH ratio of 2.0. So, these three mixes were synthesized at similar SH molarity, SS/SH, and AL/FA ratios. All three factors were synthesized at medium or high-level content in these mixtures. GPC synthesized at higher AL/FA ratios presents higher water content in the mixture. In these studies (Aliabdo; Abd Elmoaty; Salem, 2016; Sathonsaowaphak; Chindaprasirt; Pimraksa, 2009), it was reported that the increase of voids resulted from the increase of water content, which had no role in the chemical reaction, resulting in increased water absorption. Also, based on the study by Lavanya, and Jegan (2015), it was concluded that the increase in water absorption indicated the presence of higher void content due to the incomplete process of geopolymerization. So, according to these findings, in the present work, the higher water absorption results in the GP12, GP14, and GP15 mixes also may be due to the increase of voids resulting from the medium/high contents present in the mixture, which had no role in the chemical reaction, increasing water absorption (Aliabdo; Abd Elmoaty; Salem, 2016; Lavanya; Jegan, 2015; Sathonsaowaphak; Chindaprasirt; Pimraksa, 2009).

5.2.3 Compressive strength cubic molds

APPENDIX G presents the results of the compressive strength tests for all samples, including the composition, standard deviation, and coefficient of variation. Figure 24 presents the average results of compressive strength tests.

Figure 24 - Average compressive strength at 28 days in cubs.



Source: Author (2024).

As depicted in Figure 24, the highest compressive strength was obtained by a GPC mix. GP11 achieved an average compressive strength of 29.4 MPa, surpassing even the cement composition REF, which achieved approximately 26.9 MPa. So, the slightly lower compressive strength of REF and the higher compressive strength of GPC from the preliminary tests to the final tests may be attributed to the alteration in the quantities and proportion of FA and aggregates, which positively impacted the GPC mixes and negatively the OPC mix. On the other hand, the anticipated positive impact of the alteration in the FA and aggregates in the GPC mixes was based on GPC studies. The study by Rickard *et al.* (2011) argued that higher FA content provides a denser and more compacted microstructure to the GPC matrix. Additionally, FA particles enhance movement among the aggregate particles due to their spherical form and smooth surface (Ahmed *et al.*, 2021; Rickard *et al.*, 2011). Also, in another study, Al-Azzawi, Yu, and Hadi (2018), it was observed that increasing the FA content results in an increase in the volume of fine fraction particles in the GPC matrix. The increase fills the voids and pores

between the aggregate particles, thereby improving the compressive strength of FA-BGPC (Ahmed *et al.*, 2021; Al-Azzawi; Yu; Hadi, 2018). These studies have demonstrated the improved properties of GPC when using similar quantities of FA and aggregates (Deb; Nath; Sarker, 2014; Ghafoor *et al.*, 2021; Nath; Sarker, 2014, 2017; Ramujee; PothaRaju, 2017).

In both preliminary and final tests, GP11 and GP15 were the two GPC with the highest compressive strength. In the preliminary tests, GP15 achieved the highest compressive strength among the GPC mixes, reaching 25.4 MPa while GP11 ranked second with an average of 20.9 MPa. However, in the final tests, the GP11 and GP15 achieved a compressive strength of 29.4 and 27.2 MPa, respectively, with GP11 surpassing GP15. This difference could be attributed to the fact that FA is the primary aluminosilicate source in the GPC mixture. As the amount of FA content increases, silica and alumina levels also increase, affecting polymerization reactions and increasing C-A-S-H and N-A-S-H gels (Ahmed *et al.*, 2021; Parveen *et al.*, 2018). From the final test results, the change in FA and aggregate quantities favored the factors used for GP11 synthesis, leading to an increase in the compressive strength of the GP11 mix compared to the GP15 mix.

The GP11 composition has a molarity of 10 M, SS/SH ratio of 1.5, and AL/FA ratio of 0.70. Comparatively, GP7 has the same molarity and AL/FA ratio but a higher SS/SH ratio of 2.5. Despite this difference, GP11 achieved higher compressive strength. Among all GPC mixes in Figure 24, GP11 is uniquely synthesized at low SS/SH ratio (1.5). In the study by Ghafoor *et al.* (2021), reductions in compressive strength of FA-BGPC were observed with increasing SS/SH ratio. This behavior was observed while increasing the SS/SH ratio from 1.5 to 2, and from 2 to 2.5. The reductions in compressive strength were attributed to the subsequent decrease in SH solution and hydroxide ions (OH^-), reducing the formation of the three-dimensional network of sodium aluminosilicates hydrate [N-A-S-H] gel (Ghafoor *et al.*, 2021). Hence, compared to GP7, the higher compressive strength result of GP11 can be attributed to the fact that the compressive strength increased with decreasing SS/SH ratio. Similar behavior was reported in other studies (Ghafoor *et al.*, 2021; Phoo-Ngernkham *et al.*, 2015; Ridtirud; Chindaprasirt; Pimraksa, 2011).

Compared to other GPCs, the highest compressive strength of GP11 also may be attributed to another fact. The GP11 mix was synthesized using high AL/FA ratio of 0.70.

According to findings from a study by Joseph, and Mathew (2012), it was reported that the compressive strength increased as the AL/FA ratio increased. The improvement in FA-BGPC strength may be attributed to the fact that increasing the AL/FA ratio enhances the Si species content and the $\text{SiO}_2/\text{Al}_2\text{O}_3$ ratio, resulting in more Si-O-Si bonds, which are stronger compared to Si-O-Al (Al Bakri, A.M.M. *et al.*, 2012; Aliabdo; Abd Elmoaty; Salem, 2016; Joseph; Mathew, 2012). Similarly, the improvement in GPC properties due to increasing AL/FA ratio has been reported in these studies (Ahmed *et al.*, 2021; Aliabdo; Abd Elmoaty; Salem, 2016; Hardjito *et al.*, 2004; Scholar; Ganesh Babu-Professor; Santhanam-Assistant Professor, 2008). Similarly, GP7 was also synthesized using an AL/FA ratio of 0.70 and presented higher compressive strength compared to GP3, GP12, and GP14. Compared to other GPC mixes, GP7 achieved a medium compressive strength of 26.7 MPa.

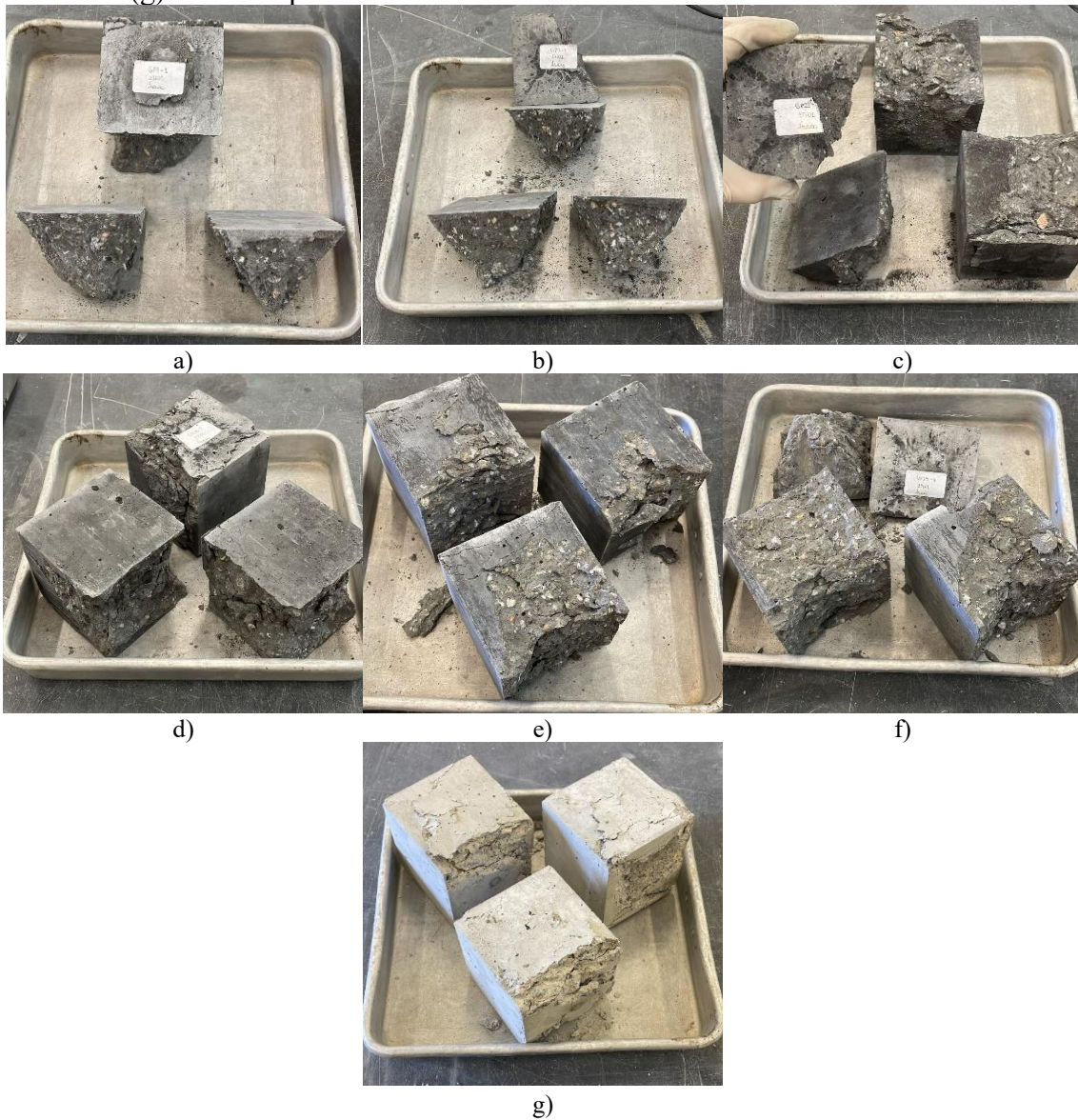
After GP11, the geopolymer GP15 achieved the second higher compressive strength result, which was 27.2 MPa. GP15 was synthesized using a molarity of 16 M, SS/SH ratio of 2.5, and AL/FA ratio of 0.525. Compared to the other five geopolymers in Figure 24, GP15 is the only one with a molarity of 16 M. In a study by B. Siva Konda Reddy, J. Varaprasad, and K. Naveen Kumar Reddy (2010), FA-BGPC mixes were synthesized using molarities of 10 M, 12 M, 14 M, and 16 M. The results showed that the compressive strength of GPC mixes continuously increased with increasing SH molarity from 10 M to 16 M (B. Siva Konda Reddy; J. Varaprasad; K. Naveen Kumar Reddy, 2010). Similar behavior was reported in other studies (Baharom *et al.*, 2019; Das; Shrivastava, 2021; Jaydeep; Chakravarthy, 2013; Vora; Dave, 2013). Additionally, it was reported by Aliabdo, Abd Elmoaty, and Salem (2016) that increasing SH molarity up to 16 M improves FA-BGPC properties. However, beyond 16 M, desirable properties decrease due to a lower rate of polymerization taking place as a result of the high SH concentration (Aliabdo; Abd Elmoaty; Salem, 2016). The improvement in GPC properties while increasing SH molarity up to 16 M was reported in these studies (Al Bakri, A M M *et al.*, 2012; Aliabdo; Abd Elmoaty; Salem, 2016; Hardjito *et al.*, 2004). In general, increasing the SH molarity improves the compression strength of GPC, which may be attributed to the higher dissolution of silicon and aluminum particles in the geopolymerization process (Ahmed *et al.*, 2021; Ghafoor *et al.*, 2021; Görhan; Kürklü, 2014; Nath; Sarker, 2017); through the leaching out of silica and alumina with the high concentration of SH (Aliabdo; Abd Elmoaty; Salem, 2016; Chindaprasirt *et al.*, 2009a).

Geopolymers GP3, GP12, and GP14 are positioned as the three central nodes of the DOE. Consequently, it was anticipated that these three geopolymers would demonstrate comparable compressive strength once they were produced using the DOE's medium factors: a molarity of 10 M, SS/SH ratio of 2.0, and AL/FA ratio of 0.525. Figure 24 reveals that these mixes presented lower compressive strength.

Compared to GP7 and GP11, which were synthesized with an AL/FA of 0.70, the GP3, GP12, and GP14 were synthesized with a ratio of 0.525. This variance in composition may contribute to the lower compressive strength observed in GP3, GP12, and GP14. The reduced AL/FA ratio potentially led to a lower Si species content in the mixture, resulting in weaker Si-O-Si bonds and decreased compressive strength (Al Bakri, A.M.M. *et al.*, 2012; Aliabdo; Abd Elmoaty; Salem, 2016; Joseph; Mathew, 2012). Compared to GP15, which was synthesized with a high molarity of 16 M, GP3, GP12, and GP14 were formulated with medium molarity of 10 M. Similarly, the lower compressive strength of GP3, GP12, and GP14 may also be influenced by the lower concentration of SH in the mixture, resulting in the lower dissolution of silicon and aluminum particles during the geopolymerization process (Ahmed *et al.*, 2021; Ghafoor *et al.*, 2021; Görhan; Kürklü, 2014; Nath; Sarker, 2017).

To depict the final compressive strength test procedure, photographs of the cubic specimens were registered after the compression test in Figure 25. Also, the highest-performance sample from each composition was selected for future research in microstructure analyses (Figure 26).

Figure 25 - (a-f) Geopolymers GP3, GP7, GP11, GP12, GP14, and GP15, respectively
(g) REF composition.



Source: Author (2024).

Figure 26 - Selection of samples to future research.



Source: Author (2024).

6 CONCLUSIONS AND FUTURE RESEARCH

6.1 Conclusions

FA-BGPC utilization can avoid the disposal of an excessive quantity of FA which negatively affects the environment and requires large land area occupation, turning the waste and low-cost material into a beneficial and useful product.

The mix REF, which was produced using OPC, presented the highest compressive strength result in the preliminary tests (27.3 MPa), but was surpassed in the flexural strength results in the preliminary tests and in the compressive strength results in the final tests by GPC mixes. In the preliminary tests, the GP3, GP4, GP7, GP8, GP10, GP11, GP12, GP14, and GP15 achieved higher flexural strength, compared to REF. Geopolymer GP11 presented the highest flexural strength result in the preliminary tests (6 MPa), and the highest compressive strength result in the final tests (29.4 MPa), even higher than the flexural and compressive strength of the cement-based mix REF (4.2 MPa and 26.9 MPa, respectively). The final test results offered higher reliability than preliminary tests.

Compared to all mixes, the geopolymers GP5 and GP7 presented the highest and lowest water absorption through capillarity, respectively. The GP7, GP8, and GP12 mixes presented lower water absorption by capillarity, compared to REF. The GP13 presented the lowest water absorption by immersion. Also, only GP12 and GP15 mixes presented higher water absorption, compared to REF.

GPC technology has the potential to replace the traditional concrete in the construction sector, but its adoption can be difficult because the current standards focus on Portland cement-based concretes. FA-BGPC utilization instead of OPC concrete has the potential to achieve similar mechanical properties and reduce the impact caused by cement production over global warming and FA disposal.

6.2 Future research

Some significant topics about FA-BGPC that would complement this study.

- Mix Design Procedure for FA-BGPC: it can improve the properties of the materials used for GPC synthesis. This could be done with true fine refinements in the mixture quantities and proportion between FA and aggregates according to the amount of alkaline solution used in each GPC;

- Scanning Electron Microscope (SEM), Fourier Transform Infrared Spectroscopy (FTIR), X-ray Diffraction (XRD) analyses: additional analyses could provide very significant details of the microstructure of FA-BGPC, the existence of microcracks, incomplete formation of the dense matrix, amorphous and crystalline structures, unreacted FA;
- Heat-cured FA-BGPC: heat cured conditions could significantly improve the mechanical strength of GPC. This condition contributes to the complete reaction between FA and the alkaline activator, resulting in a denser matrix;
- Blended FA, such as FA-GGBFS or FA-MK GPC: another aluminosilicate source material combined may provide improved properties, such as workability and setting time;
- Influence of W/GPS ratio on workability, microstructure, and mechanical properties of FA-BGPC: study on the influence of water addition and other additives, such as superplasticizer, may offer the optimum limits to be used in the GPC syntheses and achieve desirable properties;
- Fire resistance: previous studies have shown that GPC has superior performance under elevated temperatures compared to OPC concrete;
- Compressive strength of FA-BGPC at other ages, especially after 28 days.

REFERENCES

ABDULLAH, Mohd Mustafa Al Bakri *et al.* Fly Ash-based Geopolymer Lightweight Concrete Using Foaming Agent. **International Journal of Molecular Sciences**, [s. l.], v. 13, n. 6, p. 7186–7198, 2012.

AHMED, Hemn Unis *et al.* Compressive Strength of Sustainable Geopolymer Concrete Composites: A State-of-the-Art Review. **Sustainability**, [s. l.], v. 13, n. 24, p. 13502, 2021.

AL BAKRI, A.M.M. *et al.* **Optimization of alkaline activator/fly ash ratio on the compressive strength of manufacturing fly ash-based geopolymer.** [S. l.: s. n.], 2012. v. 110–116

AL BAKRI, A M M *et al.* THE PROCESSING, CHARACTERIZATION, AND PROPERTIES OF FLY ASH BASED GEOPOLYMER CONCRETE. **Rev. Adv. Mater. Sci.**, [s. l.], p. 90–97, 2012.

AL-AZZAWI, Mustafa; YU, Tao; HADI, Muhammad N.S. Factors Affecting the Bond Strength Between the Fly Ash-based Geopolymer Concrete and Steel Reinforcement. **Structures**, [s. l.], v. 14, p. 262–272, 2018. Disponível em: Acesso em: 19 maio 2024.

ALBITAR, M. *et al.* Durability evaluation of geopolymer and conventional concretes. **Construction and Building Materials**, [s. l.], v. 136, p. 374–385, 2017. Disponível em: Acesso em: 25 abr. 2024.

ALIABDO, Ali A.; ABD ELMOATY, Abd Elmoaty M.; SALEM, Hazem A. Effect of water addition, plasticizer and alkaline solution constitution on fly ash based geopolymer concrete performance. **Construction and Building Materials**, [s. l.], v. 121, p. 694–703, 2016. Disponível em: Acesso em: 25 abr. 2024.

ALMUTAIRI, Ahmad L. *et al.* Potential applications of geopolymer concrete in construction: A review. **Case Studies in Construction Materials**, [s. l.], v. 15, p. e00733, 2021.

ÁLVAREZ-AYUSO, E. *et al.* Environmental, physical and structural characterisation of geopolymer matrixes synthesised from coal (co-)combustion fly ashes.

Journal of Hazardous Materials, [s. l.], v. 154, n. 1–3, p. 175–183, 2008. Disponível em: Acesso em: 24 mar. 2024.

ANA PAULA SILVA NATAL. **Production of Geopolymers from Fly Ash for Wastewater Treatment**. 2023. [s. l.], 2023. Disponível em: <http://hdl.handle.net/10198/28717>. Acesso em: 11 abr. 2024.

ANDREW, Robbie M. Global CO₂ emissions from cement production, 1928–2018. **Earth System Science Data**, [s. l.], v. 11, n. 4, p. 1675–1710, 2019.

ASSI, Lateef N. *et al.* Review of availability of source materials for geopolymer/sustainable concrete. **Journal of Cleaner Production**, [s. l.], v. 263, p. 121477, 2020.

ASTM INTERNATIONAL. **ASTM C 642 Standard Test Method for Density, Absorption, and Voids in Hardened Concrete**. [S. l.], 2006.

ASWATHY, N. N.; RITZY, R. Effect of Metakaolin in the Mechanical Properties of Ambient Cured Flyash Based Geopolymer Concrete. *In*: [S. l.: s. n.], 2020. p. 871–879.

B. SIVA KONDA REDDY; J. VARAPRASAD; K. NAVEEN KUMAR REDDY. Strength and workability of low lime fly-ash based geopolymer concrete. **Indian Journal of Science and Technology**, [s. l.], v. Vol. 3, 2010.

BAHAROM, Shahrizan Bin *et al.* **Effect of Heat Curing Temperatures on Fly Ash-Based Geopolymer Concrete Article in International Journal of Engineering and Technology**. [S. l.: s. n.], 2019. Disponível em: <https://www.researchgate.net/publication/330242016>. .

BAJPAI, Rishabh *et al.* Environmental impact assessment of fly ash and silica fume based geopolymer concrete. **Journal of Cleaner Production**, [s. l.], v. 254, p. 120147, 2020. Disponível em: Acesso em: 22 mar. 2024.

BELLUM, Ramamohana Reddy; MUNIRAJ, Karthikeyan; MADDURU, Sri Rama Chand. Influence of activator solution on microstructural and mechanical properties of geopolymer concrete. **Materialia**, [s. l.], v. 10, p. 100659, 2020.

BENHELAL, Emad; SHAMSAEI, Ezzatollah; RASHID, Muhammad Imran. Challenges against CO₂ abatement strategies in cement industry: A review. **Journal of**

Environmental Sciences, [s. l.], v. 104, p. 84–101, 2021. Disponível em: Acesso em: 26 mar. 2024.

BUSCH, Pablo *et al.* Literature review on policies to mitigate GHG emissions for cement and concrete. **Resources, Conservation and Recycling**, [s. l.], v. 182, p. 106278, 2022.

CHINDAPRASIRT, Prinya *et al.* Comparative study on the characteristics of fly ash and bottom ash geopolymers. **Waste Management**, [s. l.], v. 29, n. 2, p. 539–543, 2009a. Disponível em: Acesso em: 25 abr. 2024.

CHINDAPRASIRT, Prinya *et al.* Comparative study on the characteristics of fly ash and bottom ash geopolymers. **Waste Management**, [s. l.], v. 29, n. 2, p. 539–543, 2009b. Disponível em: Acesso em: 24 mar. 2024.

CHITHAMBARAM, S. Jeeva *et al.* Effect of parameters on the compressive strength of fly ash based geopolymer concrete. **Structural Concrete**, [s. l.], v. 19, n. 4, p. 1202–1209, 2018a.

CHITHAMBARAM, S. Jeeva *et al.* Effect of parameters on the compressive strength of fly ash based geopolymer concrete. **Structural Concrete**, [s. l.], v. 19, n. 4, p. 1202–1209, 2018b.

CRISTELO, Nuno *et al.* Recycling municipal solid waste incineration slag and fly ash as precursors in low-range alkaline cements. **Waste Management**, [s. l.], v. 104, p. 60–73, 2020. Disponível em: Acesso em: 17 jun. 2024.

DAS, Sourav K.; SHRIVASTAVA, Sandeep. Siliceous fly ash and blast furnace slag based geopolymer concrete under ambient temperature curing condition. **Structural Concrete**, [s. l.], v. 22, n. S1, p. E341–E351, 2021.

DAVIDOVITS, Joseph. **Geopolymer: Chemistry and Applications**. 5th edition. [S. l.: s. n.], 2020.

DE VARGAS, Alexandre Silva *et al.* The effects of Na₂O/SiO₂ molar ratio, curing temperature and age on compressive strength, morphology and microstructure of alkali-activated fly ash-based geopolymers. **Cement and Concrete Composites**, [s. l.], v. 33, n. 6, p. 653–660, 2011. Disponível em: Acesso em: 24 mar. 2024.

DEB, Partha Sarathi; NATH, Pradip; SARKER, Prabir Kumar. The effects of ground granulated blast-furnace slag blending with fly ash and activator content on the workability and strength properties of geopolymer concrete cured at ambient temperature. **Materials & Design (1980-2015)**, [s. l.], v. 62, p. 32–39, 2014.

DEUTSCHE NORM. **DIN 1048-5 Testing Concrete - Testing of Hardened Concrete (Specimens Prepared in Mould)**. [S. l.], 1996.

EISA, M. S.; FAHMY, E. A.; BASIOUNY, M. E. Using metakaolin-based geopolymer concrete in concrete pavement slabs. **Innovative Infrastructure Solutions**, [s. l.], v. 7, n. 1, p. 1, 2022.

EUROPEAN STANDARD; EUROPEAN COMMITTEE FOR STANDARDIZATION. **NP EN 196-1 Métodos de ensaios de cimentos - Parte 1: Determinação das resistências mecânicas**. [S. l.], 2006.

EUROPEAN STANDARD; EUROPEAN COMMITTEE FOR STANDARDIZATION. **NP EN 933-1 2014 Ensaios das propriedades geométricas dos agregados Parte 1: Análise granulométrica Método da peneiração**. [S. l.], 2014.

EUROPEAN STANDARD; EUROPEAN COMMITTEE FOR STANDARDIZATION. **NP EN 12390-1 Testing hardened concrete - Part 1: Shape, dimensions, and other requirements for specimens and moulds**. [S. l.], 2003a.

EUROPEAN STANDARD; EUROPEAN COMMITTEE FOR STANDARDIZATION. **NP EN 12390-3 Testing hardened concrete - Part 3: Compressive strength of test specimens**. [S. l.], 2009.

EUROPEAN STANDARD; EUROPEAN COMMITTEE FOR STANDARDIZATION. **NP EN 12620 2003 Agregados para betão**. [S. l.], 2003b.

FANG, Guohao *et al.* Workability and mechanical properties of alkali-activated fly ash-slag concrete cured at ambient temperature. **Construction and Building Materials**, [s. l.], v. 172, p. 476–487, 2018.

FAWZY, Samer *et al.* Strategies for mitigation of climate change: a review. **Environmental Chemistry Letters**, [s. l.], v. 18, n. 6, p. 2069–2094, 2020.

FERDOUS, M W; KAYALI, O; KHENNANE, A. A DETAILED PROCEDURE OF MIX DESIGN FOR FLY ASH BASED GEOPOLYMER CONCRETE. **International Institute for FRP in Construction**, [s. l.], p. 11–13, 2013.

FERNÁNDEZ-JIMÉNEZ, A.; PALOMO, A.; CRIADO, M. Microstructure development of alkali-activated fly ash cement: a descriptive model. **Cement and Concrete Research**, [s. l.], v. 35, n. 6, p. 1204–1209, 2005.

FU, Qiang *et al.* The microstructure and durability of fly ash-based geopolymer concrete: A review. **Ceramics International**, [s. l.], v. 47, n. 21, p. 29550–29566, 2021. Disponível em: Acesso em: 30 mar. 2024.

GANESH, A. Chithambar; MUTHUKANNAN, M. Development of high performance sustainable optimized fiber reinforced geopolymer concrete and prediction of compressive strength. **Journal of Cleaner Production**, [s. l.], v. 282, p. 124543, 2021. Disponível em: Acesso em: 23 mar. 2024.

GHAFOOR, M. Talha *et al.* Influence of alkaline activators on the mechanical properties of fly ash based geopolymer concrete cured at ambient temperature. **Construction and Building Materials**, [s. l.], v. 273, p. 121752, 2021.

GÖRHAN, Gökhan; KÜRKLÜ, Gökhan. The influence of the NaOH solution on the properties of the fly ash-based geopolymer mortar cured at different temperatures. **Composites Part B: Engineering**, [s. l.], v. 58, p. 371–377, 2014.

GOSWAMI, Kakali Priyam; PAKSHIRAJAN, Kannan; PUGAZHENTHI, G. Process intensification through waste fly ash conversion and application as ceramic membranes: A review. **Science of The Total Environment**, [s. l.], v. 808, p. 151968, 2022. Disponível em: Acesso em: 30 mar. 2024.

GRABIAS-BLICHAZ, Ewelina; FRANUS, Wojciech. A critical review on mechanochemical processing of fly ash and fly ash-derived materials. **Science of The Total Environment**, [s. l.], v. 860, p. 160529, 2023. Disponível em: Acesso em: 30 mar. 2024.

HADI, Muhammad N.S.; FARHAN, Nabeel A.; SHEIKH, M. Neaz. Design of geopolymer concrete with GGBFS at ambient curing condition using Taguchi method. **Construction and Building Materials**, [s. l.], v. 140, p. 424–431, 2017.

HANIFA, Mohd *et al.* A review on CO₂ capture and sequestration in the construction industry: Emerging approaches and commercialised technologies. **Journal of CO₂ Utilization**, [s. l.], v. 67, p. 102292, 2023.

HANNANEE AHMAD ZAIDI, Fakhryna *et al.* Performance of Geopolymer Concrete when Exposed to Marine Environment. **IOP Conference Series: Materials Science and Engineering**, [s. l.], v. 551, n. 1, p. 012092, 2019.

HARDJITO, D. *et al.* On the development of fly ash-based geopolymer concrete. **ACI Materials Journal**, [s. l.], v. 101, n. 6, p. 467–472, 2004.

HU, Wei *et al.* Mechanical property and microstructure characteristics of geopolymer stabilized aggregate base. **Construction and Building Materials**, [s. l.], v. 191, p. 1120–1127, 2018. Disponível em: Acesso em: 24 mar. 2024.

IBRAHIM, Omar Mohamed Omar *et al.* Effect of horizontal joints on structural behavior of sustainable self-compacting reinforced concrete beams. **Advances in Concrete Construction**, [s. l.], v. 10, n. 5, p. 455–462, 2020.

JAYDEEP, S; CHAKRAVARTHY, B J. Study On Fly Ash Based Geo-Polymer Concrete Using Admixtures. **International Journal of Engineering Trends and Technology (IJETT)**, [s. l.], v. 4, 2013. Disponível em: <http://www.ijettjournal.org>.

JOSEPH, Benny; MATHEW, George. Influence of aggregate content on the behavior of fly ash based geopolymer concrete. **Scientia Iranica**, [s. l.], v. 19, n. 5, p. 1188–1194, 2012.

KARTHIK, A.; SUDALAIMANI, K.; VIJAYA KUMAR, C. T. Investigation on mechanical properties of fly ash-ground granulated blast furnace slag based self curing bio-geopolymer concrete. **Construction and Building Materials**, [s. l.], v. 149, p. 338–349, 2017. Disponível em: Acesso em: 8 abr. 2024.

LABORATÓRIO NACIONAL DE ENGENHARIA CIVIL - PORTUGAL.
LNEC E 393 - Betões: Determinação da absorção de água por capilaridade. [S. l.], 1993a.

LABORATÓRIO NACIONAL DE ENGENHARIA CIVIL - PORTUGAL.
LNEC E 394 - Betões: Determinação da absorção de água por imersão. [S. l.], 1993b.

LAVANYA, Ganesan; JEGAN, Josephraj. Durability Study on High Calcium Fly Ash Based Geopolymer Concrete. **Advances in Materials Science and Engineering**, [s. l.], v. 2015, p. 1–7, 2015.

LEHNE, Johanna; PRESTON, Felix. **Chatham House Report Making Concrete Change Innovation in Low-carbon Cement and Concrete**. [S. l.: s. n.], 2018. Disponível em: www.chathamhouse.org.

LUHAR, S *et al.* Impact of incorporation of volcanic ash on geopolymerization of eco-friendly geopolymer composites: A review. **IOP Conference Series: Materials Science and Engineering**, [s. l.], v. 572, n. 1, p. 012001, 2019.

LUHAR, Salmabanu; KHANDELWAL, Urvashi. A Study on Water Absorption and Sorptivity of Geopolymer Concrete. **International Journal of Civil Engineering**, [s. l.], v. 2, n. 8, p. 1–9, 2015.

LUHAR, Ismail; LUHAR, Salmabanu. A Comprehensive Review on Fly Ash-Based Geopolymer. **Journal of Composites Science**, [s. l.], v. 6, n. 8, p. 219, 2022. Disponível em: <https://www.mdpi.com/2504-477X/6/8/219>.

MADDALENA, Riccardo; ROBERTS, Jennifer J.; HAMILTON, Andrea. Can Portland cement be replaced by low-carbon alternative materials? A study on the thermal properties and carbon emissions of innovative cements. **Journal of Cleaner Production**, [s. l.], v. 186, p. 933–942, 2018.

MANIKANDAN, P.; VASUGI, V. A Critical Review of Waste Glass Powder as an Aluminosilicate Source Material for Sustainable Geopolymer Concrete Production. **Silicon**, [s. l.], v. 13, n. 10, p. 3649–3663, 2021.

MUSTAFA, A M *et al.* **Effect of Na₂SiO₃/NaOH Ratios and NaOH Molarities on Compressive Strength of Fly-Ash-Based Geopolymer/ACI Materials** **Journal**. [S. l.: s. n.], 2012.

NATH, Pradip; SARKER, Prabir Kumar. Effect of GGBFS on setting, workability and early strength properties of fly ash geopolymer concrete cured in ambient condition. **Construction and Building Materials**, [s. l.], v. 66, p. 163–171, 2014.

NATH, Pradip; SARKER, Prabir Kumar. Flexural strength and elastic modulus of ambient-cured blended low-calcium fly ash geopolymer concrete. **Construction and Building Materials**, [s. l.], v. 130, p. 22–31, 2017.

NGUYEN, Hong Ha T. *et al.* Emerging waste-to-wealth applications of fly ash for environmental remediation: A review. **Environmental Research**, [s. l.], v. 227, p. 115800, 2023. Disponível em: Acesso em: 30 mar. 2024.

NUAKLONG, Peem; SATA, Vanchai; CHINDAPRASIRT, Prinya. Properties of metakaolin-high calcium fly ash geopolymer concrete containing recycled aggregate from crushed concrete specimens. **Construction and Building Materials**, [s. l.], v. 161, p. 365–373, 2018. Disponível em: Acesso em: 24 mar. 2024.

OJHA, Avinash; AGGARWAL, Praveen. Durability performance of low calcium Flyash-Based geopolymer concrete. **Structures**, [s. l.], v. 54, p. 956–963, 2023. Disponível em: Acesso em: 8 maio 2024.

OZCELIKCI, Emircan *et al.* A comprehensive study on the compressive strength, durability-related parameters and microstructure of geopolymer mortars based on mixed construction and demolition waste. **Journal of Cleaner Production**, [s. l.], v. 396, p. 136522, 2023. Disponível em: Acesso em: 19 abr. 2024.

PACHECO-TORGAL, Fernando; CASTRO-GOMES, João; JALALI, Said. Alkali-activated binders: A review. Part 2. About materials and binders manufacture. **Construction and Building Materials**, [s. l.], v. 22, n. 7, p. 1315–1322, 2008. Disponível em: Acesso em: 25 abr. 2024.

PARVEEN *et al.* Mechanical and microstructural properties of fly ash based geopolymer concrete incorporating alccofine at ambient curing. **Construction and Building Materials**, [s. l.], v. 180, p. 298–307, 2018. Disponível em: Acesso em: 19 maio 2024.

PAVITHRA, P. *et al.* A mix design procedure for geopolymer concrete with fly ash. **Journal of Cleaner Production**, [s. l.], v. 133, p. 117–125, 2016.

PHOO-NGERNKHAM, Tanakorn *et al.* Effects of sodium hydroxide and sodium silicate solutions on compressive and shear bond strengths of FA–GBFS geopolymer. **Construction and Building Materials**, [s. l.], v. 91, p. 1–8, 2015. Disponível em: Acesso em: 24 mar. 2024.

POLOJU, Kiran Kumar; SRINIVASU, Kota. Impact of GGBS and strength ratio on mechanical properties of geopolymer concrete under ambient curing and oven curing. **Materials Today: Proceedings**, [s. l.], v. 42, p. 962–968, 2021.

QAIDI, Shaker M.A. *et al.* Ultra-high-performance geopolymer concrete: A review. **Construction and Building Materials**, [s. l.], v. 346, p. 128495, 2022. Disponível em: Acesso em: 23 mar. 2024.

RAMUJEE, Kolli.; POTHARAJU, M. Mechanical Properties of Geopolymer Concrete Composites. **Materials Today: Proceedings**, [s. l.], v. 4, n. 2, p. 2937–2945, 2017.

REDDY, M. Srinivasula; DINAKAR, P; RAO, B. Hanumantha. Mix design development of fly ash and ground granulated blast furnace slag based geopolymer concrete. **Journal of Building Engineering**, [s. l.], v. 20, p. 712–722, 2018.

REHAN, R.; NEHDI, M. Carbon dioxide emissions and climate change: Policy implications for the cement industry. **Environmental Science and Policy**, [s. l.], v. 8, n. 2, p. 105–114, 2005.

RICKARD, William D.A. *et al.* Assessing the suitability of three Australian fly ashes as an aluminosilicate source for geopolymers in high temperature applications. **Materials Science and Engineering: A**, [s. l.], v. 528, n. 9, p. 3390–3397, 2011. Disponível em: Acesso em: 19 maio 2024.

RIDTIRUD, Charoenchai; CHINDAPRASIRT, Prinya; PIMRAKSA, Kedsarin. Factors affecting the shrinkage of fly ash geopolymers. **International Journal of Minerals, Metallurgy, and Materials**, [s. l.], v. 18, n. 1, p. 100–104, 2011. Disponível em: <http://link.springer.com/10.1007/s12613-011-0407-z>.

SATHONSAOWAPHAK, Apha; CHINDAPRASIRT, Prinya; PIMRAKSA, Kedsarin. Workability and strength of lignite bottom ash geopolymer mortar. **Journal of Hazardous Materials**, [s. l.], v. 168, n. 1, p. 44–50, 2009a. Disponível em: Acesso em: 25 abr. 2024.

SATHONSAOWAPHAK, Apha; CHINDAPRASIRT, Prinya; PIMRAKSA, Kedsarin. Workability and strength of lignite bottom ash geopolymer mortar. **Journal of Hazardous Materials**, [s. l.], v. 168, n. 1, p. 44–50, 2009b. Disponível em: Acesso em: 25 abr. 2024.

SCHOLAR, RSathia-PhD; GANESH BABU-PROFESSOR, K; SANTHANAM-ASSISTANT PROFESSOR, Manu. **DURABILITY STUDY OF LOW CALCIUM FLY ASH GEOPOLYMER CONCRETE**. [s. l.: s. n.], 2008. Disponível em: <https://www.researchgate.net/publication/237643013>. .

SCRIVENER, Karen L.; JOHN, Vanderley M.; GARTNER, Ellis M. Eco-efficient cements: Potential economically viable solutions for a low-CO₂ cement-based materials industry. **Cement and Concrete Research**, [s. l.], v. 114, p. 2–26, 2018.

SHAHEDAN, Noor Fifinatasha *et al.* Properties of a New Insulation Material Glass Bubble in Geopolymer Concrete. **Materials**, [s. l.], v. 14, n. 4, p. 809, 2021.

SHI, Caijun; QU, Bo; PROVIS, John L. Recent progress in low-carbon binders. **Cement and Concrete Research**, [s. l.], v. 122, p. 227–250, 2019.

SIDDIKA, Ayesha *et al.* Waste Glass in Cement and Geopolymer Concretes: A Review on Durability and Challenges. **Polymers**, [s. l.], v. 13, n. 13, p. 2071, 2021.

SULTHAN, Faiz. Literature Review On Geopolymer Mortar Using Agricultural Waste As Precursor. **Article in International Journal of Scientific & Technology Research**, [s. l.], v. 8, p. 8, 2019. Disponível em: www.ijstr.org.

SUMAJOUW, D. M.J. *et al.* Fly ash-based geopolymer concrete: Study of slender reinforced columns. **Journal of Materials Science**, [s. l.], v. 42, n. 9, p. 3124–3130, 2007.

TALHA JUNAID, M. *et al.* A mix design procedure for low calcium alkali activated fly ash-based concretes. **Construction and Building Materials**, [s. l.], v. 79, p. 301–310, 2015.

TEIXEIRA, E. R.; CAMÕES, A.; BRANCO, F. G. Synergetic effect of biomass fly ash on improvement of high-volume coal fly ash concrete properties. **Construction and Building Materials**, [s. l.], v. 314, p. 125680, 2022. Disponível em: Acesso em: 17 jun. 2024.

TÖBELMANN, Daniel; WENDLER, Tobias. The impact of environmental innovation on carbon dioxide emissions. **Journal of Cleaner Production**, [s. l.], v. 244, p. 118787, 2020. Disponível em: Acesso em: 26 mar. 2024.

VERMA, Manvendra *et al.* Geopolymer Concrete: A Material for Sustainable Development in Indian Construction Industries. **Crystals**, [s. l.], v. 12, n. 4, p. 514, 2022.

VINICIO TIOSSI SCHINCAGLIA. **CONCRETE BLOCKS WITH INCORPORATION OF DIATOMACEOUS EARTH**. 2022. Master thesis - Instituto Politécnico de Bragança, Portugal, 2022. Disponível em: <http://hdl.handle.net/10198/25866>. Acesso em: 19 mar. 2024.

VORA, Prakash R.; DAVE, Urmil V. Parametric Studies on Compressive Strength of Geopolymer Concrete. **Procedia Engineering**, [s. l.], v. 51, p. 210–219, 2013.

WANG, Chao *et al.* High value-added applications of coal fly ash in the form of porous materials: A review. **Ceramics International**, [s. l.], v. 47, n. 16, p. 22302–22315, 2021. Disponível em: Acesso em: 30 mar. 2024.

WONGKEO, Watcharapong; SEEKAEW, Saravadee; KAEWRAHAN, Orawan. Properties of high calcium fly ash geopolymer lightweight concrete. **Materials Today: Proceedings**, [s. l.], v. 17, p. 1423–1430, 2019. Disponível em: Acesso em: 6 maio 2024.

WORLD METEOROLOGICAL ORGANIZATION. **State of the Global Climate in 2022**. [s. l.: s. n.], 2022. Disponível em: <https://public.wmo.int/en/our-mandate/climate/wmo-statement-state-of-global-climate>. Acesso em: 5 set. 2023.

XIE, Jianhe *et al.* Effects of combined usage of GGBS and fly ash on workability and mechanical properties of alkali activated geopolymer concrete with recycled aggregate. **Composites Part B: Engineering**, [s. l.], v. 164, p. 179–190, 2019.

XIE, Tianyu; OZBAKKALOGLU, Togay. Behavior of low-calcium fly and bottom ash-based geopolymer concrete cured at ambient temperature. **Ceramics International**, [s. l.], v. 41, n. 4, p. 5945–5958, 2015.

YANG, Yuyu *et al.* Monitoring global cement plants from space. **Remote Sensing of Environment**, [s. l.], v. 302, p. 113954, 2024.

ZAIDI, Fakhryna Hannanee Ahmad *et al.* Assessment of Geopolymer Concrete for Underwater Concreting Properties. **Archives of Metallurgy and Materials**, [s. l.], p. 677–684, 2021.

ZHANG, Peng *et al.* Fabrication and engineering properties of concretes based on geopolymers/alkali-activated binders - A review. **Journal of Cleaner Production**, [s. l.], v. 258, p. 120896, 2020a. Disponível em: Acesso em: 30 mar. 2024.

ZHANG, Peng *et al.* Properties of fresh and hardened fly ash/slag based geopolymer concrete: A review. **Journal of Cleaner Production**, [s. l.], v. 270, p. 122389, 2020b. Disponível em: Acesso em: 30 mar. 2024.

ZHOU, Wei *et al.* A comparative study of high- and low-Al₂O₃ fly ash based-geopolymers: The role of mix proportion factors and curing temperature. **Materials and Design**, [s. l.], v. 95, p. 63–74, 2016.

ZHOU, Shuaikang *et al.* Relationship between Moisture Transportation, Efflorescence and Structure Degradation in Fly Ash/Slag Geopolymer. **Materials**, [s. l.], v. 13, n. 23, p. 5550, 2020.

APPENDIX

APPENDIX A - Particle analysis of gravel.

Sieves (mm)	Trapped in the sieves		Accumulated retained (%)	Accumulated past (%)
	Mass (g)	Percentage (%)		
16.000	0.00	0.00	0.00	100.00
14.000	0.00	0.00	0.00	100.00
12.500	0.00	0.00	0.00	100.00
10.000	54.40	2.51	2.51	97.49
8.000	615.60	28.38	30.89	69.11
6.300	775.40	35.75	66.64	33.36
4.000	628.10	28.96	95.60	4.40
2.000	62.20	2.87	98.46	1.54
1.000	7.70	0.36	98.82	1.18
0.500	2.40	0.11	98.93	1.07
0.250	2.40	0.11	99.04	0.96
0.125	3.30	0.15	99.19	0.81
0.063	5.60	0.26	99.45	0.55
<0.063	11.90	0.55	100.00	0.00
TOTAL	2169.00			

Source: Adapted from Vinicio Tiozzi Schincaglia (2022).

APPENDIX B - Particle analysis of sand.

Sieves (mm)	Trapped in the sieves		Accumulated retained (%)	Accumulated past (%)
	Mass (g)	Percentage (%)		
16.000	0.00	0.00	0.00	100.00
14.000	0.00	0.00	0.00	100.00
12.500	0.00	0.00	0.00	100.00
10.000	0.00	0.00	0.00	100.00
8.000	0.00	0.00	0.00	100.00
6.300	0.00	0.00	0.00	100.00
4.000	16.90	1.67	1.67	98.33
2.000	65.50	6.47	8.14	91.86
1.000	78.40	7.74	15.88	84.12
0.500	231.30	22.84	38.73	61.27
0.250	427.90	42.26	80.99	19.01
0.125	139.00	13.73	94.72	5.28
0.063	47.20	4.66	99.38	0.62
<0.063	6.30	0.62	100.00	0.00
TOTAL	1012.50			

Source: Adapted from Vinicio Tiozzi Schincaglia (2022).

APPENDIX C - Mass and dimensions of prisms in the preliminary tests.

Designation	Mix no.	Mass (g)	Dimensions		
			L (mm)	W (mm)	H (mm)
REF-OPC	REF-1	563.7	16.0	3.9	4.0
	REF-2	570.2	16.0	4.0	3.9
	REF-3	567.2	16.0	4.0	3.9
GP1-16-2.0-0.35	GP1-1	662.3	16.0	4.1	4.2
	GP1-2	682.0	16.0	4.4	4.2
	GP1-3	685.7	16.1	4.5	4.3
GP2-4-2.0-0.35	GP2-1	605.1	16.2	4.2	4.2
	GP2-2	620.6	16.0	4.1	4.2
	GP2-3	566.9	16.1	4.1	4.1
GP3-10-2.0-0.525	GP3-1	650.2	16.2	4.3	4.2
	GP3-2	630.3	16.0	4.2	4.0
	GP3-3	637.7	16.0	4.2	4.1
GP4-4-2.5-0.525	GP4-1	611.9	16.0	4.0	4.1
	GP4-2	632.0	16.0	4.1	4.1
	GP4-3	658.6	16.0	4.1	4.2
GP5-10-1.5-0.35	GP5-1	620.1	16.0	4.3	4.0
	GP5-2	617.1	16.0	4.2	4.0
	GP5-3	627.5	16.1	4.1	4.1
GP6-4-1.5-0.525	GP6-1	604.6	16.1	4.1	4.0
	GP6-2	606.7	16.1	4.1	4.0
	GP6-3	606.0	16.0	4.1	4.1
GP7-10-2.5-0.70	GP7-1	608.7	16.1	4.1	4.0
	GP7-2	626.2	16.0	4.1	4.0
	GP7-3	628.5	16.0	4.3	4.3
GP8-16-2.0-0.70	GP8-1	590.2	15.9	4.0	3.9
	GP8-2	630.8	16.1	4.1	4.0
	GP8-3	618.1	16.0	4.1	4.0
GP9-4-2.0-0.70	GP9-1	599.5	16.0	4.0	4.0
	GP9-2	589.7	16.0	4.0	4.0
	GP9-3	599.4	16.0	4.0	4.0
GP10-16-1.5-0.525	GP10-1	640.4	16.1	4.1	4.0
	GP10-2	608.3	16.0	4.1	4.0
	GP10-3	651.4	16.1	4.1	4.1
GP11-10-1.5-0.70	GP11-1	644.3	16.1	4.1	4.1
	GP11-2	618.1	16.1	4.2	4.0
	GP11-3	620.1	16.1	4.0	4.1
GP12-10-2.0-0.525	GP12-1	593.6	16.1	4.1	4.0
	GP12-2	638.3	16.1	4.1	4.2
	GP12-3	624.4	16.1	4.1	4.1
GP13-10-2.5-0.35	GP13-1	570.0	15.9	4.1	3.8
	GP13-2	597.1	16.0	4.2	3.9
	GP13-3	592.1	16.0	4.1	4.0
GP14-10-2.0-0.525	GP14-1	579.9	16.0	4.2	3.8
	GP14-2	597.9	15.9	4.1	4.0
	GP14-3	616.4	16.0	4.3	4.0
GP15-16-2.5-0.525	GP15-1	608.6	16.0	4.1	4.0
	GP15-2	610.9	16.0	4.1	4.2
	GP15-3	602.4	16.0	4.1	4.0

APPENDIX D - Flexural and compressive strength in the preliminary tests.

Designation	Mix no.	Flexural Strength		Compressive Strength - 1st halve and 2nd halve			
		kN	MPa	kN	MPa	kN	MPa
REF-OPC	REF-1	1.68	3.9	50.61	31.6	45.13	28.2
	REF-2	2.04	4.8	41.17	25.7	41.95	26.2
	REF-3	1.68	3.9	41.29	25.8	41.71	26.1
GP1-16-2.0-0.35	GP1-1	1.44	3.4	18.52	11.6	14.08	8.8
	GP1-2	1.44	3.4	9.65	6.0	11.14	7.0
	GP1-3	1.68	3.9	10.09	6.3	10.78	6.7
GP2-4-2.0-0.35	GP2-1	0	0	0	0	0	0
	GP2-2	0	0	0	0	0	0
	GP2-3	0	0	0	0	0	0
GP3-10-2.0-0.525	GP3-1	2.28	5.3	27.23	17.0	34.03	21.3
	GP3-2	2.16	5.1	37.66	23.5	51.57	32.2
	GP3-3	2.28	5.3	23.41	14.6	23.04	14.4
GP4-4-2.5-0.525	GP4-1	2.04	4.8	27.11	16.9	17.74	11.1
	GP4-2	2.04	4.8	11.68	7.3	18.13	11.3
	GP4-3	2.28	5.3	37.54	23.5	29.14	18.2
GP5-10-1.5-0.35	GP5-1	0.24	0.6	0.57	0.4	0.23	0.1
	GP5-2	0.96	2.3	10.71	6.7	7.61	4.8
	GP5-3	0.72	1.7	0.61	0.4	0	0.0
GP6-4-1.5-0.525	GP6-1	0.60	1.4	7.57	4.7	8.96	5.6
	GP6-2	0.72	1.7	8.16	5.1	12.26	7.7
	GP6-3	0.84	2.0	7.12	4.5	8.83	5.5
GP7-10-2.5-0.70	GP7-1	2.28	5.3	16.09	10.1	23.56	14.7
	GP7-2	2.40	5.6	23.77	14.9	33.64	21.0
	GP7-3	2.28	5.3	38.79	24.2	17.78	11.1
GP8-16-2.0-0.70	GP8-1	2.40	5.6	25.14	15.7	10.49	6.6
	GP8-2	2.63	6.2	25.79	16.1	26.57	16.6
	GP8-3	2.52	5.9	20.51	12.8	21.37	13.4
GP9-4-2.0-0.70	GP9-1	1.68	3.9	13.41	8.4	18.71	11.7
	GP9-2	1.68	3.9	27.34	17.1	25.60	16.0
	GP9-3	1.80	4.2	29.63	18.5	19.04	11.9
GP10-16-1.5-0.525	GP10-1	2.16	5.1	20.14	12.6	25.85	16.2
	GP10-2	2.04	4.8	22.69	14.2	22.07	13.8
	GP10-3	2.16	5.1	18.37	11.5	22.27	13.9
GP11-10-1.5-0.70	GP11-1	2.75	6.4	33.12	20.7	37.19	23.2
	GP11-2	2.40	5.6	30.17	18.9	33.69	21.1
	GP11-3	2.52	5.9	32.86	20.5	33.66	21.0
GP12-10-2.0-0.525	GP12-1	2.04	4.8	21.81	13.6	21.56	13.5
	GP12-2	1.92	4.5	33.04	20.7	31.64	19.8
	GP12-3	2.16	5.1	21.28	13.3	22.11	13.8
GP13-10-2.5-0.35	GP13-1	0.96	2.3	16.61	10.4	16.27	10.2
	GP13-2	1.08	2.5	19.96	12.5	20.69	12.9
	GP13-3	1.20	2.8	20.88	13.1	20.34	12.7
GP14-10-2.0-0.525	GP14-1	1.80	4.2	34.75	21.7	34.40	21.5
	GP14-2	2.04	4.8	33.44	20.9	29.51	18.4
	GP14-3	1.92	4.5	33.20	20.8	28.70	17.9
GP15-16-2.5-0.525	GP15-1	1.92	4.5	46.10	28.8	49.28	30.8
	GP15-2	1.92	4.5	39.29	24.6	34.51	21.6
	GP15-3	2.04	4.8	35.14	22.0	39.23	24.5

APPENDIX E - Weight measurements of the samples in the test of capillarity.

Designation	Mass (g)					
	0 h	3 h	6 h	24 h	48 h	72 h
REF-OPC	2323.14	2329.50	2331.09	2335.20	2337.31	2337.42
GP1-16-2.0-0.35	2282.44	2288.91	2290.97	2298.20	2303.12	2306.90
GP2-4-2.0-0.35	2202.06	2246.00	2262.96	2283.94	2285.33	2285.33
GP3-10-2.0-0.525	2302.07	2306.35	2308.06	2317.49	2323.62	2323.78
GP4-4-2.5-0.525	2259.95	2266.91	2268.52	2274.66	2279.25	2282.47
GP5-10-1.5-0.35	2241.40	2280.83	2295.75	2332.65	2335.86	2337.38
GP6-4-1.5-0.525	2262.35	2272.22	2274.96	2286.29	2295.02	2301.23
GP7-10-2.5-0.70	2304.94	2306.33	2306.66	2310.08	2310.40	2310.40
GP8-16-2.0-0.70	2331.05	2334.70	2335.82	2340.15	2341.31	2341.31
GP9-4-2.0-0.70	2288.18	2294.18	2296.05	2303.30	2306.15	2306.15
GP10-16-1.5-0.525	2281.21	2284.34	2284.61	2293.34	2302.26	2307.06
GP11-10-1.5-0.70	2334.64	2338.80	2340.27	2345.40	2349.66	2349.66
GP12-10-2.0-0.525	2266.63	2270.33	2271.76	2276.05	2277.98	2277.98
GP13-10-2.5-0.35	2261.12	2270.41	2272.01	2294.18	2304.65	2310.14
GP14-10-2.0-0.525	2278.21	2281.78	2283.07	2297.87	2307.33	2309.98
GP15-16-2.5-0.525	2264.28	2266.91	2267.97	2279.77	2290.62	2295.04

Source: Author (2024).

APPENDIX F - Absorption of water in the test of capillarity in g/mm².

Designation	Absorption of water (g/mm ²)					
	0 h	3 h	6 h	24 h	48 h	72 h
REF-OPC	0	0.00064	0.00080	0.00121	0.00142	0.00143
GP1-16-2.0-0.35	0	0.00065	0.00085	0.00158	0.00207	0.00245
GP2-4-2.0-0.35	0	0.00439	0.00609	0.00819	0.00833	0.00833
GP3-10-2.0-0.525	0	0.00043	0.00060	0.00154	0.00215	0.00217
GP4-4-2.5-0.525	0	0.00070	0.00086	0.00147	0.00193	0.00225
GP5-10-1.5-0.35	0	0.00394	0.00543	0.00913	0.00945	0.00960
GP6-4-1.5-0.525	0	0.00099	0.00126	0.00239	0.00327	0.00389
GP7-10-2.5-0.70	0	0.00014	0.00017	0.00051	0.00055	0.00055
GP8-16-2.0-0.70	0	0.00036	0.00048	0.00091	0.00103	0.00103
GP9-4-2.0-0.70	0	0.00060	0.00079	0.00151	0.00180	0.00180
GP10-16-1.5-0.525	0	0.00031	0.00034	0.00121	0.00211	0.00258
GP11-10-1.5-0.70	0	0.00042	0.00056	0.00108	0.00150	0.00150
GP12-10-2.0-0.525	0	0.00037	0.00051	0.00094	0.00113	0.00113
GP13-10-2.5-0.35	0	0.00093	0.00109	0.00331	0.00435	0.00490
GP14-10-2.0-0.525	0	0.00036	0.00049	0.00197	0.00291	0.00318
GP15-16-2.5-0.525	0	0.00026	0.00037	0.00155	0.00263	0.00308

Source: Author (2024).

APPENDIX G - Compressive strength in the final tests.

Designation	Mix No.	Mass (g)	Compressive strength			
			MPa	Average (MPa)	Standard deviation (MPa)	Coefficient of variation (%)
REF-OPC	REF-1	2284.37	27.02	26.94	0.44	1.64
	REF-2	2310.74	26.46			
	REF-3	2288.21	27.33			
GP3-10-2.0-0.525	GP3-1	2305.60	20.94	19.73	1.05	5.33
	GP3-2	2311.30	19.09			
	GP3-3	2310.70	19.15			
GP7-10-2.5-0.70	GP7-1	2321.10	27.10	26.69	1.01	3.80
	GP7-2	2297.50	27.44			
	GP7-3	2282.70	25.54			
GP11-10-1.5-0.70	GP11-1	2309.40	28.29	29.37	0.98	3.35
	GP11-2	2298.97	29.62			
	GP11-3	2320.77	30.21			
GP12-10-2.0-0.525	GP12-1	2271.41	22.53	22.33	0.92	4.13
	GP12-2	2268.95	21.32			
	GP12-3	2295.26	23.13			
GP14-10-2.0-0.525	GP14-1	2321.90	24.64	23.34	1.13	4.85
	GP14-2	2269.20	22.80			
	GP14-3	2277.00	22.58			
GP15-16-2.5-0.525	GP15-1	2287.70	27.61	27.19	1.37	5.02
	GP15-2	2287.40	28.29			
	GP15-3	2257.10	25.66			

Source: Author (2024).



O12 | Optimizing the synthesis of geopolymers from fly ash: A Box-Behnken design for enhanced mechanical performance in sustainable construction materials

Ana Paula Ferreira ^{1,2,3*}, Isaac A. Oliveira ^{1,2,6}, José Luis D. Tuesta ^{1,4}, Debora Macanjo ^{1,5}, Rodrigo A. Pereira ⁶, José A. Peres ³, Helder T. Gomes ^{1,2}

¹Centro de Investigação de Montanha (CIMO), Instituto Politécnico de Bragança, Campus de Santa Apolónia, 5300-253 Bragança, Portugal

²Laboratório Associado para a Sustentabilidade e Tecnologia em Regiões de Montanha (SusTEC), Instituto Politécnico de Bragança, Campus de Santa Apolónia, 5300-253 Bragança, Portugal

³Centro de Química de Vila Real (CQVR), Universidade de Trás-os-Montes e Alto Douro, Quinta de Prados, 5000-801, Vila Real, Portugal

⁴Department of Chemical and Environmental Technology, ESCET, Rey Juan Carlos University, Móstoles, Spain

⁵Centro de Materiais e Tecnologia Construtivas (C-MADE), Universidade Beira Interior (UBI)

⁶Department of Agricultural Engineering, Federal University of Lavras, Trevo Rotatório Professor Edmir Sá Santos Universidade Federal de, Lavras - MG, 37203-202, Brasil

*anapaula.silva@ipb.pt

Abstract: This research delves into the synthesis of geopolymers from fly ash, emphasizing the process optimization through a Box-Behnken design. Key parameters, including molar concentration of NaOH, Na₂SiO₃/NaOH and alkali solution/fly ash mass ratios, are systematically explored to enhance the flexural and compressive strength properties of the geopolymers, aligning with the burgeoning interest in sustainable construction materials. The geopolymer production process, meticulously optimized using the Box-Behnken design, aims to achieve materials with superior flexural and compressive strengths, evaluated through bending and compression tests, providing quantitative insights into the material's resistance to deformation and load-bearing capacity, essential factors for assessing its suitability in construction applications^{1,2}. Produced in prismatic quadrangular molds, measuring approximately 16 mm in length, 4 mm in width and 4 mm in height, the geopolymers boast masses of around 600 g. The production methodology involves combining an alkaline solution (consisting of waterglass and NaOH) through magnetic stirring, followed by fly ash and aggregates (stone, sand and water) into paddle stirrers. Among the 15 geopolymers analyzed, one formulation (considering NaOH 16 M, Na₂SiO₃/NaOH = 2.5 and an alkali solution/fly ash ratio = 0.525 (g/L)), distinguished itself with the highest compression strength of 25.4 MPa. Simultaneously, a geopolymer prepared considering NaOH 16 M, Na₂SiO₃/NaOH = 1.5 and an alkali solution/fly ash ratio = 0.525 (g/L), excelled in flexural strength with a result of 6 MPa. The superior compression strength of the former formulation and the heightened flexural strength of the latter, provide valuable insights in the quest to tailor geopolymers to meet diverse construction and materials engineering requirements.

Keywords: Geopolymers; Fly Ash; Box-Behnken Design; Sustainable Construction Materials; Mechanical Strength

Acknowledgments: The authors are grateful to the Foundation for Science and Technology (FCT, Portugal) for financial support through national funds of FCT/MCTES (PIDDAC) to CIMO (UIDB/00690/2020 and UIDP/00690/2020), CQVR (UIDB/00616/2020) and SusTEC (LA/P/0007/2020). Ana Paula Ferreira thanks her doctoral Grant with reference PRT/BD/153090/2021, financed by FCT, with funds from NORTE2020, under Program MIT Portugal, Jose L. Diaz de Tuesta acknowledges the financial support through the program of Atracción al Talento of Comunidad de Madrid (Spain) for the individual research grants 2020-T2/AMB-19836 and 2022-T1/AMB-23946.

References:

1. Khawaji, M. Hydration, Microstructure, and Properties of Fly Ash-Based Geopolymer: A Review. *Materials Science-Poland* **41**, 263-287 (2023), doi: 10.2478/msp-2023-0006.
2. Gaurav, G., Kandpal, S. C., Mishra, D. & Kotoky, N. A comprehensive review on fly ash-based geopolymer: a pathway for sustainable future. *J Sustain Cem Based Mater* 1–45 (2023) doi:10.1080/21650373.2023.2258122.